AN ABSTRACT OF THE DISSERTATION OF

Anthony Janicek for the degree of Doctor of Philosophy in Biological & Ecological Engineering presented on March 27, 2015.

Title: Cathode Development and Reactor Design for Scaling-up Microbial Fuel Cells.

Abstract approved:

_____

Hong Liu

Developing new wastewater treatment technologies which will off-set the high-energy cost associated with treatment is necessary to maintain both water and energy security. Microbial fuel cell technology represents one such option. However, there are still many obstacles to overcome before practical application of this technology can be realized. Improving cathode and reactor design while lowering cost and increasing performance will remove two major obstacles to scale-up and move MFC technology one-step closer to practical application.

Metal supporting materials are increasingly being used as base materials for microbial fuel cell (MFC) cathodes. However, the potential for corrosion may limit their use as base materials of MFCs during scale-up and long-term operation. In the first study included in this dissertation, the electrochemical performance, power generation in MFCs, hydrostatic pressure tolerance, and stability of activated carbon (catalyst) cathodes with carbon cloth or different size metal mesh as base materials were investigated. Electrochemical testing results showed that the finest stainless steel mesh (250x250 openings per inch) outperformed carbon cloth cathodes by 10-

40% at current densities ranging from 6 to 11.2 A m^{-2} over the typical cathode operating range of 0.1 V to 0 V. When tested in MFCs, however, carbon cloth based cathodes out performed all stainless steel mesh cathodes by as much as 34%, reaching 1.72 W m^{-2}; probably due to the corrosion and salt build-up on the surface of the stainless steel mesh cathodes. Carbon cloth cathodes also maintained high static pressure heads of 1.9 m. The high electrochemical performance, hydrostatic pressure tolerance, and corrosion resistance of carbon cloth suggest that carbon fiber based materials may be more suitable than metal based materials for use as MFC cathodes base material for some applications.

Replacing precious metal catalysts by inexpensive activated carbon (AC) is a breakthrough in microbial fuel cell (MFC) cathode fabrication. In the next study covered by this dissertation, activated carbon powders made from bamboo, peat, coal, coconut, and hardwood sources were characterized in terms of their surface area, pore size distribution, surface chemistry, and conductivity to better understand the linkages between the physical and chemical properties of AC and their electrochemical performance with carbon cloth as the base material. The bamboo-based AC demonstrates the highest potential for use as a catalyst for carbon cloth based cathode, reaching -10.6 A m^{-2} and 11.27 A m^{-2} at 0V with loading of 25mg cm^{-2} and 50mg cm^{-2}, respectively. The maximum power density reached 3.3 W m^{-2} in CEA-MFCs and 2.6 W m^{-2} in cube-MFCs, respectively. These power densities are much higher than that typically reported for single-chamber MFCs with activated carbon catalysts. The higher proportion of micorpore surface area/volume, higher conductivity, and lower C/O ratio may all contribute to the higher performance. These results demonstrate

that activated carbon/carbon cloth cathodes are capable of achieving high performance with very low potential for corrosion, making them more suitable for use in scaling-up MFCs.

To further advance MFC technology toward scale-up, developing more efficient reactors that maintain performance during scale-up is paramount for practical application to be realized. When MFCs are scaled up, however, increasing reactor size has typically resulted in decreased power density. Furthermore, the voltage output of a single MFC is normally less than 0.8 V, often less than 0.3 V at maximum power output, which greatly limits the application of MFCs. In the next study, a novel scaled-up MFC configuration that contains multiple cloth electrode assemblies in which the MFCs were internally connected in series (iCiS CEA-MFC) was developed. The iCiS CEA-MFC, equivalent to 3 CEA-MFCs, produced a high voltage output over 1.8 V and a maximum power density of 3.5 W m^{-2} using cathodes containing activated carbon as the catalyst. This power density is 6% higher than that reported for a similar smaller CEA-MFC, indicating that power can be maintained during scale-up with a greater than 33-fold increase in total cathode surface area and greater than 20-fold increase in reactor volume. The maximum power density occurred at an HRT of 80 min and an acetate concentration of 5.9 gL^{-1}, which is significantly higher than that typically reported for MFCs. High stability was also demonstrated based on the performance of the iCiS CEA-MFC containing activated carbon/carbon cloth cathodes over a period of one year of operation. The high power and stability is likely due, in part, to a more efficient means of current collection caused by the internal series connection, which avoids the use of expensive current

collectors. These results clearly demonstrate the great potential of this MFC design for further scaling-up.

However, serial electrical connection of MFCs can result in unbalanced voltage between individual MFCs, which can lead to voltage reversal, causing decreased voltage and power output and electrode material deterioration. In the final study, voltage reversal in newly designed iCiS-MFC stacks with metal mesh or carbon cloth as the cathode base material is examined. Serious corrosion was observed in the MFC stacks with the stainless steel cathode base material, which may have been caused and further worsened by repeated voltage reversal. Higher power output and stability was observed in the MFC stack using carbon cloth as the cathode base material. Conditions related to MFC continuous operation including pump stoppage, gas build-up within the reactor, and rapid decreases in external resistance at high current density, were also examined to determine their relation to voltage reversal and MFC performance. Although negative MFC voltages occurred in some MFCs and the total reactor voltage decreased 67 to 85% under these operational conditions, full recovery following voltage reversal was observed after normal operating conditions were restored in the MFC stacks. These results indicate that voltage reversal can be avoided through proper operation and design of MFC stacks and in the event voltage reversal occurs, full recovery is possible with the iCiS CEA-MFC.

Cathode Development and Reactor Design for Scaling-up Microbial Fuel Cells

by
Anthony Janicek

A DISSERTATION

submitted to

Oregon State University

in partial fulfillment of
the requirements for the
degree of

Doctor of Philosophy

Presented March 27, 2015
Commencement June 2015

Doctor of Philosophy dissertation of Anthony Janicek presented on March 27, 2015

APPROVED:

Major Professor, representing Biological & Ecological Engineering

Head of the Department of Biological & Ecological Engineering

Dean of the Graduate School

I understand that my dissertation will become part of the permanent collection of Oregon State University libraries. My signature below authorizes release of my dissertation to any reader upon request.

Anthony Janicek, Author

ACKNOWLEDGEMENTS

I would like to express my sincere gratitude to Dr. Hong Liu for all of her support and guidance throughout my time at OSU and especially for her advice regarding experimental design and her invaluable feedback on the manuscripts that were prepared from my research and this dissertation. Her advice was critical in enabling me to distil a cohesive dissertation and high quality manuscripts from the large amount of research that I performed during my time at OSU. I consider myself very fortunate to have worked with her these last 4 years.

I would also like to thank Dr. Yanzhen Fan for all his help and advice regarding electrochemical analysis, MFC design, and reactor operation. I sincerely appreciate all the time he took out of his busy schedule to further my understanding of all aspects of MFC technology.

I would also like to thank my committee members Dr. Tyler Radniecki, Dr. Dipankar Koley, and Dr. Todd Jarvis for serving on my committee and for their helpful comments.

Thank you also to my lab mates Carol Abourachid, Ningshengjie Gao, Shoutao Xhu, Cheng Li, Luguang Wang, and Keaton Lesnik for all their moral support.

Most importantly, I would like to thank my wife Melissa for all her support and understanding throughout the last four years, especially the last 6 months as I prepared this dissertation and the associated manuscripts.

CONTRIBUTION OF AUTHORS

Hong Liu provided experimental oversight and revisions to all manuscripts

Yanzhen Fan provided guidance with experimental design, MFC design, and revisions to all manuscripts

Ningshengjie Gao provided assistance with interpretation of XPS results presented in Chapter 3

TABLE OF CONTENTS

Page

TABLE OF CONTENTS (Continued)

Page

LIST OF FIGURES

LIST OF FIGURES (Continued)

Figure Page

LIST OF FIGURES (Continued)

Figure Page

LIST OF FIGURES (Continued)

Figure Page

Figure Page

LIST OF TABLES

Table Page

1. INTRODUCTION

As population increases, the demand for water also increases. In the last century, water use has been growing at a rate more than double the rate of population increase [1]. This increase in water use has led to an increase in the amount of wastewater generated. It is estimated that all of the wastewater produced annually amounts to six times more water than exists in all the world's rivers [2]. Every day, 2 million tons of sewage, industrial, and agricultural waste is discharged into the world's waterways [3]. Discharging untreated wastewater contaminates freshwater and coastal ecosystems, threatens food security and access to safe drinking water and ultimately results in major health and environmental management challenges [3]. In developed nations, wastewater infrastructure is often inadequate or deteriorating, while in developing nations it is often non-existent [3,4]. In the U.S. alone, capital investment in wastewater infrastructure is estimated to be $298 billion over the next 20 years with more than 20% of that needed for treatment plants [4].

Compounding the problems associated with the enormous capital investment required for wastewater infrastructure is the significant cost associated with the operation of treatment plants. A significant portion of treatment cost is directly attributable to energy consumption. Currently wastewater treatment consumes approximately 3% of the electricity generated in the U.S. [5,6]. Based on the most recent energy use statistics available, this represents a cost of nearly $11 billion annually [7]. With a finite supply of water, an ever-increasing population, and the enormous cost associated with treatment, finding more efficient and cost effective

means of treating wastewater has become more important than ever. Developing new treatment technologies which will off-set this high-energy cost is necessary to maintain both water and energy security.

Domestic, industrial, and agricultural wastewaters with high organic content represent a possible source of energy, which could offset the high cost associated with wastewater treatment. It has been estimated that the energy contained in wastewater in the form of soluble and insoluble organic matter is 10 times that needed for treatment [8]. Capturing even a fraction of this energy would make wastewater treatment a net-energy producing process [9,10]. Microbial fuel cell (MFC) technology has the potential to capture a portion of this energy directly as electricity. Through the use of exoelectrogenic bacteria, MFC technology releases the energy contained in wastewater while simultaneously treating it. This process occurs when bacteria growing on the anode oxidize soluble organic matter contained in the wastewater and transfer the electrons to the anode while releasing protons at the same time (Figure 1.1 a). Current is produced when electrons flow through an external circuit and protons migrate from the anode to the cathode. At the cathode, the electrons reduce an electron acceptor, typically oxygen in the presence of hydrogen ions, ultimately forming a reduced compound such as water.

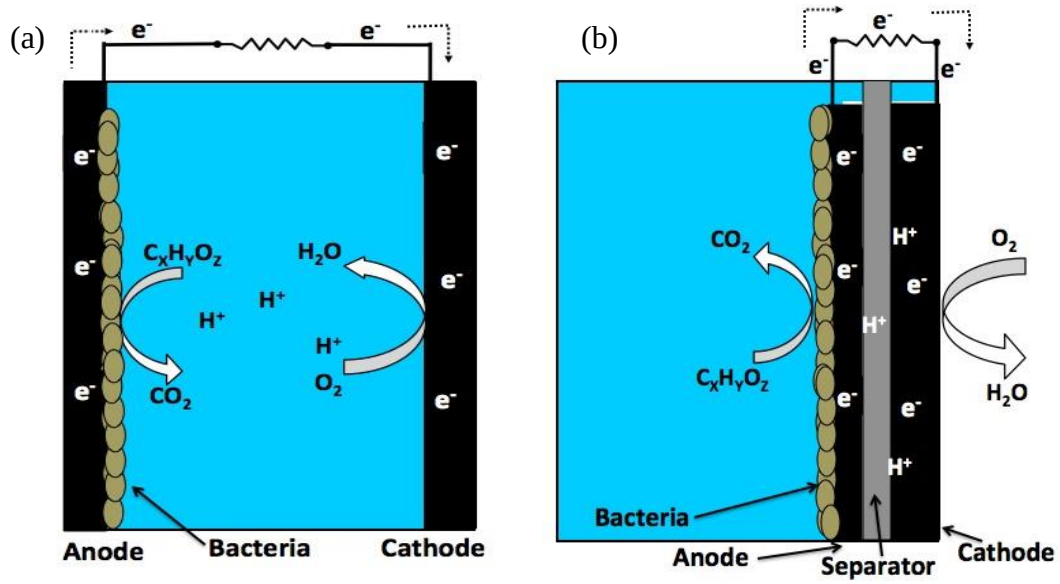

FIGURE 1.1:(a) Schematic showing the processes occurring within a single chamber MFC; and (b) schematic showing the same processes in a cloth electrode assembly (CEA)-MFC.

1.1 PROGRESSION OF MFC RESEARCH

The ability of bacteria to produce electrical current has been known for over 100 years [11]. However, it wasn't until recently that prospects for practical application of MFC technology increased when it was discovered electric current could be generated from wastewater [10,12]. During the same time period, advances in MFC design increased achievable power densities several fold, as indicated by Figure 1.2, further increasing the prospects for practical application [13–16]. In recent years, research into MFC technology has increased exponentially leading to a deeper fundamental understanding of MFC processes as well as advances in MFC design and operation, bringing this technology even closer to the possibility of practical application.

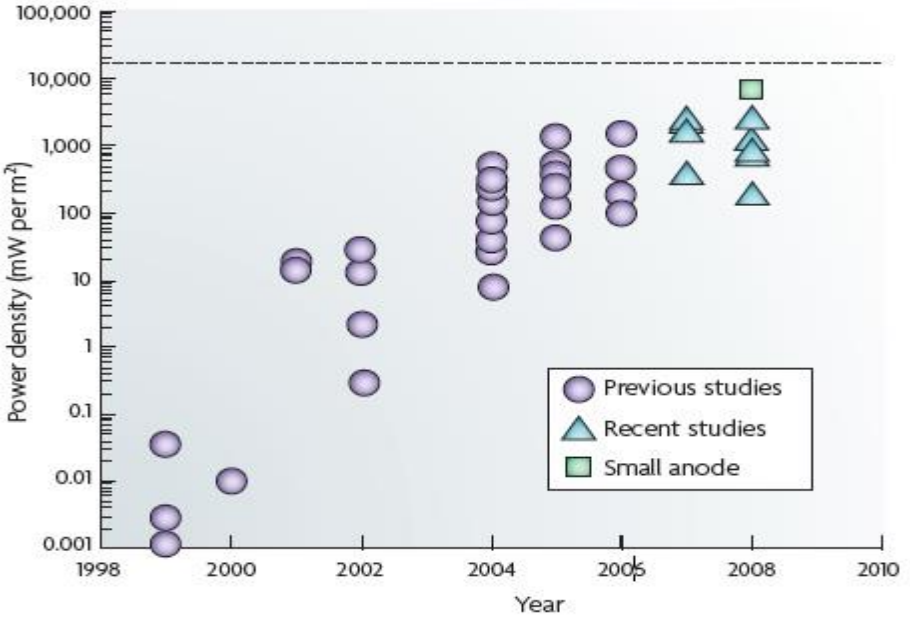

FIGURE 1.2: Increases in power density achieved in MFCs from 1998 to 2008 (figure adapted in part from [16]).

1.2 ADVANTAGES OF MFC TECHNOLOGY IN WASTEWATER TREATMENT

Biological wastewater treatment consists of a broad range of technologies that can be separated into aerobic and anaerobic processes (i.e., by the terminal electron acceptor used). Aerobic treatment methods are the most common biological treatment methods for both municipal and industrial wastewater treatment. However, aerobic treatment methods are extremely energy intensive, as they require entrainment of oxygen into the wastewater for use by bacteria. Although aerobic methods are fast, they typically consume 30% or more of the electrical energy required by treatment plants in order to maintain dissolved oxygen levels in wastewater [5,17].

On the other hand, anaerobic treatment processes are generally slower than aerobic processes as there is less energy available when terminal electron acceptors other than oxygen are used. However, anaerobic treatment methods have the potential to be net energy producing processes. Methane gas, produced during the final step in anaerobic treatment processes, is used to generate electricity when it is combusted in the gas engine of a generator. However, converting the energy contained in the methane indirectly into electricity results in significant losses, with only 30 to 40% of the energy contained in the gas converted to electricity with the remainder given off as heat [9]. In addition, methane is an extremely powerful greenhouse gas [18]. As a result, incomplete combustion and escaping gases will have detrimental effects on the environment.

There are several potential advantages of MFC technology over anaerobic technology for energy generation with simultaneous wastewater treatment. The most significant advantage is that the energy contained within wastewater can be converted directly into electricity. Theoretically, direct electron transfer would result in greater conversion efficiencies than other waste to energy technologies. Another advantage is that electricity production in MFCs is much cleaner than anaerobic methods that generate methane, which is significantly more harmful than carbon dioxide as a greenhouse gas. Regarding treatment, MFCs may produce a higher quality effluent with lower sludge production compared to traditional anaerobic technologies due to the combination of aerobic and anaerobic processes associated with MFC operation [19].

1.3 MFC COMPONENTS & MATERIALS

There are typically four main components to MFCs: (1) bacteria, (2) the anode, (3) the cathode, and (4) separators. Bacteria convert the energy contained in the soluble organic matter of wastewater directly to electricity (electrons). The bacteria then transfer the electrons to the anode, which is connected to the cathode via an external circuit. Protons released during the oxidation of organic matter by the bacteria migrate through solution to the cathode where they combine with oxygen and electrons to form water. Depending on the configuration, the anode can be placed at the opposite end of the chamber from the cathode or sandwiched into an electrode-separator structure through use of a membrane or other separator material (Figure 1.1). For configurations in which the anode and cathode are at opposite ends of the chamber, separators are generally not used.

1.3.1 Exoelectrogens

The electrochemically active bacterial species that have the capability to transfer electrons extracellularly to an electrode are termed exoelectrogens [20]. There are over 20 species of bacteria that are known exoelectrogens [16,21]. These bacteria can transfer electrons to an electrode through chemical mediators or directly through outer membrane proteins or bacterial nanowires [20,22]. Mixed cultures of exoelectrogens have shown to produce higher power than pure cultures in MFCs likely due to the synergistic interactions within the mixed bacterial community [23]. Mixed cultures of bacteria come from diverse genetic groups with core group

members of high power generating mixed cultures coming from *Geobacter*, *Aminophilus*, *Sedimentibacter*, *Acetoanaerobium*, and *Spirochaeta* [24].

1.3.2 Anodes

The anode is the location of electron transfer from bacteria in MFCs. Anodes used in MFCs are typically made from carbon-based materials due to the high conductivity, chemical stability, and biocompatibility. Higher surface area can promote electron transfer and bacterial attachment [20,25]. The following carbon-based materials have been reported for use as MFCs anodes: graphite brush [15,26], carbon veil [27,28], graphite felt [29,30], carbon felt [31], carbon cloth [14,32], carbon paper [33], graphite rods [34], granular graphite [35], and granular activated carbon [34]. The highest power densities have been achieved using carbon cloth anodes and graphite brush anodes [14,15,36].

1.3.3 Cathodes

The cathode is probably the most challenging component of MFC architecture as it is crucial to maintain a three-phase interface between air (oxygen), water (proton), and solid (electrode) to allow the oxygen reduction reaction (ORR) to take place [12,37]. The cathode is also typically the limiting factor to performance in many MFCs and represents a significant portion of the total cost [25]. Among the different types of cathodes that have been used in MFCs, air cathodes have demonstrated the capability of generating high power densities, representing the best

option for practical applications. Air-cathodes used in MFCs typically consist of a catalyst layer, gas diffusion layer, and a conductive base material.

1.3.3.1 Catalysts and catalyst binder

The catalyst layer is the site of the oxygen reduction reaction (ORR) and is typically attached to the solution facing side of the cathode. Precious metal catalysts, such as platinum, have widely been used as the catalyst for the ORR. However, recently inexpensive activated carbon has been used as an alternative to precious metal catalysts, resulting in comparable performance [37–43]. The chemical and physical properties of the activated carbon are dependent upon the source material the activated carbon is made from and procedure used to prepare it. Commercially available activated carbons made from different source materials have recently been examined for use as catalysts in MFC cathodes [44,45]. Although different chemical and physical properties were examined to determine the effect on performance, conflicting results between studies were obtained as to which properties influence performance. These conflicting results suggest that performance of AC powders, as catalysts for MFC cathodes, cannot be predicted by a single physical or chemical property alone or that further investigation is needed. As activated carbon is in powder form, a binder is required to help coalesce the powder and fix it to the supporting base material. Typically polytetraflouroethylene (PTFE) is used as the binder for activated carbon cathodes due to the low cost, ease of use, and high stability compared to other binders [37,40–42,46,47].

1.3.3.2 Gas Diffusion Layers

The gas diffusion layer, is fixed to the air-facing side of the supporting base material, and allows for oxygen diffusion into the cathode structure while preventing leakage of the solution from the MFC. The most typical gas diffusion layers used for MFC cathodes consist of PTFE or polymeric organosilcon based compounds such as polydimethylsiloxane (PDMS). Gas diffusion layers are typically mixed with conductive carbon black and applied to the supporting base material as paste or paint depending on the structure of the cathode [36,37,48]. Curing of gas diffusion layers is required in order to provide the microporous structure that allows for gas diffusion into the catalyst layer while at the same time preventing leakage of solution through the air-facing side of the cathode [49]. Although PDMS and PTFE are similarly priced, PTFE represent a better option for scale-up and practical application, as cure times are relatively short and preparation comparatively more simple.

1.3.3.3 Supporting Base Material

The base material is used as both a current collector and a supporting material for the catalyst layer and gas diffusion layer. Important characteristics for base materials are conductivity, stability, and durability. Both metal-based and carbon-based materials have been used as supporting base materials in MFCs. Carbon-based materials such as carbon cloth [14,25,36], carbon paper [50], and carbon felt [51], and metal-based materials such as stainless steel mesh [37,38,45,52], nickel mesh [40], and nickel foam [42] have been investigated for use as base materials in MFC cathodes. For activated carbon cathodes used in MFCs, stainless steel mesh is the

most widely used base material due to the lower cost and higher conductivity compared to carbon-based materials [37–39,43–45,52–55]. However, recent studies suggest that corrosion of metal base materials is possible under certain conditions [54,56]. This suggests that metal based electrode supporting materials may lack the stability needed and therefore may be limited in their application in MFCs. Although widely used as a supporting base material for precious metal catalysts in MFC cathodes due to high strength and chemical stability, carbon cloth has not been thoroughly investigated as a base material for activated carbon cathodes for use in MFCs.

1.3.3.3.1 Current Collectors

When MFC electrode size is increased or if a base material with low conductivity is used as the supporting material, a current collector is required to enhance electron travel over long distances [12]. Current collectors can either be incorporated as the electrode base material or can be a separate wire or mesh that attaches to the electrode base material. In either case, current collectors serve to reduce the overall internal resistance by reducing the ohmic losses of the electrode [25]. In MFCs, current collectors have been made from titanium mesh, titanium wire, graphite plates, gold, copper, and stainless steel mesh [12,25]. Precious metal current collectors are cost prohibitive for scaling up MFC technology. Although MFCs operate at low current densities, the energy loss can be as much 2 orders of magnitude greater when single point connection is used compared to optimized connections in electrode configurations with surface area greater than 1 m^2 [57]. If current

collectors are used, stable and inexpensive materials should be chosen and the points of connection to the base material should be optimized to maximize current collection.

1.3.4 Separators

Separators are typically used when the anode is in close proximity to the cathode or in two-chamber MFCs (see section 1.4). Separators can prevent short circuit between the anode and cathode. Separator materials used in MFCs have consisted of cation exchange membranes (CEM) [58,59], anion exchange membranes (AEM) [59,60], and materials such as cloth [14], nylon and glass fiber [61]. It is generally recommended that the use of CEMs and AEMs should be avoided if possible due to their high cost compared with other separator materials [36,62]. Although the use of a separator is not required in single-chamber MFCs, its use allows for decreased electrode spacing and prevents oxygen diffusion into the anode chamber which can have detrimental effects on biofilms and the total fraction of substrate that is converted into electricity (i.e., coulombic efficiency) [14,33,63,64]. Cloth based separator materials have shown to provide the greatest promise for practical applications due to the low cost, high power densities, and the high coulombic efficiency attainable with this material.

1.4 MFC CONFIGURATION & DESIGN FACTORS RELATING TO PERFORMANCE

1.4.1 MFC configurations

While many different MFC designs have been reported in the literature such as single and dual chamber cube and cylindrical type reactors [26,32,65,66], dual chambered H-cell reactors [66], plate and tube shaped reactors [26,36,50], the majority of scale-up studies use reactors that are tubular or flat plate in design [26–30,34,60,67–71]. Both tubular and flat plate designs can consist of dual or single chamber configurations. Dual chamber MFCs typically contain aqueous cathode chambers using biological catalysts or chemical oxidants such as ferricianide, permanganate, or dissolved oxygen. Configurations that use aqueous cathode chambers are not suitable for practical application due to the low power associated with biological catalysis or the cost associated with replenishing the aqueous oxidant.

Single chamber MFCs, which consist of an anode and cathode in a shared electrolyte, have shown increased power generation compared to dual chamber configurations due to decreased internal resistance resulting from increased ion diffusion rates [62,63,72]. A single chamber MFC may contain a separator, such as those mentioned in section 1.3.4 (Figure 1.1 b). Single chamber MFCs using separators, such as the cloth electrode assembly (CEA)-MFC depicted in Figure 1.1 b, typically produce higher power compared to configurations that don't contain separators due to the decreased internal resistance associated with the decreased electrode spacing [14]. Although the presence of the separator contributes to the internal resistance, electrode spacing can be significantly decreased compared to designs that don't use a separator. As a result, internal resistance is decreased due to faster ionic diffusion rates compared to configurations with larger electrode spacing.

There are many different configurations of tubular and flat plate single chamber MFCs reported in the literature, which will be discussed in more detail below.

1.4.1.1 Tubular Reactor Configurations

Scaled-up, tube shaped configurations typically consist of a tubular anode surrounded by a separator to electrically isolate the anode from the cathode. The tubular shape of the reactor is typically a product of the cylindrical structural material used. For example, scaled-up reactors have been designed using supporting materials such as PVC [29,30,60,67,73–75] (Figure 1.3b, 1.3c, 1.3d, 1.4b, 1.4e), polypropylene [27,76,77] (Figure 1.4a), cylindrical bottles [26] (Figure 1.3a), measuring cylinders [28] (Figure 1.4d), nylon tubing [68] (Figure 1.4c), and a cation exchange membrane formed into a tube [71] (Figure 1.3c). Anodes in these reactors consist of a cylindrical brush (graphite or carbon fiber), granular material (granular activated carbon or graphite granules), or a flat electrode (Figure 1.4f, 1.4g), made of some type of conductive fabric (carbon cloth, felt, or veil) formed into a cylinder (Table 1) The anodes, or anode chamber, are then wrapped by some type of membrane or separator material (Table 1) to electrically isolate the anode from the cathode. The cathode is then wrapped around the separator. Cathodes made of carbon cloth, carbon fiber, or carbon veil containing Pt, MnO2, or activated carbon as the catalyst have been reported (Table 1). Only 3 studies report using a biologically catalyzed cathode [68,69,78], one of which used graphite fiber brush cathodes, the only such design reported. Depending on type of membrane or separator material used, the electrode/membrane or electrode/separator structure has been termed a membrane

electrode assembly (MEA) [77], a membrane cathode assembly (MCA) [29], or a cloth cathode assembly (CCA) [30]. The configuration can also be reversed with a cylindrical anode chamber surrounding a cathode tube [68]. Relatively few tubular designs have been reported that use no separator [26,34,79].

FIGURE 1.3: Tubular brush anode reactors. (A) Cylindrical bottle batch reactor; (B) perforated PVC brush anode reactor; (C) cation exchange membrane brush anode reactor; (D) u-shaped tubular brush anode reactor. Figure adapted in part from [80].

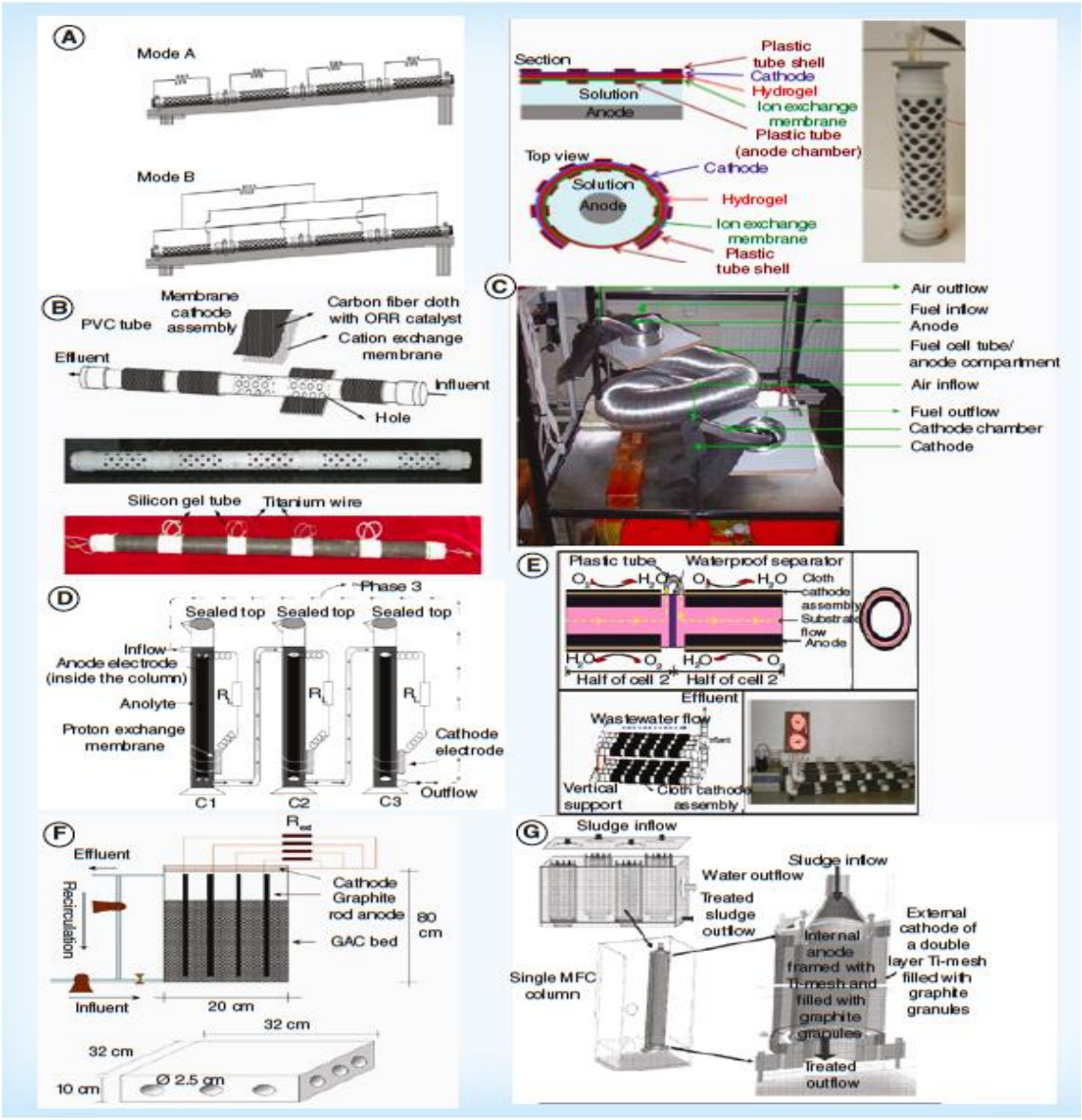

FIGURE 1.4: Tubular reactors with sandwiched membrane/electrode structures. (A) Longitudinal modular tubular reactor with membrane electrode assembly; (B) tubular stack reactor made with membrane cathode assembly; (C) inner cathode tubular reactor; (D) tubular column reactor; (E) tubular stack reactor made with membrane cathode assembly; (F) multi anode/cathode reactor; (G) tubular reactor with granular graphite anode/cathode chambers. Figure adapted in part from [80].

TABLE 1: Summary of design characteristics for reactors reported in the literature. Figure adapted in part from [80].

Volume	Anode Type	Cathode Type	Separator/ Membrane	Specific Area (m^2 m^{-3})	Figure
1 L	graphite fiber brush	air cathode, carbon cloth with Pt	None	13	1a
~1 L	carbon veil	air, cathode, carbon cloth, 0.5 mg cm^{-2} Pt	CEM	43	2 a
~ 1.5 L	graphite felt	air cathode,carbon fiber, MnO_2 catalyst	CEM	12.5	2 b
2 L	carbon brush	carbon cloth with Pt/AC or AC only as catalyts	CEM or AEM	119.5	1 b
2.5 L	carbon cloth	carbon cloth, biocathode	perforated nylon tubing	40	2 c
2.7 L	carbon veil	carbon veil	PEM	40	2 d
2.7 L	carbon veil	carbon veil	PEM	40	2 d
3.6 L	carbon brush	air cathode, carbon cloth with Pt catalyst	CEM	73.3	1 c
4 L	carbon brush	carbon cloth with Pt/AC or AC only as catalyts	CEM	-----	1 d
10 L	graphite felt	GORE-TEX cloth, conductive catalytic layer	water proof air-permeable layer, layer of GORE-TEX cloth	62	2 e
20 L	graphite rods, granular activated carbon	air cathode, carbon cloth with Pt or MnO_2 as catalyst	none	0.3	2 f
67 L	graphite granules, titanium mesh	graphite granules, titanium mesh	nylon mesh	-----	2 g
1.5 L	-----	air cathode, carbon paper, 0.5 mg/cm^2 Pt	PEM	21.3	3 a
1.5 L	-----	air cathode, carbon paper, 0.5 mg/cm^2 Pt	PEM		3 a
3.5 L	carbon felt	carbon felt biocathode	CEM	5.6	3 b
5 L	titanium plate/mesh with mixed metal oxide coating	titanium plate/mesh with mixed metal oxide coating and ferric iron	CEM	100	-----
7.5 L	granular graphite	carbon felt, biocathode	CEM	25.2	3 c
20 L	titanium plate/mesh with mixed metal oxide coating	titanium plate/mesh with mixed metal oxide coating	CEM	100	-----

Most tubular designs reported were operated in continuous flow mode. As a result further scale-up can be achieved by connecting additional tubular MFC modules together in series by extending the length of the tube, forming an MFC stack [30]. It is believed that the tubular design allows for near optimal cross-sectional dimensions to be maintained during scale-up [27,68,76,81]. As a result, minimal dead space is likely to occur in the reactor thereby creating near plug flow conditions allowing for a sufficiently mixed, relatively steady-state flow regime [27].

1.4.1.2 Flat Plate Reactor Configurations

Fewer studies have been reported on flat plate designs than on tubular designs [26,31,35,50,58,82]. Flat plate configurations typically consist of rectangular anode chambers with some type of a membrane or separator material sandwiched between the anode and cathode. The supporting structural material is typically Plexiglass or some other type of easily machine-able plastic [31,35,50,58,82,83] (Figure 1.5a,b, c). The anodes and cathodes in these designs have been made of granular graphite (anode only), carbon felt, carbon paper, and titanium plates/mesh (Table 1). Both chemical and biological catalysts have been used to catalyze the reaction at the cathode (Table 1). One flat plate design was similar to the bipolar plate design used in PEMFCs [58,82]. The key feature of the flat plat design is that the distance between the anode and cathode is minimized thereby increasing ionic diffusion rates and reducing internal resistance compared to other designs in which electrode spacing is larger [14,36,64]. As with tubular designs, most flat plate designs were operated in

continuous flow mode (Table 1) and individual flat plat modules can be connected to form larger MFC stacks during scale-up [35,58].

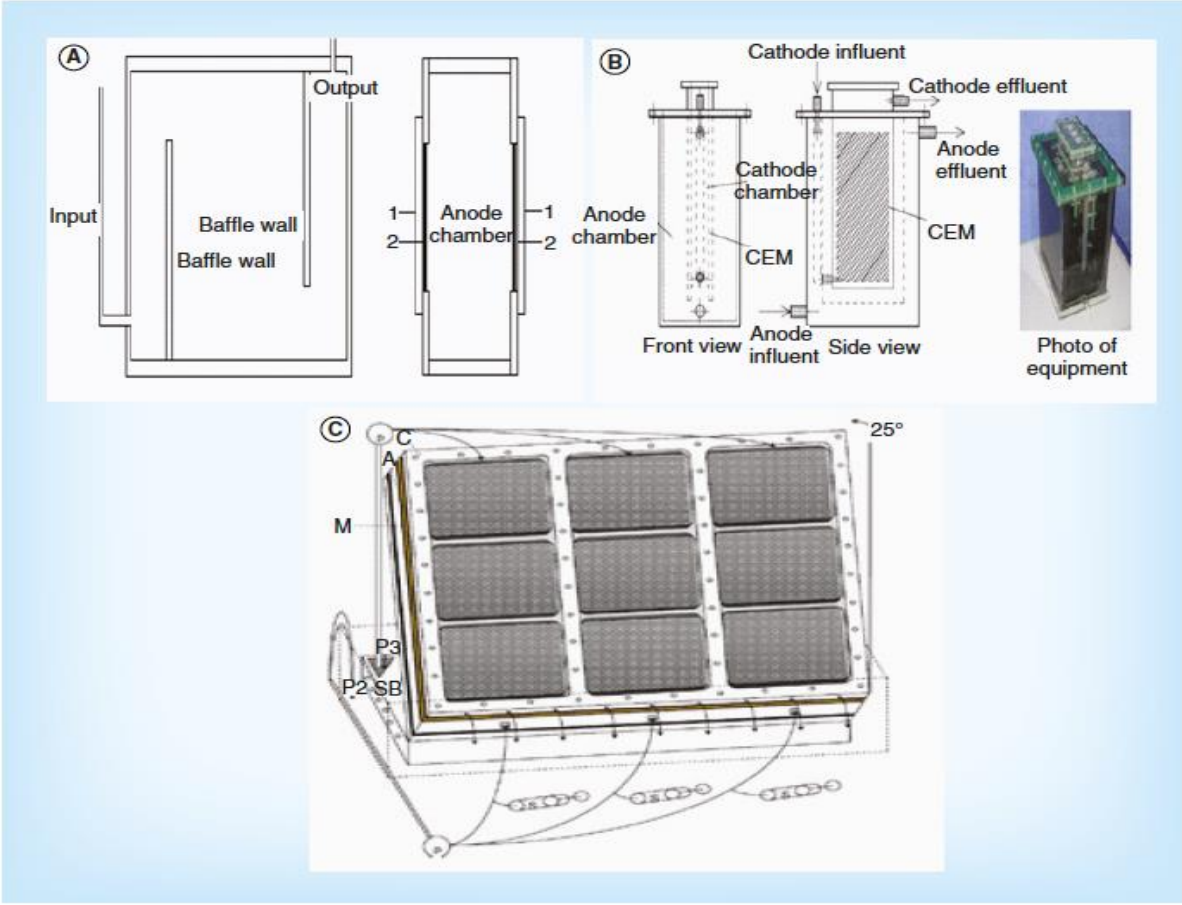

FIGURE 1.5: (A) Baffled flat plate reactor; (B) inner cathode flat plate reactor; (C) flat plate stack reactor. Figure adapted in part from [80]

1.4.1.3 Multiple MFC connection

Connecting MFCs into stacks of multiple individual MFCs allows for both series and parallel hydraulic and electrical connection. When hydraulically connected in series, influent flows sequentially through each MFC module while parallel connection results in each module receiving the same influent. Similarly, individual MFCs can be connected electrically in series to increase voltage or in parallel to

increase current [84–87]. Both series and parallel electrical connection allows for useful voltages and currents to be produced, which are a requirement if practical application of MFC technology is to be realized.

When connected electrically in series, unbalanced voltage between individual cells often occurs. If the imbalance in voltage is large enough, a phenomenon known as voltage reversal can occur under certain conditions. Voltage reversal results from an imbalance in voltage between cells, which is due to differences in internal resistance of individual cells. This phenomenon results in one of the electrodes switching polarity, either becoming more positive (in the case of the anode) or more negative (in the case of the cathode) than the other electrode. Voltage reversal has been shown to occur in chemical fuel cells resulting in damage to both anodes and cathodes [88–92]. In MFCs, the effect of voltage reversal on electrode materials has not been examined.

1.4.2 Design Factors Affecting Performance

1.4.2.1 Electrode Spacing

In many MFC systems, the electrolyte resistance contributes significantly to the internal resistance. While not the only limiting factor, high electrolyte resistance will ultimately restrict the maximum power achievable for a given design [62]. Reducing electrolyte resistance can be achieved either by reducing electrode spacing or increasing the conductivity of the solution. Increasing conductivity would likely require the addition of chemical buffers, which would be cost prohibitive for scaled-up practical applications. As a result, reducing electrode spacing is the most effective

way to decrease the internal resistance and increase the power attainable in a given design [14,32,33,62,64,93]. For an MFC with electrode area equal to 7 cm^2, a buffer concentration of 50 mM, and using typical values for the anode and cathode resistance [62], the internal resistance and power density at an electrode distance of 1 cm are calculated as 142 Ω and 0.907 W m^{-2}, respectively. Similarly, at a distance of 1 mm power density can be calculated as 2.34 Wm^{-2}. This represents a greater than 150% increase in power density by decreasing the electrode spacing from 1 cm to 1 mm. For systems that contain separators, a significant increase in power density was demonstrated compared to separator-less systems when electrode spacing was reduced [14].

1.4.2.2 Electrode Shape and Orientation

Electrode shape and orientation have the greatest effect on the minimum distance attainable in a given design. For the designs reported in the literature, anode type dictated the minimum attainable electrode spacing. By nature of the cylindrical brush structure, reactor configurations using brush anodes had increased electrode spacing compared to flat plate reactors and tubular reactors that did not use brush anodes (Table 1). This increased distance results in longer proton diffusion times for areas of the brush located further away from the cathode thereby increasing internal resistance and limiting power. Milliliter scale studies have shown that brush anodes are capable of achieving high power densities due to high electrode surface area and reduced effect of oxygen crossover from the cathode [15,93,94]. However, this was not the case for the scaled-up reactors presented in the literature. These reactors were

larger in both length and diameter than similar smaller reactors. If brush diameter were left the same when scaling up from the smaller scale versions, electrode spacing would be increased, ultimately reducing power. Likewise, if brush diameter were increased, anode surface area would be increased compared to smaller designs. It has been shown that increasing anode surface area with brush anode reactors at smaller scales, increased power significantly but, with similar designs at larger scales power was not significantly increased by increasing brush anode surface area [15,26,32].

In brush anode reactors, the centerline of the brush can be oriented parallel or perpendicular to the cathode. Although high power has been generated in both electrode orientations at smaller scales, larger reactors using brush anodes discussed in the literature have the centerline of the cylindrical brush oriented parallel to the tubular structure with the membrane/cathode assembly wrapped around the entire circumference of the reactor, surrounding the entire anode [60,67,71]. However, the power obtained by these reactors (operated on wastewater) was lower than that achieved by a similar smaller scale reactor also treating wastewater [95] indicating that substrate composition may not be the sole reason for reduced performance.

When brush anodes are used in flat plate reactors [26,32,93], cathodes were placed on only one or two sides of the brush anodes, which results in an inefficient use of anode area compared to the tubular designs. However, flat plate reactors with brush anodes may have an advantage over tubular reactors with brush anodes if electrode spacing can be reduced. A smaller scale (14 ml) brush anode reactor was developed in which the brush, centerline oriented parallel to the cathode, was pressed against the separator of the membrane electrode assembly. This design formed a

hemispherical brush anode shape, reducing the electrode distance by half [93]. This design has not been investigated at larger scales but does hold promise due to the reduced electrode spacing compared to the tubular designs presented in this above. This design configuration could also be extended to tubular reactors through the use of multiple brush anodes or by using smaller diameter tubing, which would flatten the brush against the separator/membrane.

Regardless of the configuration, reactors containing brush anodes will always have greater electrode spacing compared to tubular reactors and flat plate reactors that have electrodes pressed against a separator or membrane. Tubular reactors, described in the literature, with sandwiched membrane electrode structures should have similar performance as flat plat designs if electrode spacing is the same. However, several of these tubular reactors [16–19,30,31] had perforated structural material (PVC or similar material) separating the anode from the membrane/cathode assembly. Although, this likely would not increase the electrode spacing significantly, the perforated nature of the design limits the available surface area of the anode (discussed in further detail below). This in conjunction with the increased spacing could reduce performance significantly compared to flat plate designs that do not contain this limiting structural feature.

1.4.2.3 Separator Materials

In both tubular and plate reactors, electrode spacing is reduced furthest through the use of a separator material sandwiched between the anode and cathode. Most reactors listed in Table 1 used some type of separator, especially cation

exchange membranes (~75%). However, the use of membranes (cation and proton exchange membranes) should be avoided if possible due to their high cost compared with separator materials and high area specific resistance [36,62]. Under proton deficient conditions or neutral pH, proton carriers (commonly anions) are blocked by CEMs leading to high resistance and high cross membrane pH gradients [72]. Similarly, results based on separator materials have shown that internal resistance was increased due to decreased proton transport to the cathode due to the presence of the separator [61]. However, cloth separators have been shown to enhance coulombic efficiency by greatly reducing the oxygen diffusion rate while still maintaining high power densities due to greatly reduced electrode spacing and much higher ion conductivity compared to other separator materials [14,61]. Although, separator materials such as nylon mesh or perforated nylon tubing used in some reactors (Table 1) may prevent contact between electrodes, the impermeable material ultimately reduces the available area of the electrodes, which ultimately reduces performance.

In membrane-less configurations, oxygen diffusion through the cathode can reduce coulombic efficiency as well as potentially interfere with activity of anaerobic bacteria on the anode [14,33,63,64]. The effect of oxygen is further exacerbated when the anode is in close proximity to the cathode. As a result, separators are a critical component of design, allowing electrode spacing to be reduced as much as possible. It is important to select separators based on material type as well as mass transfer properties. Reactors described in this review (Table 1) using CEMs or other separator material would likely experience increased performance through the use of better separator materials.

It should be noted that separators (or membranes) have been observed to deform in both smaller and larger scale flat plate MFCs [58,96]. Separator deformation can decrease anode compartment volume, increase the spacing between electrodes, trapping gas, and ultimately reducing performance. This problem is likely less common in smaller reactors due to the small electrode and separator sizes used. However, as reactor size increases, electrode and separator size will increase, which increases the chance for deformation. Supporting structures may need to be designed that maintain the electrode/separator structure while still maximizing the available area of the electrodes.

1.4.2.4 Surface Area to Volume Ratio

Reducing the electrode spacing can also reduce the surface area to volume ratio, depending on the configuration used. Size and effective electrode surface area will ultimately determine the maximum power attainable for a given design. Scaling up typically results in an increase in electrode area. Depending on the type of electrode material used, larger electrode area can result in increased internal resistance due to the increased distance electrons travel through the material. It has been shown that although increasing anode surface area can increase power, it does not affect performance as much as increasing cathode surface area [26,32] which is currently the limiting factor with respect to performance. In particular it is important to maintain cathode specific surface area (i.e., surface area to volume ratio) when scaling up, as volumetric power density is a function of this parameter. Cathode specific surface areas, for reactors described in this review, are presented in Table 1. High specific surface area does not necessarily correspond to higher power densities.

However, many other factors contribute to the performance of these reactors. Factors such as electrode spacing, anode surface area, separators, substrate, and hydraulic retention time all play a role in determining power output. As a result, it is not possible to draw any conclusions based on this parameter. However, in more controlled experiments [26,36], higher cathode specific area led to higher volumetric power densities.

1.4.2.5 Materials and Structural Supports

Some reactors contain surface modified electrodes to reduce the internal resistance by increasing surface area and conductivity [58,82,83]. Electrode surface modification of both the anode and cathode has shown to increase performance [97,98]. However, in two such cases reported in the literature, titanium mesh was used as part of the modification. This type of electrode would likely be cost prohibitive when produced at larger scales during scale-up. In addition, structural supports used in some tubular reactors, such as PVC or polypropylene tubing, not only act to further separate electrodes but also reduce proton transfer thereby increasing internal resistance. Using perforated piping as structural supports lowers the percentage of open area between the electrodes due to the perforations, reducing the area available for proton transfer, which ultimately reduces performance. This was likely the main reason for decreased performance when scaling up from a similar smaller version of the tubular brush anode reactors operated on wastewater described above. Similarly, another tubular design [60] used a perforated pipe as the structural support for the membrane electrode assembly. Although this supporting structure was on the exterior of the cathode and did not reduce the available area between the

electrodes, oxygen availability to the cathode needed for the oxygen reduction reaction was likely limited due to the lower open area created by the perforated pipe. Structural supports should be chosen so that interference with necessary electrode interactions and processes is limited.

1.5 CHALLENGES & OBJECTIVES

Among the many factors that affect the scaling-up of MFCs, the cathode is currently the limiting factor with respect to both performance and cost. As a result, developing high performing and stable cathodes is paramount for practical application of MFC technology to be realized. Examination of the stability of different base materials as well as the effect of chemical and physical properties of activated carbon on MFC cathode performance will allow for the development of cathodes suitable for scaled-up applications. Furthermore, increasing electrode size and connecting MFCs into stacks represents the greatest potential for scaling-up MFCs. However, using this strategy requires more efficient means of current collection to be developed. As a result, designing more efficient reactors that maintain performance during scale-up and evaluating the performance over the long-term is paramount to move MFC technology closer to practical application.

This dissertation focuses on the development and optimization of low-cost cathode materials and MFC reactor design for use during scaling-up of MFC technology. More specifically, the following 4 objectives are addressed:

1) Compare carbon-based and metal-based supporting base materials with respect to stability and performance during operation in MFCs using activated carbon as the catalyst

2) Develop and optimize a cathode suitable for use during scaling-up of MFCs based on the results of objective (1).

3) Evaluate the performance of the newly designed internally connected in series (iCiS) scaled-up CEA-MFC stack using the cathode developed in (2). Evaluate the performance and stability over one year of operation.

4) Examine the effect of voltage reversal on activated carbon cathodes with carbon-based and metal-based supporting base materials. Evaluate conditions occurring under continuous flow mode that lead to voltage reversal in the iCiS CEA-MFC stack.

1.6 DISSERTATION ORGANIZATION

This dissertation is organized into 6 chapters consisting of this introduction, 4 chapters that address the stated objectives, and a final concluding chapter.

Metal supporting materials are increasingly being used as base materials for microbial fuel cell (MFC) cathodes. However, the potential for corrosion may limit their use as base materials of MFCs during scale-up and long-term operation. In Chapter 2, the electrochemical performance, power generation in MFCs, hydrostatic pressure tolerance, and stability of activated carbon (catalyst) cathodes with carbon

cloth or different size metal mesh as base materials were investigated. Electrochemical testing results showed that the finest stainless steel mesh (250x250 openings per inch) outperformed carbon cloth cathodes by 10-40% at current densities ranging from 6 to 11.2 A m^{-2} over the typical cathode operating range of 0.1 V to 0 V. When tested in MFCs, however, carbon cloth based cathodes out performed all stainless steel mesh cathodes by as much as 34%, reaching 1.72 W m^{-2}; probably due to the corrosion and salt build-up on the surface of the stainless steel mesh cathodes. Carbon cloth cathodes also maintained high static pressure heads of 1.9 m. The high electrochemical performance, hydrostatic pressure tolerance, and corrosion resistance of carbon cloth suggest that carbon fiber based materials may be more suitable than metal based materials for use as MFC cathodes base material for some applications. The results of this work were summarized in a paper by Janicek, A.; Fan, Y.; Liu, H., titled "Performance and stability of different cathode base materials for use in microbial fuel cells" published in Journal of Power Sources.

Replacing precious metal catalysts by inexpensive activated carbon (AC) is a breakthrough in microbial fuel cell (MFC) cathode fabrication. In Chapter 3, activated carbon powders made from bamboo, peat, coal, coconut, and hardwood sources were characterized in terms of their surface area, pore size distribution, surface chemistry, and conductivity to better understand the linkages between the physical and chemical properties of AC and their electrochemical performance with carbon cloth as the base material. The bamboo-based AC demonstrates the highest potential for use as a catalyst for carbon cloth based cathode, reaching -10.6 Am^{-2} and 11.27 A m^{-2} at 0V with loading of 25mg cm^{-2} and 50mg cm^{-2}, respectively. The

maximum power density reached 3.3 Wm^{-2} in CEA-MFCs and 2.6 Wm^{-2} in cube-MFCs, respectively. These power densities are much higher than that typically reported for single-chamber MFCs with activated carbon catalysts. The higher proportion of micorpore surface area/volume, higher conductivity, and lower C/O ratio may all contribute to the higher performance. These results demonstrate that activated carbon/carbon cloth cathodes are capable of achieving high performance with very low potential for corrosion, making them more suitable for use in scaling-up MFCs. The results of this work were summarized in a paper by Janicek, A.; Fan, Y.; Liu, H., titled "High Power Generation and Pressure Tolerance of an Activated Carbon/Carbon Cloth Cathode for Microbial Fuel Cells" submitted to Journal of Power Sources.

In the fourth chapter, the cathode optimized in chapter three was evaluated in a newly designed scaled-up CEA-MFC flat plate reactor containing a stack of MFCs internally connected electrically in series (iCiS). The iCiS CEA-MFC, equivalent to 3 CEA-MFCs, produced a high voltage output over 1.8 V and a maximum power density of 3.5 W m^{-2} using cathodes containing activated carbon as the catalyst. This power density is 6% higher than that reported for a similar smaller CEA-MFC, indicating that power can be maintained during scale-up with a greater than 33-fold increase in total cathode surface area and greater than 20-fold increase in reactor volume. The maximum power density occurred at an HRT of 80 min and an acetate concentration of 5.9 gL^{-1}, which is significantly higher than that typically reported for MFCs. High stability was also demonstrated based on the performance of the iCiS CEA-MFC containing activated carbon/carbon cloth cathodes over a period of one

year of operation. The high power and stability is likely due, in part, to a more efficient means of current collection caused by the internal series connection, which avoids the use of expensive current collectors. These results clearly demonstrate the great potential of this MFC design for further scaling-up. The results of this work were summarized in a paper by Janicek, A.; Gao, N; Fan, Y.; Liu, H., titled "Stable and High Voltage and Power Output of Scaled-up CEA-MFCs Internally Connected in Series (iCiS)" submitted to Energy and Environmental Science.

Serial electrical connection of MFCs can result in unbalanced voltage between individual MFCs, which can lead to voltage reversal, causing decreased voltage and power output and electrode material deterioration. In Chapter 5, voltage reversal in newly designed iCiS CEA-MFC stacks with metal mesh or carbon cloth as the cathode base material is examined. Serious corrosion was observed in the MFC stacks with the stainless steel cathode base material, which may have been caused and further worsened by repeated voltage reversal. Higher power output and stability was observed in the MFC stack using carbon cloth as the cathode base material. Conditions related to MFC continuous operation including pump stoppage, gas build-up within the reactor, and rapid decreases in external resistance at high current density, were also examined to determine their relation to voltage reversal and MFC performance. Although negative MFC voltages occurred in some MFCs and the total reactor voltage decreased 67 to 85% under these operational conditions, full recovery following voltage reversal was observed after normal operating conditions were restored in the MFC stacks. These results indicate that voltage reversal can be avoided through proper operation and design of MFC stacks and in the event voltage

reversal occurs, full recovery is possible with the iCiS CEA-MFC. The results of this work were summarized in a paper by Janicek, A.; Fan, Y.; Liu, H., titled “Stability and Voltage Reversal /Recovery of Internally Connected in Series (iCiS) CEA-MFC Stacks” submitted to Water Research.

2. Performance and Stability of Different Cathode Base Materials for Use in Microbial Fuel Cells

Anthony Janicek, Yanzhen Fan, and Hong Liu

ABSTRACT

Metal supporting materials are increasingly being used as base materials for microbial fuel cell (MFC) cathodes. However, the potential for corrosion may limit their use as base materials of MFCs during scale-up and long-term operation. In this study, the electrochemical performance, power generation in MFCs, hydrostatic pressure tolerance, and stability of activated carbon (catalyst) cathodes with carbon cloth or different size metal mesh as base materials are investigated. Electrochemical testing results show that the finest stainless steel mesh (250x250 openings per inch) outperforms carbon cloth cathodes by 10-40% at current densities ranging from 6 to 11.2 A m^{-2} over the typical cathode operating range of 0.1 V to 0 V. When tested in MFCs, however, carbon cloth based cathodes out perform all stainless steel mesh cathodes by as much as 34%, reaching 1.72 W m^{-2}; probably due to the corrosion and salt build-up on the surface of the stainless steel mesh cathodes. Carbon cloth cathodes also maintained high static pressure heads of 1.9 m. The high electrochemical performance, hydrostatic pressure tolerance, and corrosion resistance of carbon cloth suggest that carbon fiber based materials may be more suitable than metal based materials for use as MFC cathodes base material for some applications.

2.1 INTRODUCTION

Microbial fuel cell (MFC) technology has the unique ability to convert the organic matter in wastewater directly into electricity while treating the wastewater at the same time. However, the compositions of real waste streams can have drastic impacts on performance during practical applications [80]. The complex nature of many waste streams could ultimately limit performance by damaging electrodes and separator materials. As a result, selecting suitable materials for construction of MFC components that maintain desired performance is key for practical application to be realized.

Cathode is typically the limiting factor to performance in many MFCs and represents a significant portion of the total cost [25]. Among the different types of cathodes that have been used in MFCs, air cathodes have demonstrated the capability of generating high power densities in MFCs, representing a great potential for practical applications. Air-cathodes used in MFCs typically consist of a catalyst layer, gas diffusion layer, and a conductive base material. The catalyst layer, which is the site of the oxygen reduction reaction (ORR), is attached to the solution facing side of the cathode. The gas diffusion layer, is fixed to the air-facing side of the supporting base material, and allows for oxygen diffusion into the cathode structure while preventing leakage of the solution from the MFC. The base material is used as both a current collector and a supporting material, for the catalyst layer and gas diffusion layer.

The use of conductive carbon fabrics as base materials for MFC air-cathodes is very common, as carbon fabrics are known for their high strength, good

conductivity and chemical stability [25,99,100]. The electrical properties of carbon fabrics can be controlled through the method in which carbon fibers are formed and through the raw material used to form carbon fibers. Carbon fibers typically have a diameter around 10 μm and are assembled into bundles that contain 1,000 to 10,000 fibers [99]. As a result, carbon cloth can be produced with much higher surface area compared to other supporting materials used for electrode base materials in MFCs.

Due to lower cost and higher conductivity than many carbon based materials, stainless steel mesh [37,38,45,52], nickel mesh [39,40], and nickel foam [42] have been investigated as new base materials for MFC cathodes. However, recent studies have shown that corrosion of stainless steel mesh [54] and nickel foam [56] is possible when used in MFCs, which results in an increased ohmic resistance and a decreased performance [42,56]. For example, greater than 33% decrease in maximum power due to corrosion, which has been attributed to adsorbed protons at the interface of activated carbon and stainless steel mesh, has been shown to occur after acid pretreatment of activated carbon [44,54]. A similar decrease in power density was shown to occur as a result of corrosion due to low cathode potentials at which corrosion is more thermodynamically favorable [56]. This suggests that metal based electrode supporting materials may lack the stability needed and therefore may be limited in their application in MFCs for treating certain types of wastewaters.

Recent studies have compared the performance of metal based activated carbon cathodes to carbon cloth based cathodes using platinum as the catalyst in MFCs [39,40,43], demonstrating comparable results between the two materials for both electrochemical and MFC tests. However, only one metal mesh size was used to

make the comparison in these studies and a comparison between based materials with the same catalyst (activated carbon) was not made. One study examined the effect of different metal mesh sizes on performance, focused on more coarse mesh sizes (ranging from 30x30 to 120x120 openings per inch) and a comparison with carbon fiber based materials was not made [101]. Finer metal mesh sizes have the potential to lead to better performance, compared to more coarse mesh sizes, due to their larger specific surface area. Furthermore, hydrostatic pressure tolerance and stability of MFC base materials, which are critical for large scale and long term operation, have not been well studied.

In this study, the performance and stability of activated carbon cathodes with stainless steel mesh or carbon cloth based materials were investigated. The electrochemical performance in both electrochemical cells and MFCs and the hydrostatic pressure tolerance of cathodes fabricated under different conditions were characterized. Stability as determined by susceptibility to corrosion and salt build-up on the cathode surface were also examined and discussed.

2.2 EXPERIMENTAL

2.2.1 Cathode Fabrication.

Cathodes were constructed with carbon cloth (CC, fuelcellearth.com) or of stainless steel mesh of four different sizes (mcmaster.com) as the base material, activated carbon powder (AC, VWR) as the catalyst, carbon black (Vulcan XC-72R) to increase conductivity, and PTFE as the binder. The stainless steel mesh sizes, characterized by the number of openings per inch, were 250x250 (SS-250), 200x200

(SS-200), 150x150 (SS-150), and 100x100 (SS-100). Activated carbon and carbon powder were combined at mass ration of 9:1 (AC:CP) and mixed with ethanol for 15 minutes. PTFE (60 wt%) was then added to the mixture at a mass ratio of 3:1 (AC to PTFE) and heated at 50°C until a slurry was formed. The slurry was then applied evenly to the solution facing side of the carbon cloth cathode, air-dried overnight, and pressed at ~100 psi at activated carbon mass loading of 17.5 mg cm^{-2}. The other side of the carbon cloth, the air facing side, was prepared by applying diffusion layers as previously reported [102]. Additional cathodes were also constructed with the same procedure as above without the pressing step.

2.2.2 Electrochemical Analysis

Cathode polarization curves were generated using linear sweep voltammetry with a potentiostat (G300, Gamery Instruments, Inc.) in a three-electrode electrochemical test cell. The test cell was constructed from PVC and measured 3 cm in diameter by 2 cm in length (empty bed volume of ~12 ml). The test cell consisted of a cylindrical single-chamber with the working electrode (cathodes with area equal to 0.7 cm^2) placed at one end of the chamber and the counter electrode (anode) placed at the other end. The reference electrode consisted of a Ag/AgCl reference (MF-2052 RE-5B, Bioanalytical Systems, USA) placed in a 200 µl pipet tip which was modified by heating and bending so that the tip faced the working electrode. The counter electrode consisted of a square piece of platinum foil (2.12 × 2.12 cm^2). Tests were conducted in a medium solution containing the following (per liter): KCl, 0.13 g; NH_4Cl, 0.31 g; $NaH_2PO_4*H_2O$, 2.92 g; and $Na_2HPO_4*7H_2O$, 7.735 g. LSV

experiments were conducted by varying potential from +300 mV to -200 mV at a scan rate 0.1 mV s^{-1}.

2.2.3 Pressure Tests

Pressure tolerance of cathodes was determined by measuring the static pressure head. The testing device consisted of a test piece holder (cathode test piece area equal to 7 cm^2) constructed from PVC piping and attached to a tube 2.5 m in length. The apparatus was filled with growth medium solution prepared as previously described [14]. Starting at 10 cm the tubing was raised in 5 cm increments above the test piece holder and left to stand for several hours. Tests were ended when medium solution leaked through the cathode. The pressure tolerance was recorded as the static head measurement prior to the height at which leaking occurred. The average and standard deviation of 3 to 4 cathodes was reported for each test condition.

2.2.4 MFC Construction & Operation

Cube-MFCs were used to determine cathode performance. The MFCs were constructed as previously described [14] with an empty bed volume ~ 12 ml. Carbon cloth (CCP, fuelcellearth.com) was used as the anode material while cathodes were as described above. All data for cathodes presented in this study was obtained by placing new cathodes into fully operational cube-MFCs. Polarization curves were generated as previously described [103] once the voltage had stabilized, typically within 5 to 6 batches after cathodes were placed in MFCs. MFCs were inoculated as previously described [36] using a medium solution containing the following (per

liter): acetate, 5.9 g; KCl, 0.13 g; NH_4Cl, 0.31 g; $NaH_2PO_4*H_2O$, 2.92 g; and $Na_2HPO_4*7H_2O$, 7.735 g. All experiments were conducted in duplicate or triplicate.

2.3 RESULTS

2.3.1 Electrochemical performance

The CC cathode maintained the highest current densities (> -60 A m^{-2} at -0.2V) at cathode potentials more negative than -0.1 V (Figure 2.1 a) reaching over 120% greater than all other cathodes tested at a cathode potential of -0.2 V. However, over the cathode operating range of 0.1 V to 0 V, the SS-250 mesh cathode reached the highest current density of -6 A m^{-2} to -11.2 A m^{-2}, which is 10 to 40 % higher than both the CC (-4.3 A m^{-2} at 0.1 V and -10.2 A m^{-2} at 0V) and SS-200 mesh (-4.3 A m^{-2} at 0.1 V and -9.8 A m^{-2} at 0V) cathodes (Figure 2.1 b). The performance of the SS-150 and SS-100 mesh cathodes were similar, more than16 to 40% less than the SS-250 mesh cathode over the cathode operating range.

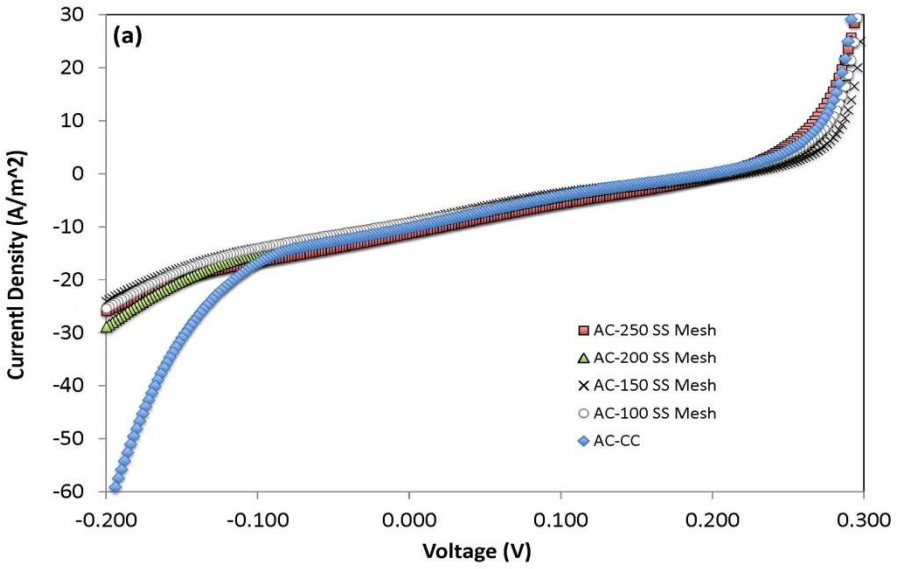

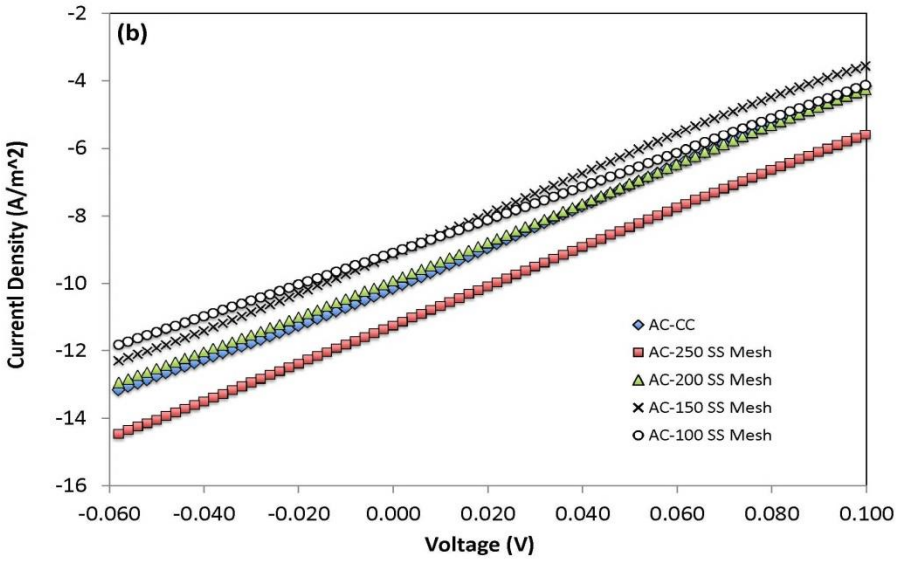

FIGURE 2.1: Current density as a function of voltage for the carbon cloth (CC) and stainless steel (SS) mesh activated carbon cloth cathodes (a) showing higher performance of CC cathode at more negative cathode operating potentials; and (b) close up of figure (a) showing the performance of CC and SS mesh cathodes over the typical cathode operating range. Samples were tested in triplicate.

2.3.2 Performance of Cathodes in MFCs

The MFC with the CC cathode achieved the highest power density of 1.72 ± 0.06 W m^{-2} over a period of 30 days (~30 batches) (Figure 2.2 & 2.3a). The maximum power density decreased with mesh size from 1.56 ± 0.06 W m^{-2}, for the SS-250 mesh cathode, to 1.28 ± 0.05 W m^{-2}, for the SS-110 mesh cathode. Furthermore, there was inconsistency between batches for all of the SS mesh samples (Figure 2.3b and c). Although decreasing slightly during the first 4 days, the CC cathode remained stable over more than 30 days of operation, even increasing slightly after 16 days of operation.

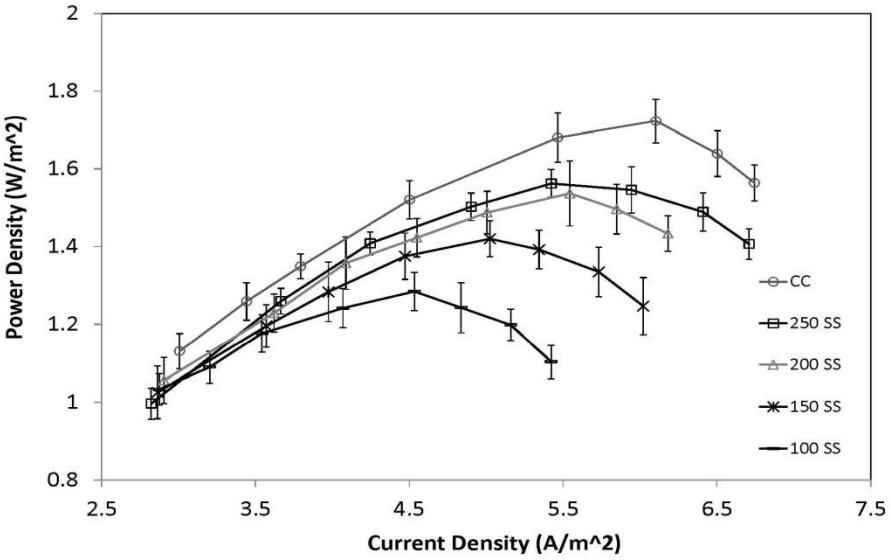

FIGURE 2.2: Polarization curves for MFCs containing activated carbon/carbon cloth and activated carbon/stainless steel mesh cathode

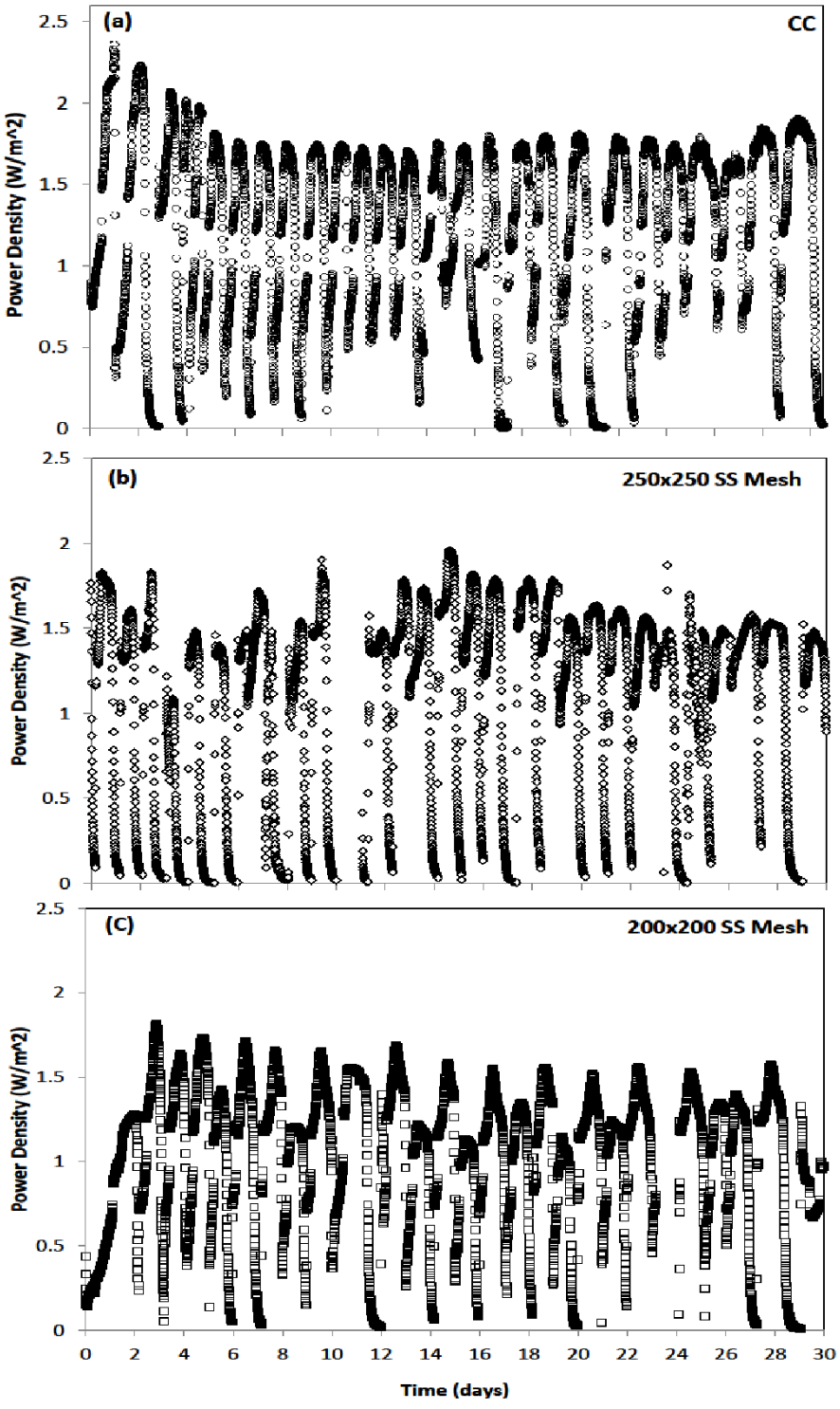
(a)
CC
(b)
250x250 SS Mesh
(C)
200x200 SS Mesh
Power Density (W/m^2)
Time (days)
0
0.5
1
1.5
2
2.5
0
2
4
6
8
10
12
14
16
18
20
22
24
26
28
30

FIGURE 2.3: Power density as a function of time for (a) activated carbon/carbon cloth cathode; (b) activated carbon/250 stainless steel mesh cathode; (c) activated carbon/200 stainless steel mesh.

2.3.3 Hydrostatic Pressure Tolerance of AC Cathodes

The static pressure head of cathodes was measured to determine pressure tolerance of different base material with AC catalyst coated using different procedure. When the catalyst was pasted onto the cathode base materials without pressing, all cathodes maintained high static pressure heads of 1.83 ± 0.05 m to 1.98 ± 0.03 m The SS mesh cathodes maintained static pressure heads 7.5 to 8.7% greater than that of the CC cathode (1.83 m) (Figure 2.4a). However, the catalyst on all un-pressed samples sloughed off upon removal from the testing device, indicating that the pasted catalyst could not stick to the based material without pressing. As a result, un-pressed samples were not evaluated in electrochemical cells and in MFCs. When the catalyst was pressed onto the cathode base material (at ~100 psi), there was a significant difference between the CC cathode and the SS mesh cathodes (Figure 2.4 b). The CC cathode maintained the highest static pressure at 1.83 ± 0.14 m. This result was 265 to 330% greater than that achieved by any of the SS mesh cathodes which all had average static pressure heads less than 0.5 m. In addition, there was greater variation in results between different samples of the same mesh type compared to that of carbon cloth, suggesting that the pressing procedure had a detrimental effect on sample homogeneity for cathodes with metal mesh based materials.

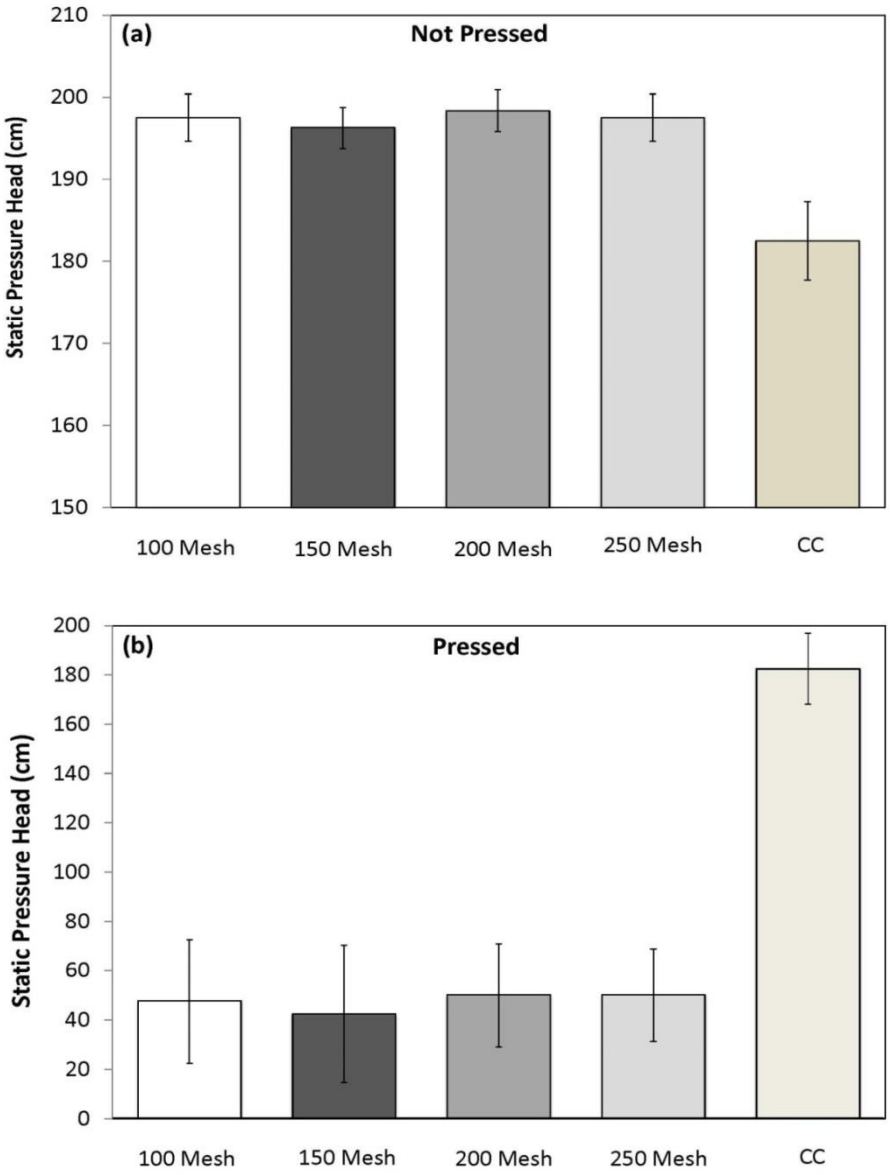

FIGURE 2.4: Static hydraulic pressure head for the carbon cloth and stainless steel mesh activated carbon cathodes (a) cathodes not pressed; and (b) cathode pressed at ~ 100 psi.

2.3.4 Corrosion and Salt Build-up

No corrosion or salt formation appeared on either side of the CC cathode after more than 30 days of operation in MFCs. For all of the stainless steel mesh cathodes, however, corrosion and salt formation began to appear on the outer surface (air facing side) of the cathode within 3-5 batches (Figure 2.5 a and b). The corrosion appeared both green and reddish-brown in color. Corrosion and salt formation on the exterior side of SS mesh cathodes increased with time and was more severe on the interior side for all SS mesh cathodes after 30 days operation (Figure 2.5a). Salt formation can occur under alkaline conditions when the solution leaks through the cathode surface and dries on the air facing side, forming a salt crystal build-up on the outer surface of the cathode [30,34]. Although no obvious leakage was observed on the SS cathode in this study, salt formation still occurred possibly due to micropore formation through the cathode surface from the pressing process.

(a) (b)

FIGURE 2.5: Photographs of stainless steel mesh cathodes showing (a) corrosion; and (b) salting out after operation in MFCs for 30 or more days.

2.4 DISCUSION

2.4.1 Performance of stainless steel cathodes with different mesh sizes

Comparing the different stainless steel mesh cathodes only, power production increased with finer mesh size and followed the trend predicted by the electrochemical performance shown from LSV experiments. Both electrochemical performance and power production could be correlated to higher specific surface area (Table 2). The surface area of metal mesh materials is dependant on wire diameter, opening size, percent open area, and number of openings per inch. The increased performance of the cathodes with finer mesh sizes compared to more coarse mesh sizes was possibly due to the greater available surface area for contact with the catalyst. In addition, the smaller wire diameter, resulting in a lower cathode thickness, may have allowed faster oxygen transfer rates into the catalyst compared to thicker cathodes with larger wire diameters. Similarly, greater number of openings per inch may have allowed for more even oxygen transfer compared to cathodes with fewer openings per inch and larger wire diameters.

TABLE 2: Comparison of cathode and base material characteristics

Sample	Mesh Opening Size (mm)	Fractional Open Area	Wire Diamter (mm)	Base Material Specific Surface Area (mm^{-1})	Cathode Thickness (mm)
SS-100	0.140	30%	0.114	12.4	0.40
SS-150	0.104	38%	0.066	18.6	0.30
SS-200	0.074	34%	0.053	24.7	0.30
SS-250	0.061	36%	0.041	30.9	0.25
CC	---	---	---	4452.7	0.60

The result for the stainless steel mesh cathodes obtained in this study is contradictory to that previously shown when several cathodes with different stainless steel mesh sizes, using platinum as the catalyst, were compared [101]. Such difference was possibly caused by the different mesh size selected, different cathode fabrication procedure, and different catalysts and loading. In the previous study, only more coarse mesh sizes ranging from 30x30 to 120x120 were examined. Platinum catalyst and Nafion ink was painted on the stainless steel base material at a loading of 0.5 mg cm^{-2}. Such a cathode preparation procedure likely limited the penetration of catalyst when the finer mesh cathodes with smaller opening sizes were used [101]. For the AC cathode in this study, the AC catalyst (17.5 mg cm^{-2}) formed a paste with PTFE and was pressed into the metal mesh, ensuring greater contact between catalyst and based material, resulting better performance with finer SS mesh.

2.4.2 Performance of carbon cloth cathodes compared to stainless steel

The electrochemical performance of the CC cathode was greater than, the stainless steel cathodes at mesh sizes of 100x100 - 200x200 openings per inch (Table

2). The much higher specific surface area may, at least in part, be the reason for this phenomenon. The specific surface area of the CC cathode was as much as 360 times greater than that of the SS mesh cathodes (Table 2). Higher surface area of the current collecting material allows for greater contact at the three-phase interface resulting in greater performance [42,45].

However, the SS-250 mesh outperformed the CC cathode by 10 to 40% over the typical operating range of 0 V to 0.1V, respectively, in electrochemical experiments. Greater overall cathode thickness may, in part, be the reason for the lower electrochemical performance of the CC cathode (Table 2) compared to the SS-250 mesh cathode. In addition, lower conductivity of the carbon cloth compared to the stainless steel mesh may also have contributed to lower overall electrochemical performance. This result suggests that there must be an appropriate balance of reactants for the oxygen reduction reaction (ORR) at the three-phase interface created by the physical and chemical characteristics of the base material, catalyst, and diffusion layer. For example, increasing available contact surface area beyond a certain point will not necessarily increase performance unless all reactants needed for the ORR are present in sufficient amounts.

Despite the lower electrochemical performance, the CC cathode achieved the highest power density during operation in MFCs, reaching 10 to 34% greater than all other cathodes tested. This result does not correlate with the results shown from electrochemical experiments, which indicated that the SS-250 mesh would out perform all other cathodes. The lower than expected performance of both these SS mesh cathodes is likely due to corrosion of the metal base material and salt formation

on the air facing side of the cathode [34,56]. When compared to many other AC cathodes reported in the literature, the result obtained here for the CC cathode was greater than other AC cathodes [38,40,43].

2.4.3 Stability of cathodes operating in MFCs

Severe corrosion was observed on all stainless steel cathodes after 30 days of operation (Figure 5a). Corrosion of the metal base material increases internal resistance, which ultimately decreases performance and affects the stability of MFC performance. Corrosion of stainless steel can occur whenever water, oxygen, and electrolyte are present. Initially, depassivation of the stainless steel may occur as a result of a low oxygen environment. Dissolution of iron into solution occurs releasing Fe^{2+} and Fe^{3+} ions and electrons. The electrons combine with oxygen and hydrogen ions to form water. Both Fe^{2+} and Fe^{3+} ions can react with hydroxide ions to form insoluble iron hydroxides, which appear reddish brown or green depending on the iron hydroxide formed. This process likely began during start-up of the MFCs when excess electrons from the anode are not available to prevent to the oxidation of iron in the stainless steel cathode. In addition, corrosion can be exacerbated in low oxygen environments if the passive chromium oxide layer is damaged, preventing repair of the passive layer, exposing the iron beneath. The pressing process used to fix the catalyst layer to the surface of the stainless steel mesh could have damaged the passive layer of the stainless steel mesh. This damage in combination with a low oxygen environment could have contributed to the start of the corrosion. Once exposed to higher oxygen and electrolyte concentrations in the MFC during start-up,

corrosion could have been accelerated. As start-up progresses the hydroxide ion concentration at the cathode increases. The presence of excess hydroxide ions likely contributed to further corrosion even after start-up is complete.

In addition, during operation and subsequent alkalinization of the test solution, formation of salt through the cathode surface was noticed after only a few days of operation for all stainless steel mesh cathodes (Figure 2.5 b). Salt formation likely occurred as a result of damage to the diffusion layer caused by the pressing process and further enhanced with increased corrosion of the stainless steel base material. The diffusion layer acts to facilitate diffusion of air into the cathode while reducing water loss through the cathode at the same time. During the pressing process micropores may have been created, which resulted in pathways for the solution to move through the cathode to the air facing side. Salt formation has been shown to decrease performance and it has been suggested that increased internal resistance due to decreased contact of the catalyst with reactants was the cause of the decreased performance [30,34].

In many recent studies on metal based AC cathodes for use in MFCs, the phenomenon of corrosion and salt formation were not reported [38,42,43,52]. While it's not clear if these phenomena are unique to this study, aspects of the cathode fabrication procedure, such as the pressure applied to fasten the AC catalyst onto the base material and the order, wire diameter of stainless steel mesh, and thickness of the diffusion layers applied to the base material, may affect the occurrence or intensity of these phenomena. The results presented here highlight the potential for corrosion and salt formation when metal base materials are used in MFCs.

The carbon cloth cathodes, on the other hand, did not show the corrosion and salt formation issues during the period of operation. A possible reason for this fact is that the pressing process did not damage the water proofing function of the diffusion layer. As a result water could not leak through the cathode to the air facing side. Carbon cloth materials are known for their chemical stability. Carbon fiber based materials also have more compressibility, flexibility, elasticity, and a higher surface area than metal based electrode base materials. Although electrical properties of carbon cloth can be improved through raw material selection and the carbon fiber formation process, lowering the cost of carbon cloth while maintaining high conductivity would be a key challenge for large-scale manufacture and assembly of MFCs for practical uses.

2.5 CONCLUSIONS

Cathode materials with high performance and stability are crucial for many applications of MFCs. This study shows that although stainless steel mesh based AC cathodes, especially at finer sizes, can demonstrate good electrochemical performance according to LSV testing, the potential for corrosion and salt build-up exists, especially when pressure is applied to fix the AC catalyst on the base material. Corrosion and salt build-up can reduce the stability and performance of MFCs for long-term operation. Carbon cloth-based AC cathodes demonstrate higher stability (no corrosion and salt build-up issues were observed) than stainless steel based cathodes, while maintaining excellent performance in MFCs. Optimization of the AC

catalyst type/loading and diffusion layer loading as well as using more conductive carbon fiber based materials will likely increase performance further.

3. High Power Generation and Pressure Tolerance of Activated Carbon/Carbon Cloth Cathodes for Microbial Fuel Cells

Anthony Janicek, Ningshengjie Gao, Yanzhen Fan, and Hong Liu

ABSTRACT

Replacing precious metal catalysts by inexpensive activated carbon (AC) is a breakthrough in microbial fuel cell (MFC) cathode fabrication. In this study, AC powders made from bamboo, peat, coal, coconut, and hardwood sources are evaluated in terms of their electrochemical performance with carbon cloth as the base material. These ACs are also characterized in terms of their surface area, pore size distribution, surface chemistry, and conductivity to better understand the linkages between their electrochemical performance and physical and chemical properties. The bamboo-based AC demonstrates the highest potential for use as a catalyst for carbon cloth based cathode, reaching -10.6 A m^{-2} and 11.27 A m^{-2} at 0V with loading of 25mg cm^{-2} and 50mg cm^{-2}, respectively. The maximum power density reached 3.3 Wm^{-2} in CEA-MFCs and 2.6 Wm^{-2} in cube-MFCs, respectively. The high performance of the bamboo-based AC cathode was possible due to the base material used and the conductivity and surface pH of the bamboo-based AC catalyst. The hydrostatic pressure tolerance of the bamboo-based AC carbon cloth cathode is greater than 1.8 m, allowing for a more versatile cathode, suitable for use in many different reactor design configurations. These results demonstrate that activated carbon/carbon cloth cathodes are capable of achieving high performance with very low potential for corrosion, making them suitable for many MFC applications.

3.1 INTRODUCTION

There is a significant amount of energy stored in the organic matter of wastewater. Microbial fuel cell (MFC) technology has the potential to harvest this stored energy and clean wastewater simultaneously. Currently, many MFC reactor configurations are limited by cathode performance and cost for full scale applications [15,32,48,104]. Development of high performing cost-effective cathodes is crucial for realizing the practical application of MFC for wastewater treatment. Among the many improvements made in cathode fabrication, replacing precious metal catalysts such as platinum by inexpensive activated carbon (AC) is a breakthrough since it can potentially reduce cathode cost by nearly 98% [37–43,53]. Performance of activated carbon cathodes is determined by the cathode base material based material and properties of activated carbon catalyst. [38,39,43,55,105].

The base materials that have been investigated for activated carbon cathodes have mainly focused on metal-based materials, such as stainless steel mesh [37,38,45,52,106], nickel mesh [39,40], and nickel foam [42]. Although metal based materials typically have good conductivity, mechanical strength and low cost, recent studies have shown that corrosion of metal base materials can occur when used as cathodes in MFCs, which can significantly affect the electrochemical performance and stability [54,56,106]. Carbon-based materials have been used as cathode base materials in chemical fuel cells [107,108] and are widely used for platinum catalyzed cathodes in MFCs [14,32,36,72,102] due to their high chemical and electrochemical stability and large surface area. Our recent study has demonstrated that a carbon cloth/activated carbon cathode MFC can outperform stainless steel mesh cathodes by

as much as 34% in terms of power density when tested in MFCs, with high stability over a period of one month of operation [106]. However, the performance of the carbon cloth/activated carbon cathode is not optimized with respect to different types and loading of activated carbons. The linkages between the physical and chemical properties of activated carbon and their electrochemical performance with carbon cloth as base material were not well-understood either. In addition, the performance in cloth electrode assembly (CEA)-MFCs, an MFC configuration that demonstrates a great potential for power output, using the activated carbon/carbon cloth cathode was also not investigated.

In this study, six activated carbon powders derived from different sources were investigated as catalysts for carbon cloth cathodes (AC-CC). Activated carbon powders made from bamboo, peat, coal, coconut, and hardwood were characterized in terms of their surface area, pore size distribution, surface chemistry, and conductivity to better understand the linkages between the physical properties of AC and their performance with carbon cloth as the base material. Due to the higher electrochemical performance of the bamboo based AC compared to other ACs tested, the loading of the bamboo based activated carbon on carbon cloth was further optimized and then examined for hydrostatic pressure tolerance. The performance in CEA-MFCs with the optimized bamboo AC cathode was also evaluated and compared with performance in cube-MFCs and the subsequent impact of cathode biofilm on cathode performance was also evaluated. The high performance of CEA-MFCs in this study demonstrates the great potential of the selected activated carbon/carbon cloth cathode as well as the CEA-MFC configuration.

3.2 MATERIALS & METHODS

3.2.1 Cathode Fabrication

Carbon cloth (CCP, fuelcellearth.com) was used as the base material of the cathodes. Six types of AC used as the catalyst for the cathode include: coconut shell based AC, bamboo based AC, hardwood based AC, bituminous coal based AC, acid washed peat based AC, and steam activated peat based AC (buyactivatedcharcoal.com). Each type of AC was mixed with ethanol (99%) at a ratio of 1 g AC to 5 ml ethanol for 15 minutes. PTFE (60 wt%) was then added to the mixture at a mass ratio of 3:1 (AC to PTFE) and heated at 50 °C until a slurry was formed. The slurry was then applied evenly to the solution facing side of the carbon cloth cathode at a loading of 18.8 mg cm^{-2}, air-dried overnight, and pressed at ~200 psi. The other side of the carbon cloth, the air facing side, was prepared by applying diffusion layers as previously reported [102]. For comparing activated carbon loading, cathodes were prepared by combining bamboo based AC with carbon black (xc-72r) at a mass ratio of 9:1 and mixing with ethanol as stated above. The mass loadings of AC were as follows: 12.5, 18.8, 25, and 50 mg cm^{-2}. The cathodes in other experiments were fabricated using the same procedure with a bamboo based AC loading of 25 mg cm^{-2}.

3.2.2 Characterization of Activated Carbon

The total surface area, as well as meso- and micorpore cumulative pore surface area and pore volume distributions of activated carbon were determined using

an accelerated surface area and porosimetry system (ASAP 2020, Micrometrics). Micropores and mesopores were defined according to the International Union of Pure and Applied Chemistry (IUPAC) convention as less than 2 nanometers and between 2 and 50 nanometers, respectively. Nitrogen adsorption isotherms were generated by increasing relative pressure from 10-7 to 0.99 atm atm^{-1}. Total surface area was calculated from the isotherms using the Brunauer-Emmett-Teller (BET) method while meso- and micropore surface area and pore volume distributions were determined using Density Functional Theory (DFT) modeling software (Micrometrics). Although the BET method is not as accurate as other methods for determining the contribution of micropore surface area in the total surface area, it is widely used as a reliable means to compare total surface area of multiple samples [109–111]. Furthermore, the theoretical accuracy of any gas adsorption analysis technique for determining pore size distributions for pores wider than 50 nm diminishes with increasing pore width [111,112]. As a result, the characterization of surface and pore properties of activated carbons focused on total surface area determined using BET and meso/micropore distributions determined using DFT. Relative conductivity of all ACs was determined by placing 0.8 grams of AC inside a plastic cylindrical tube with brass bolts at both ends then measuring the resistance between the bolts. The same torque was applied to the bolts for each measurement to allow for an appropriate comparison. Measurements were repeated four times to ensure repeatability. Carbon surface pH was determined as previously described by soaking 0.45 g of each AC powder in 20 ml of deionized water and stirring for 16 hours [54,113]. The elemental surface composition of the AC powders was analyzed at CAMCOR (University of

Oregon, US) by X-ray photoelectron spectroscopy (ThermoScientific ESCALAB 250 X-ray Photoelectron Spectrometer, US).

3.2.3 Electrochemical Analysis

Cathodes were characterized using linear sweep voltammetry (LSV) with a potentiostat (G300, Gamery Instruments, Inc.) in a three-electrode electrochemical test cell. The test cell consisted of a cylindrical single-chamber (3 cm in diameter and 2 cm in length) with the working electrode (cathode with area equal to 0.7 cm^2) placed at one end of the chamber and the counter electrode (anode) placed at the other end. An Ag/AgCl reference electrode (MF-2052 RE-5B, Bioanalytical Systems, USA) was placed in a 200 μl pipet tip which was modified by heating and bending so that the tip faced the working electrode. A square piece of platinum foil (2.12 × 2.12 cm^2) was used as the counter electrode. Tests were conducted in a medium solution containing the following (per liter): KCl, 0.13 g; NH_4Cl, 0.31 g; $NaH_2PO_4*H_2O$, 2.92 g; and $Na_2HPO_4*7H_2O$, 7.735 g. LSV experiments were conducted by varying potential from either +300 to -400 (for LSV of different types of AC only) or +300 mV to -200 mV at a scan rate 0.1 mV s^{-1}. .

3.2.4 Pressure Tests

Pressure tolerance of cathodes was determined by measuring the static pressure head using a testing device, which consisted of a test piece holder constructed from PVC piping with a 2.5 m tube attached to it. The device was filled

with growth medium solution prepared as described above. It was previously determined that cathodes prepared using the same procedure held an average static pressure head of 180 cm [106]. As a result, 160 cm was used as the starting point for the static pressure tests. Starting at 160 cm the tubing was raised in 5 cm increments above the test piece holder and left to stand overnight. Tests were ended when medium solution leaked through the cathode. The pressure tolerance was recorded as the static head measurement prior to height at which leaking occurred. The average and standard deviation of 3 to 4 cathodes was reported for each test condition. Static pressure head of the AC-CC cathode only (designated New AC-CC), with the separator material (designated as New AC-CC-sep), and without activated carbon (carbon cloth with diffusion layers only, designated as New CC-only) were also measured to determine the effect of the catalyst and separator on pressure tolerance. Pressure tolerance of used cathodes (designated as Used-AC-CC) was also measured to determine if tolerance decreased over time with use.

3.2.5 MFC Construction & Operation

Cube-MFCs and CEA-MFCs were used to determine the newly developed cathode on the performance of MFC with different configurations. Both types of MFCs were constructed as previously described [14] with an empty bed volume ~ 12 ml. For both cube-MFCs and CEA-MFCs, carbon cloth (CCP, fuelcellearth.com) was used as the anode material while bamboo-based AC with a loading of 25mg/l was added to the carbon cloth and used as the cathode. Separator material used in the CEA-MFCs was as previously described [36]. All data for cathodes presented in this

study was obtained by placing new cathodes into fully operational cube-MFCs and CEA-MFCs, which were originally inoculated as previously described [36]. Tests were conducted in batch mode until stable power output was observed, typically 5 to 6 batches. The same medium solution used in electrochemical analysis was used with 5.9 g/L of acetate added. Polarization curves and Coulombic efficiency were determined as previously described [103]. All experiments were conducted in duplicate or triplicate.

3.3 RESULTS

3.3.1 Effect of Activated Carbon Type on Cathode Perfromance

Among the various types of ACs, the bamboo based AC cathode maintained the highest electrochemical performance over the typical cathode operating range of 0.1V to 0V while the hardwood based cathode demonstrated the lowest performance (Figure 3.1). The current density for the bamboo based AC at a cathode operating potential of 0.1 V was -3.4 A m^{-2}, which was similar to the that of both the peat and coal based AC. However, at a cathode operating potential of 0V, the current density of the bamboo based AC (-8.17 A m^{-2}) was 10 to 16% higher than the peat (-7.42 A m^{-2}) and coal (-7.0 A m^{-2}) based ACs, respectively. Similarly, the bamboo based AC was as much as 1200 to 1600% greater than the remaining ACs tested over the typical cathode operating range. Furthermore, at cathode operating potentials lower than -0.1V, the bamboo based AC was reached current densities 12 to 1500% greater than all other ACs tested.

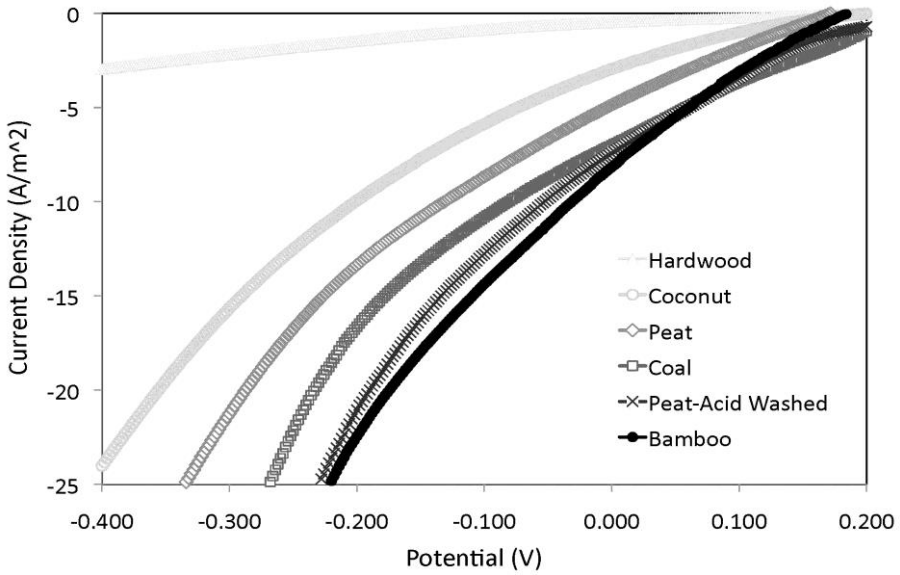

FIGURE 3.1: Current density as a function of time for carbon cloth cathodes containing activated carbon made from different source material. All curves in the figure represent the average of 3 scans with a scanning rate of 0.1 mV/s.

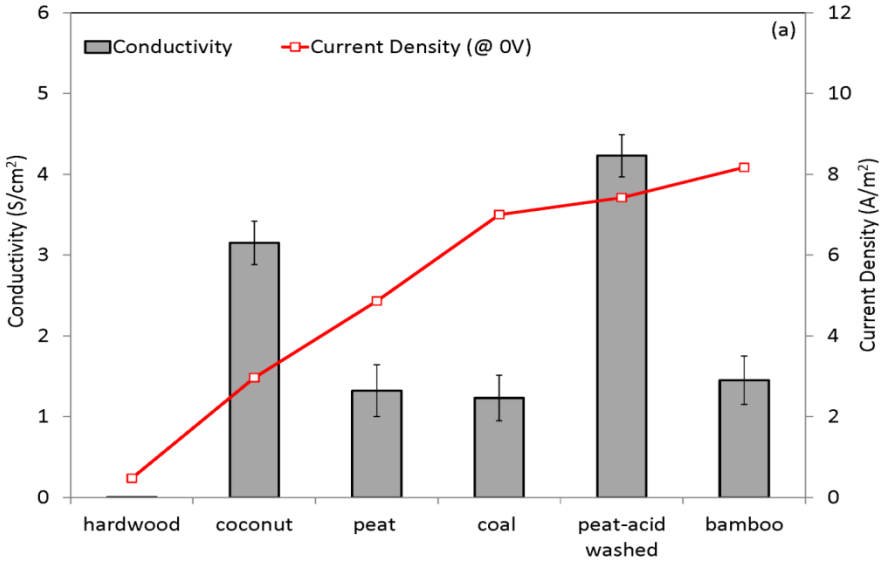

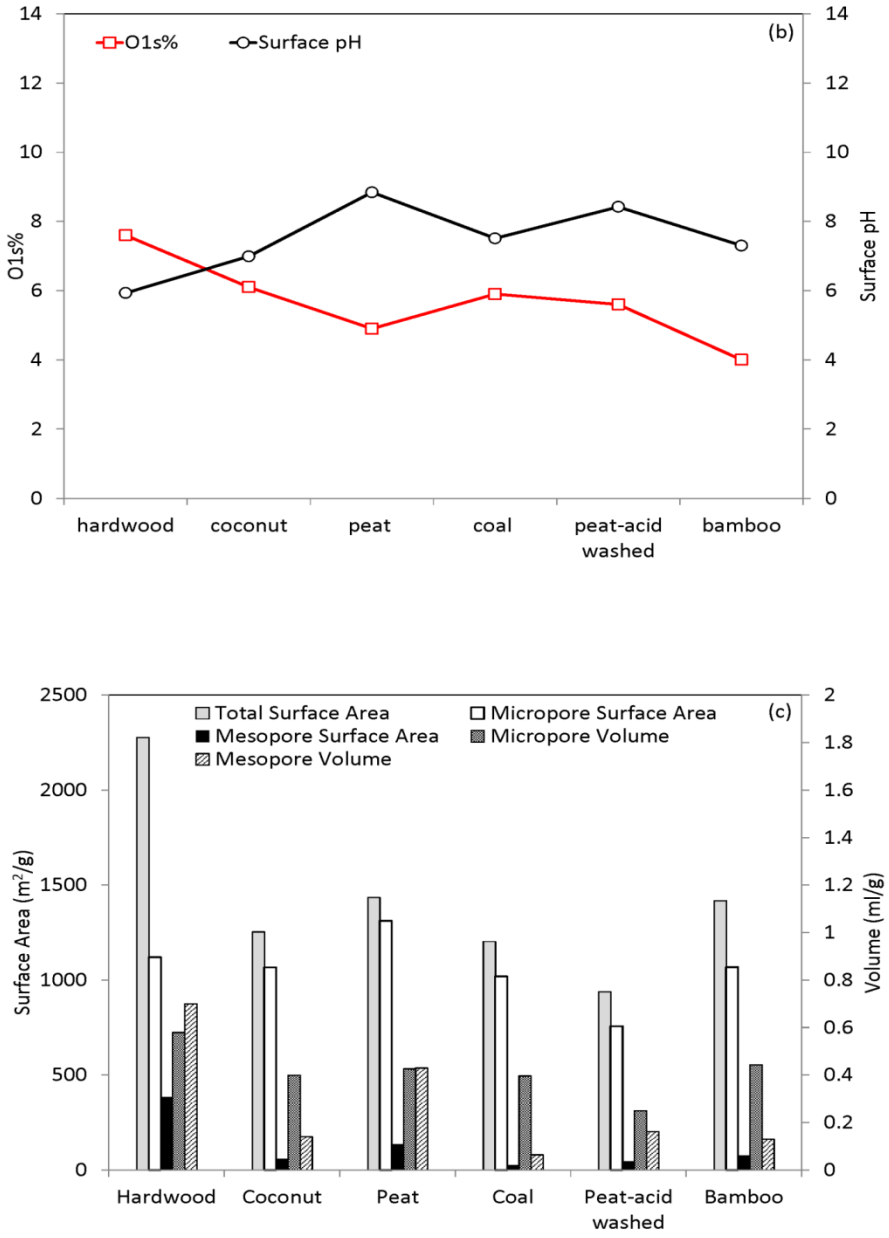

FIGURE 3.2: (a) Conductivity and current density; (b) %O1s content and surface pH; (c) total surface area, meso- and micropore surface area, and meso- and micropore volume for activated carbons made from coconut, bamboo, hardwood, peat (acid washed), peat, and bituminous coal

3.3.2 Characterization of Activated Carbon

Conductivity for all ACs was the same order of magnitude, ranging from 1.23 ±0.06 to 4.23 ±0.39 S cm^{-1}, except for the hardwood based AC which had a conductivity several orders of magnitude lower (5.7×10^{-6} S cm^{-1}). The hardwood-based AC had the lowest electrochemical performance (Figure 3.2a). Surface pH of the different ACs ranged from 5.93 for the Hardwood based AC to 8.84 for the Peat based AC (Figure 3.2b). The oxygen contents ranged from 4.2 (bamboo-based AC) to 8.3% (hardwood-based AC) with the rest as carbon, no nitrogen was detected on the surface of ACs. Total surface area of AC powders ranged from 939 m^2 g^{-1} for the peat based AC to 2276 m^2 g^{-1} for the hardwood based AC (Figure 3.2a). All samples contained a much higher percentage of micropores (< 2 nm) compared to mesopores (between 2 nm and 50 nm) (Figure 3.2b). Similarly, all samples contained higher pore volume attributable to micorpores with the exception of the hardwood based AC (Figure 2c).

3.3.3 Loading of bamboo based activated carbon on cathode performance

Due to the highest performance of bamboo based active carbon cathode in previous testing, the effect of its loading on the electrochemical performance of the cathode was further evaluated. Over the typical cathode operating range of 0V to 0.1V, doubling the loading from 12.5 to 25 mg cm^{-2} increased performance as much as 50% from -3.57 A m^{-2} at 0.1V and -7.6 A m^{-2} at 0V to -5.32 and -10.6 A m^{-2} over the same operating range (Figure 3.3). However, further doubling the loading from

25 to 50 mg cm^{-2} only increased performance 6 to 12% over the same operating range to -5.97 to -11.27 A m^{-2}, respectively.

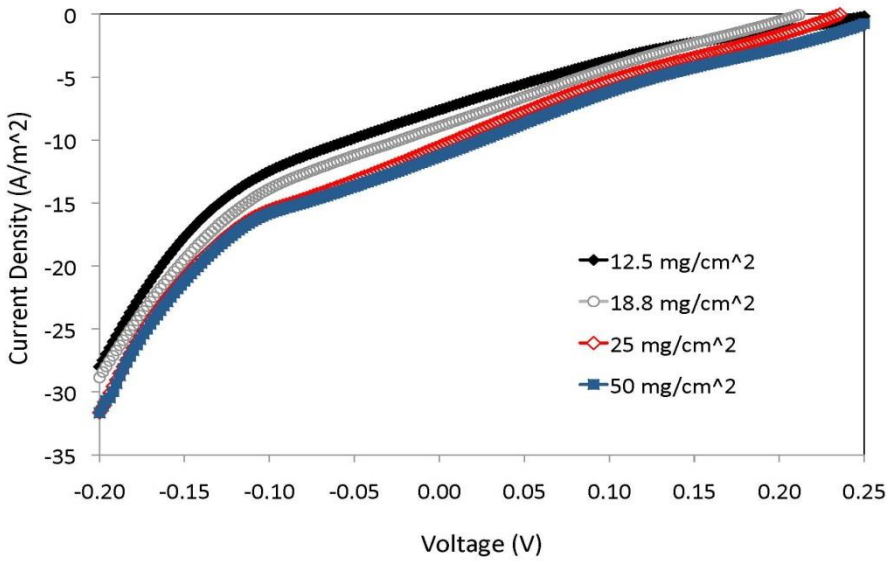

FIGURE 3.3: Current density as a function of time for carbon cloth cathodes with bamboo AC as catalyst at different loadings. All curves in the figure represent the average of 3 scans with a scanning rate of 0.1 mV/s.

3.3.4 Hydrostatic Pressure Tolerance of carbon cloth AC cathodes

The high pressure tolerance of the AC-CC cathodes allows for a more versatile cathode, suitable for use in different reactor design configurations. For example, high pressure tolerance has the most significant implications for use in vertically oriented reactor designs in which the cathode is subjected to high pressures. The new bamboo-based activated carbon/carbon cloth (AC-CC) cathode held an average of 183±14 cm (Figure 3.4). Adding a layer of separator material or an activated carbon layer did not affect the static pressure of the cathode, indicating that it's the PTFE gas diffusion layers that determined the pressure tolerance of the carbon cloth cathode material. The static pressure head of the used cathodes that operated in CEA-MFCs for over two months, maintained similar to that of the new AC-CC cathodes, suggesting the stability of the PTFE layers on the cathode.

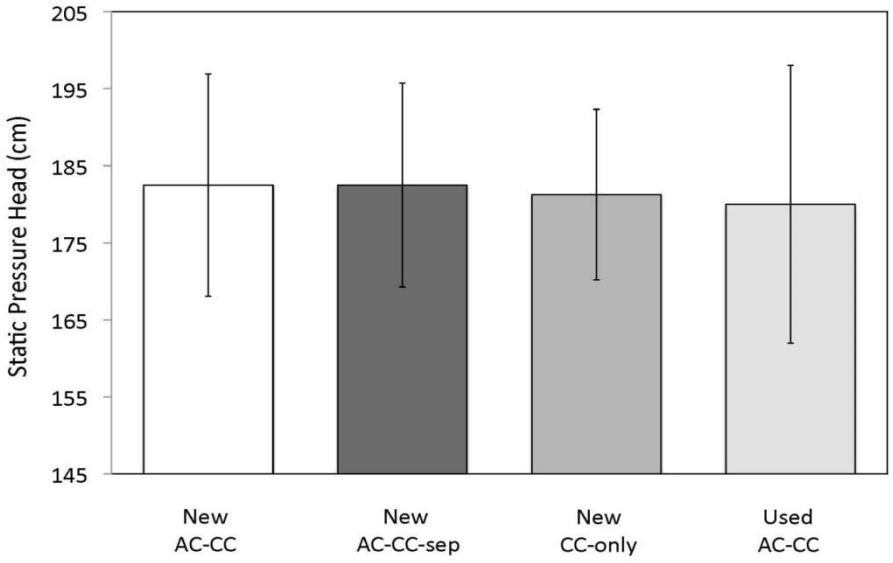

FIGURE 3.4: Static pressure head of the activated carbon/carbon cloth cathode. Sample designations are as follows: new activated carbon/carbon cloth cathode (New AC-CC), new cathode with separator material (New AC-CC-sep), new cathode with diffusion layers only (no catalyst, designated as New CC-only), used cathode after 2 months of operation (Used AC-CC), and new cathode with platinum as the catalyst (New Pt-CC). Three sample pieces were analyzed and averaged to obtain the result

3.3.5 Performance of MFCs with bamboo-based AC carbon cloth cathodes

The cube-MFCs generated an average maximum power density of 2.6 Wm^{-2} (based on polarization curves) within the first 5 batches (Figure 3.5). Power density then gradually decreased over time and stabilized at 2.2 W m^{-2} approximately sixteen batches after start-up. Coulombic efficiencies for the cube-MFCs ranged from 22 to 35%.

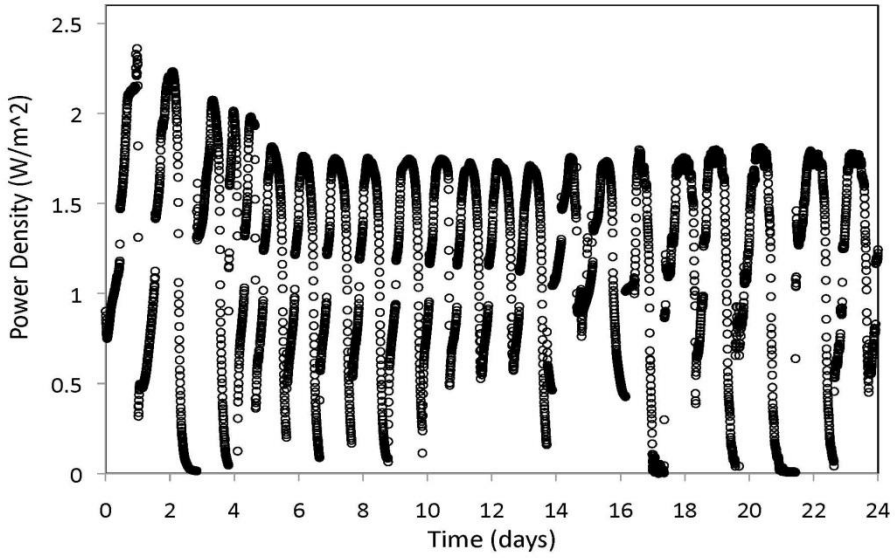

FIGURE 3.5: Power density as a function of time for cube-MFCs

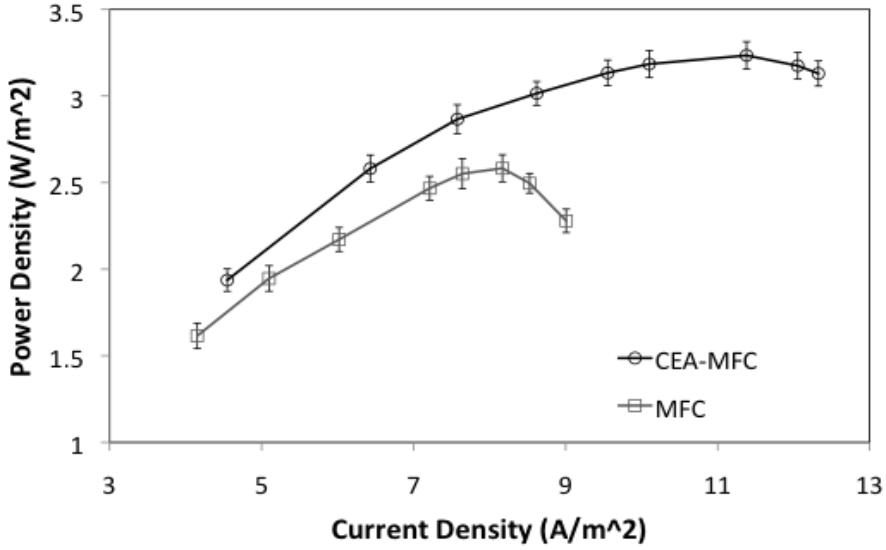

FIGURE 3.6: Polarization curves for the MFCs and CEA-MFCs

3.3.6 Performance of CEA-MFCs with bamboo-based AC carbon cloth cathode

The maximum power density of CEA-MFCs reached as high as 3.3 W m^{-2} at a current density of 10.4 A m^{-2} several batches after start-up in the CEA-MFCs (Figure

3.6). Then power density gradually decreased to a stable value corresponding to 2.9 W m^{-2} within 16 days of operation and remained stable for the duration of the experiments. Coulombic efficiencies for CEA-MFCs ranged from 61 to 78%.

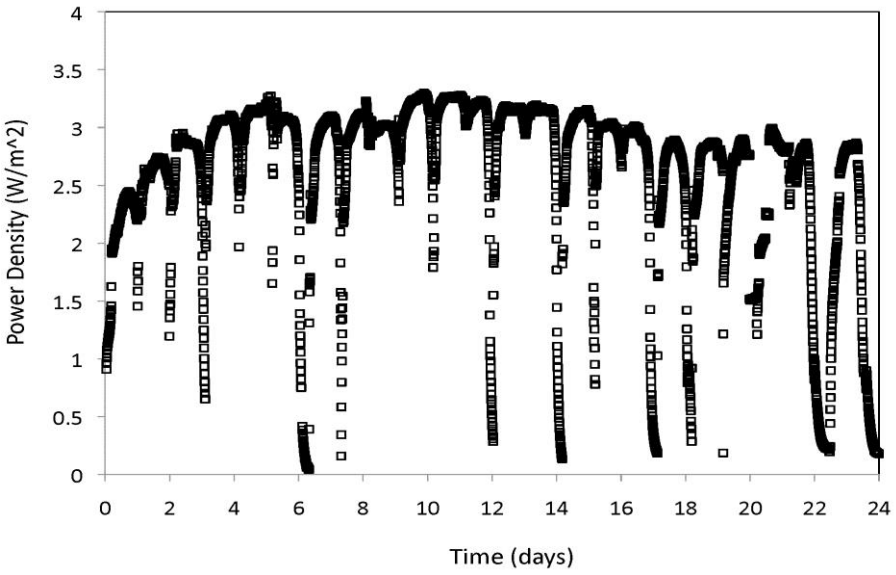

FIGURE 3.7: Power density as a function of time for the CEA-MFC

3.3.7 Cathode performance in the presence of biofilms

To understand the reasons causing the decrease of the MFCs performance, the electrochemical performance of MFC cathodes with biofilms was further evaluated. The used cathodes that had been operating in MFCs for more than 2 months showed an 11.8% and 21.6% decrease in performance at 0.1V and 0V, respectively, compared to new cathodes (Figure 3.7a and b). When the biofilm was removed from the used cathodes, the performance only slightly recovered, increased 2.7% and 3.1% at 0.1V and 0 V, respectively.

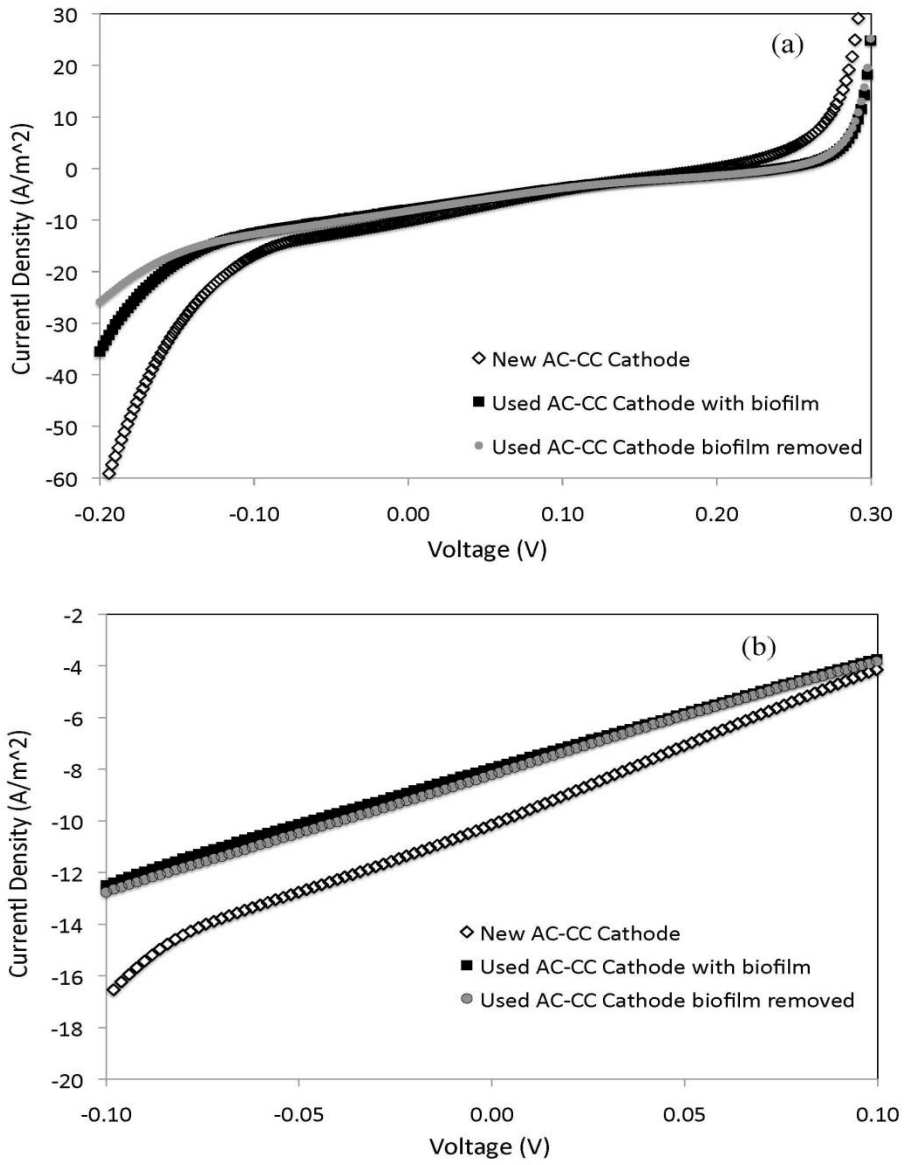

FIGURE 3.8:Current density as a function of voltage for new and used cathodes (a) full LSV scan; and (b) close-up view of the LSV curve highlighting the cathode operating range of -0.1 V to 0.1 V

3.4 DISCUSSION

Compared to cathodes using different base materials and AC source materials with no chemical modification, the current density of the activated carbon/carbon cloth (AC-CC) cathode was as much as 400% greater than that for cathodes using

nickel mesh or stainless steel as the base material and as much as 45% greater than cathodes using nickel foam at the typical cathode potential operating range of 0 V to 0.1 V (Table 3). In addition, the performance of the AC-CC cathode at lower cathode operating potentials was significantly better than all other cathodes listed in Table 3. For example, at a cathode operating potential of -0.2 V, the current density of the AC-CC cathode was more than 600% greater than all other cathodes. These results suggest that the AC-CC cathode performed significantly better than other activated carbon cathodes at higher current densities. While most MFC configurations typically do not operate at current densities greater than 10 A m^{-2}, improvements in MFC architecture have resulted in MFCs operating at higher current densities for certain configurations [36]. As a result, performance at higher current densities will become more important as advances are made to MFC architecture and biofilm performance. Furthermore, it is likely that the results described in this study are more conservative than some of the results presented in Table 3 that were obtained at higher scan rates and/or higher temperatures. Factors such as temperature, scan rate, working electrode area, number of scans, and reference placement can affect the LSV curve [114], exaggerating results.

TABLE 3: Electrochemical test comparison of activated carbon/carbon cloth cathode with different types of activated carbon metal mesh/metal foam cathodes reported in the literature

Cathode Material	Current Density at -0.2 V ($A\ m^{-2}$)	Current Density at 0V ($A\ m^{-2}$)	Current Density at 0.1V ($A\ m^{-2}$)	Temp (°C)	Working Electrode Area (cm^2)	Scan Rate (mV/s)	# of scans per sample	Reference
Carbon Cloth	64.5	10.15	4.15	22.6±0.9	0.7	0.1	3	This study
Nickle Mesh	~ 9	~5	~3.9	30	7	1	––	[7]
Stainless Steel[]	8.7	~2	~0.9	30	7	––	––	[5]
Stainless Steel	~11	~6	~3.5	30	7	0.1	––	[12]
Stainless Steel[]	~ 10	~5	~3	30	7	––	––	[10]
Nickle Foam	~ 12	~7	~3	30	7	1	3	[9]

[]Results based on chronoamperometry

There are several reasons that may contribute to the high performance of the cathodes developed in this study: the properties of AC selected, the AC loading, and the carbon cloth base material. Conductivity of AC has not been previously reported for ACs used as a catalyst in MFC cathodes. Results presented here show that conductivity is an important characteristic of the catalyst layer for determining high performance. Although an increase of conductivity from 1.23 to 4.23 S cm^{-1} does not respond to current density increases (Figure 3.2a), it is clear that ACs with very low conductivity, as with the hardwood based AC, will have much lower performance than ACs with higher conductivity. One recent study, in which cathode performance was increased significantly through the addition of conductive carbon black to the AC catalyst layer, supports this conclusion [38].

Differences in activated carbon performance as a catalyst for oxygen reduction may also be attributed to surface pH and functional groups. In general, there is an inverse relationship between surface pH and oxygen content, likely due to the presence of oxygen-containing acidic functional groups. Although the surface pH of most of the ACs tested in this study were in the range of 7.0-8.8, the low surface pH (5.9) of hardwood-based AC could be, in part, the reason for the much lower electrochemical performance as the presence of strong acid functional groups have been shown to be detrimental to the activity of the AC for ORR [44]. It has also been shown that higher performance in MFCs was attributable to the presence of nitrogen containing surface functional groups on the surface of ACs [44,53,115]. However, XPS analysis of the ACs examined here showed no nitrogen content on the surface of any ACs.

Surface area and volume have been considered key properties that affect the AC cathode performance [44] . Characterization of different ACs in this study, however, did not show direct correlation between increased electrochemical performance and total surface area, pore surface area, or pore volume. This result is contradictory to that previously reported [44] in which a strong inverse relationship was shown to exist between total surface area and performance. It was also suggested that ACs containing surface area and volume attributable to a moderate percentage of microporous structure should be selected as catalysts for MFC cathodes. However, the results of another recent study showed that an abundant micropore structure was more important than the abundance of mesopore structure for increasing ORR catalytic activity [45]. Our results and these conflicting results suggest that

performance of AC powders, as catalysts for MFC cathodes, cannot be predicted by a single physical or chemical property alone.

The electrochemical performance of cathodes increased significantly with increased bamboo AC loading from 12.5 to 25 mg cm^{-2}. Further increasing the loading from 25 to 50 mg cm^{-2} only increased performance by 6-12% over the typical cathode operating range of 0V to 0.1V, likely due to proton and oxygen mass transfer limitations resulting from the thicker catalyst layer [42,43]. The optimal loading of 25 mg cm^{-2} used for the AC-CC cathode in this study is 41% to 75% lower than the loadings used for metal mesh activated carbon cathodes [38,40,43,53].

The carbon cloth used in this study may also lead to the better performance of the cathode. A conservative estimate of the surface area of carbon cloth can be more than 125% greater than metal mesh base materials (Figure 3.9). The increased surface area provides greater contact at the interface of the three phases, which may ultimately decrease ohmic resistance [42]. Also, pressing the catalyst onto the carbon cloth in this study may provide better contact between conductive carbon black, activated carbon particles, and carbon cloth, further reducing ohmic resistance. It is also likely that mass transfer at the three-phase interface of oxygen and protons is increased as a result of the small fiber diameter and increased contact of the three phases compared to metal mesh cathodes (Figure 3.10). The larger wire diameter of the metal mesh may work to limit mass transfer while the increased open area results in decreased contact between the three phases and larger ohmic resistance.

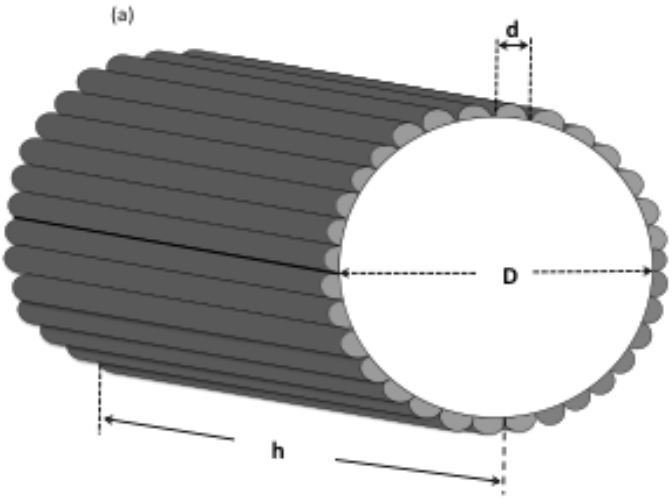

Single Carbon Fiber Yarn:

$$\frac{S_{Eff}}{S_{Geometric}} = \frac{(1/2_i \pi d_i)(1/2_e \pi D)h}{d_f h_t} = 2.4\ 6$$

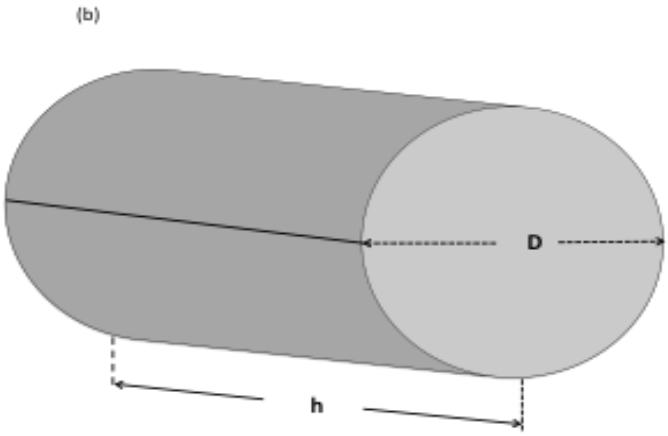

Single Metal Mesh Wire:

$$\frac{S_{EA_f}}{S_{GA_{eometric}}} \times (1^{e} - \%O^{t}p^{i}e) = \frac{1/2\pi D h}{D h} \times (0.3) = 1.0$$

FIGURE 3.9: Estimate of surface area of (a) one single yarn from carbon cloth; and (b) one single metal mesh wire. It was assumed that the carbon cloth yarn was cylindrical and that the surface area for contact was half an individual carbon fiber. In reality the carbon fiber yarn shape will not be cylindrical and more carbon fibers will likely be contacted than just one-half of the outer most fibers. As a result, the value calculated is a conservative estimate.

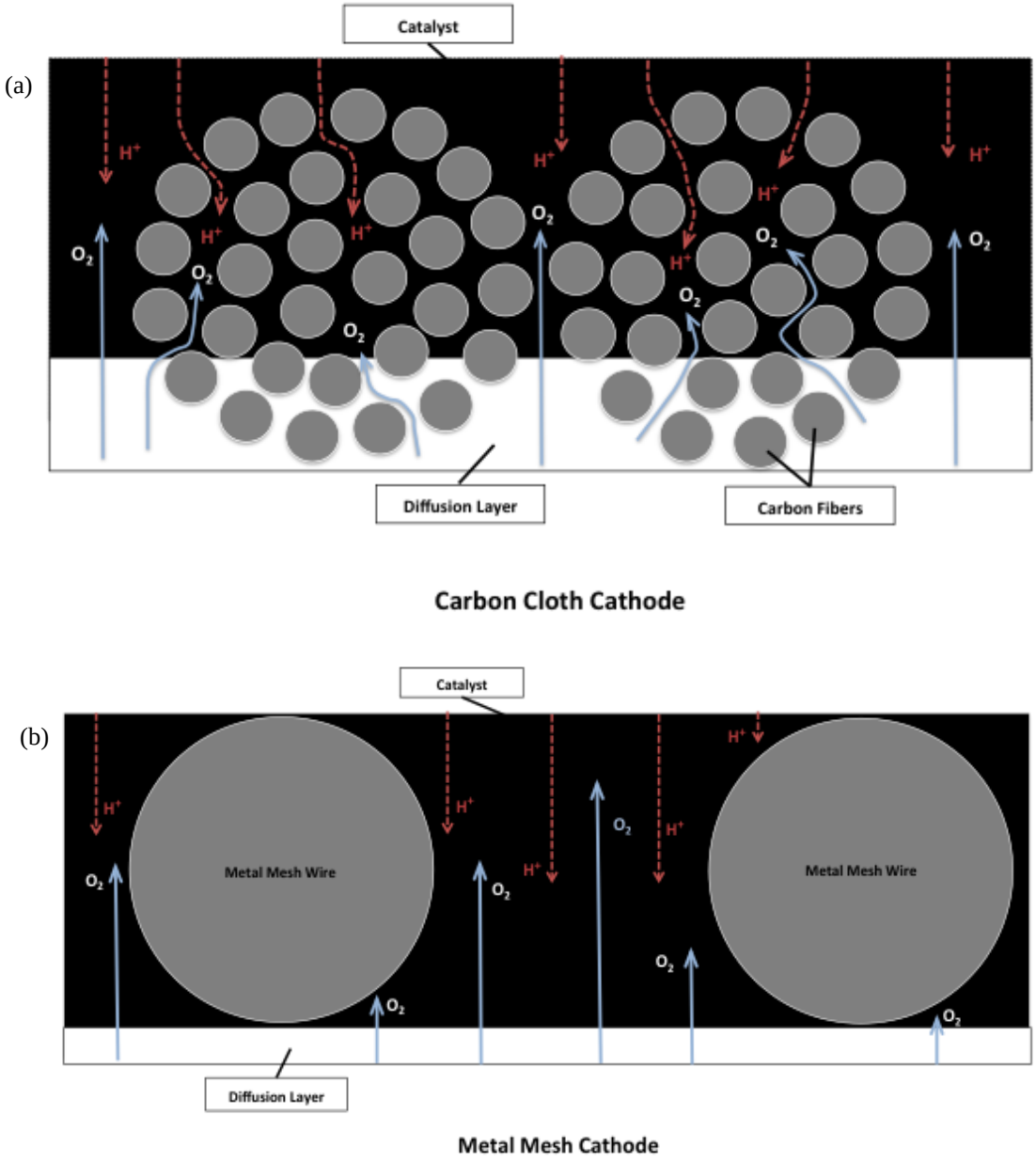

FIGURE 3.10: Schematic showing (a) Oxygen and proton transport in carbon cloth cathodes; and (b) Oxygen and proton transport in metal mesh cathodes.

The power density (3.3 W m^{-2}) obtained by the CEA-MFCs with the bamboo based AC cathode is the highest reported power density with activated carbon catalyst (based on cathode surface area), as far as we know, for a single-chamber air-cathode MFC operated in batch mode, confirming the advantages of the CEA-MFC structure for power generation [27]. Previous studies have compared AC cathodes to Pt catalyzed cathodes showing that results were similar [5,10]. As result a comparison with Pt catalyzed cathodes was not made here. Although the high power obtained here is possibly due to differences in biofilm composition compared to that used in other studies, it is likely that the cathode material plays a much more significant role in the high power generation of the cathode reported here.

3.4.1 Conclusion

Results reported here demonstrate that activated carbon/carbon cloth cathodes using bamboo-based activated carbon catalyst are capable of achieving high performance in MFCs, making them a good option for use in many MFC applications. Conductivity and surface pH are important properties for catalytic activity of activated carbon as cathode catalyst. Further development of MFC cathodes towards practical application may include: (1) optimizing the activation process for the production of activated carbon that's suitable for use as MFC cathode catalyst; (2) investigating less-expensive and more conductive carbon fabrics for use as base materials in MFCs; (3) scaling up the fabrication of cathode material; and (4) determining at which point electrode size becomes the limiting factor to cathode performance.

4. Stable and High Voltage and Power Output of Scaled-up CEA-MFCs Internally Connected in Series (iCiS-MFC)

Anthony Janicek, Yanzhen Fan, and Hong Liu

ABSTRACT

The voltage output of a single MFC is normally less than 0.8 V, often less than 0.3 V at maximum power output, which greatly limits the application of MFCs. When MFCs are scaled up, however, increasing reactor size has typically resulted in decreased power density. In this study, we developed a novel scaled-up MFC configuration that contains multiple cloth electrode assemblies in which the MFCs were internally connected in series (iCiS-MFC). The iCiS-MFC , equivalent to 3 CEA-MFCs, produced a high voltage output over 1.8 V and a maximum power density of 3.5 W m^{-2} using cathodes containing activated carbon as the catalyst. This power density is 6% higher than that reported for a similar smaller CEA-MFC, indicating that power can be maintained during scale-up with a greater than 33-fold increase in total cathode surface area and greater than 20-fold increase in reactor volume. High stability was also demonstrated based on the performance of the iCiS-MFC containing activated carbon/carbon cloth cathodes over a period of one year of operation. The high power and stability is likely due, in part, to a more efficient means of current collection through the internal series connection, which also avoids the use of expensive current collectors. These results clearly demonstrate the great potential of this MFC design for further scaling-up.

4.1 INTRODUCTION

There is a significant cost associated with wastewater treatment, which is largely attributable to energy consumption. Releasing energy stored in the high organic content in domestic, industrial, and agricultural wastewaters represent a potential means to offset this high cost. With an ever-increasing demand for wastewater treatment compounded by the enormous cost associated with treatment plant operation, finding more efficient and cost effective means of treating wastewater has become more important than ever. Developing new treatment technologies which will off-set this high-energy cost is necessary to maintain both water and energy security.

Microbial fuel cell (MFC) technology represents one such alternative. Currently, scaling-up is a key challenge for practical application of MFC technology. There are two general strategies for scaling-up MFCs: increasing the size of individual MFCs and connecting multiple MFCs into a stack [30,57]. However, increasing reactor size typically results in decreased power generation [58,80]. It has been suggested that connecting multiple MFCs into a stack could be a more effective way of generating power [116,117].

When connected into a stack, MFCs can be connected electrically in series to increase voltage. The open circuit voltage of an individual air cathode MFC is around 0.8V with an operating voltage less than 0.4 V at its maximum power output due to electrochemical losses. Such a low voltage output greatly limits the practical application of MFCs for power generation.

Increasing voltage output through series electrical connection has the potential to result in lower power loss compared to other means of boosting voltage due to the lack of conversion energy loss. Serial connection, producing higher voltage but lower current than parallel connection, may also lead to lower power loss in electricity collection and transmission. However, in spite of many attempts, current MFC stack designs have not achieved the ideal voltage output with an overall voltage decrease ranging from 30-98% for serial connection of 2-4 MFCs [58,86,87,118]. Using power managing system can booster voltage output of parallel connected MFCs, however, the addition of another system can further increase the complexity, thus reduce the reliability of MFC system. Furthermore, the maximum power density or energy output might be affected significantly[119–123]. A more efficient MFC stack design capable of high power and voltage outputs are critical for successful scaling up of MFC technology.

Among the various MFC designs, the cloth electrode assembly (CEA)-MFC, which contains a compact electrode/separator design resulting in minimized electrode spacing, has demonstrated high performance and treatment efficiency at several milliliter scales [14,106,124]. This reactor design replaces the membranes with low-cost and low-resistance separators, thus lowering its contribution to the internal resistance of MFCs and greatly increasing the performance of MFCs [14]. The CEA design also has great advantage over other MFC designs in terms of maintaining its performance during scale-up, as the electrode spacing is fixed and thus keeps the specific internal resistance as low as 20 $m\Omega\ m^2$ [14,62,124]. A stable power density of 3.3 Wm^{-2} was achieved using activated carbon as cathode catalyst during 24 days

of operation in batch mode. The high power, relatively low-cost, good scale-up potential, and stability of CEA-MFCs suggest that this configuration may be the best option for MFC stack development.

When MFC are scaled up or connected into stacks, a current collector is typically required to reduce ohmic losses of the electrode [12]. Current collectors can either be incorporated as the electrode base material or can be a separate wire or mesh that attaches to the electrode base material [25]. In MFCs, current collectors have been made from titanium mesh, titanium wire, graphite plates, gold, and stainless steel mesh [12,25]. Use of stainless steel may not be suitable for MFC applications due to the potential for severe corrosion, which ultimately leads to reduced performance [106]. Precious metal current collectors are also cost prohibitive for scaling up MFC technology. Although MFCs operate at low current densities, the energy loss can be as much 2 orders of magnitude greater when single point connection is used compared to optimized connections in a larger scale operation (electrode area of 1 m^2) [57]. As a result, a more efficient means of current collection is needed while avoiding the use of expensive or unstable current collectors.

In this study, we present a new MFC stack configuration, CEA-MFCs internally connected in serial (iCiS-MFC), in which the anode and the adjacent cathode share the same base material, i.e. carbon cloth, avoiding the need of a current collector. An iCiS-MFC equivalent to 3 MFCs was built and operated for approximately one year to demonstrate its long term stability in producing high voltage output and power density.

4.2 MATERIALS & METHODS

4.2.1 Reactor design and construction

A double iCiS air-cathode CEA-MFC (3 on each side) was constructed with a total effective surface area of 480 cm^2 (for the double CEA-MFC) and a liquid volume of 240 ml (Figure 4.1a). Each CEA-MFC was placed in between 3 PVC frames. The internal frame, which served as the anode chamber, contained 3 openings measuring 20 cm by 4 cm by 1 cm. Cathodes and anodes were internally connected and made from the same piece of carbon cloth (CCP, fuelcellearth.com) (Figure 4.1b). The end MFC's electrodes were connected to the external circuit via a titanium wire, forming a double iCiS CEA-MFC stack with 3 MFC connected in series on the top (designated as Stack A) and 3 on the bottom (designated as Stack B) (Figure 4.1a). A non-woven fabric layer was sandwiched between the anode and cathode of each CEA-MFC as previously described [124]. In order to prevent gas from becoming trapped between the anode and cathode, 1 cm x 1 cm slits, as previously described, were cut into the anode to provide a means for gas to be released [124] . Carbon cloth cathodes were constructed as previously described with an activated carbon loading of 25 mg cm^{-2} [125]. Each MFC was labeled according to the position in Stack A (MFC1, MFC2, MFC3) and Stack B (MFC1, MFC2, MFC3) according to Figure 4.1a.

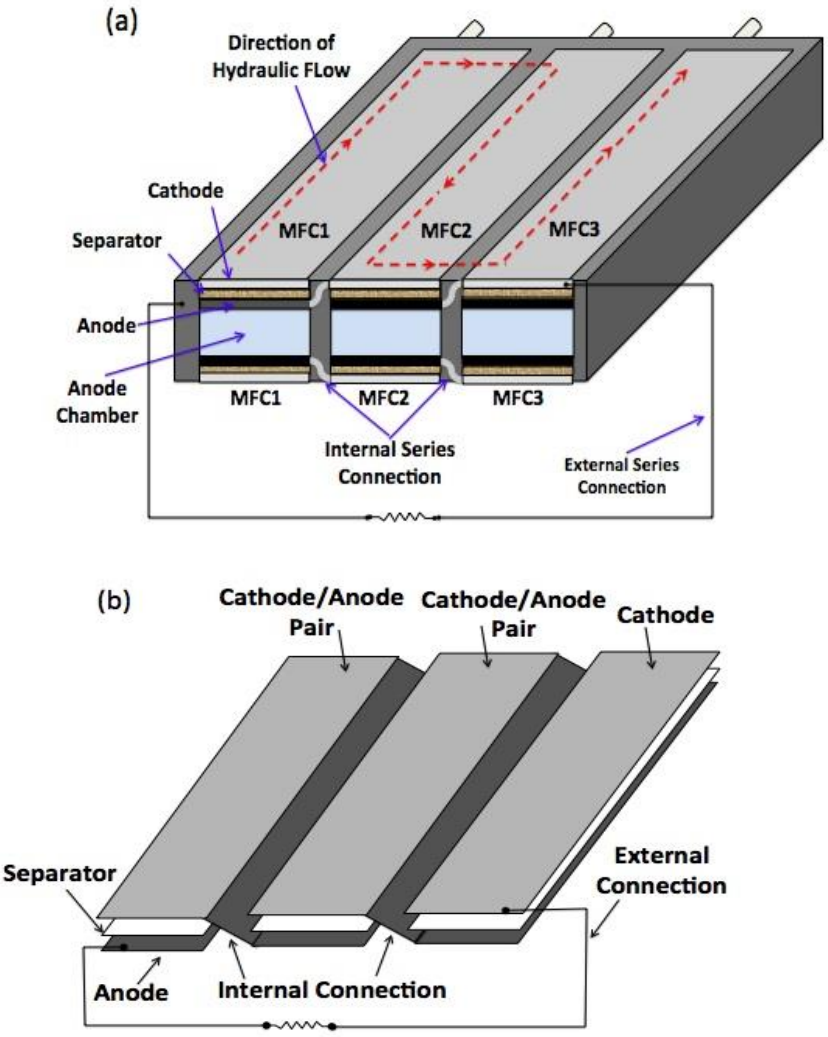
(a)
Direction of Hydraulic FLow
Cathode
Separator
MFC1
MFC2
MFC3
Anode
Anode Chamber
MFC1
MFC2
MFC3
Internal Series Connection
External Series Connection
(b)
Cathode/Anode Pair
Cathode/Anode Pair
Cathode
Separator
External Connection
Anode
Internal Connection

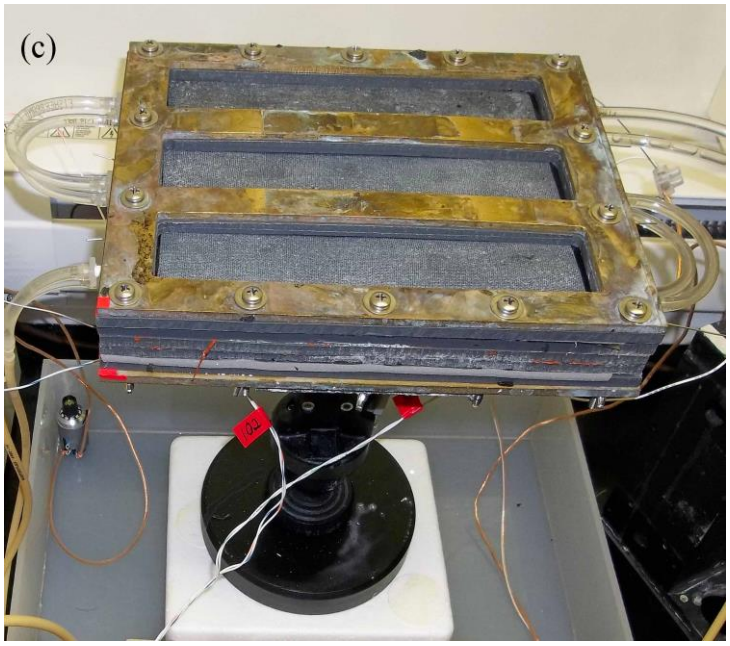

FIGURE 4.1: (a) Schematic of iCiS CEA-MFC stacks containing 3 CEA-MFCs connected internally in series on the top (initially Stack B) and 3 on the bottom (initially Stack A). Also shown are the internal and external electrical connections, direction of hydraulic flow, and position/naming of individual MFCs within the reactor; (b) Schematic showing the anode/cathode pairs, each made from a single piece of carbon cloth (resulting in the internal electrical connection); and (c) photograph of the reactor.

4.2.2 MFC operation and analysis

The MFC was inoculated with a mixed bacterial culture as previously described [124]. Acetate (5.9 g/L or 1 g/L) was used as the substrate and the medium solution contained the following (per liter), unless otherwise specified: NH_4Cl, 1.5 g; KCl, 0.13 g; $NaH_2PO_4*H_2O$, 4.67 g; $Na_2HPO_4*7H_2O$, 12.4 g; and mineral (12.5 ml) and vitamin (12.5 ml) solutions as reported [126]. The MFC experiments were operated at 32 ± 1°C in a temperature controlled chamber. The reactor was operated hydraulically in series. The reactor was initially operated in batch mode to facilitate start-up of the reactor. The system was switched to the continuous flow mode after three days as the power output started to increase significantly. Then the reactor was

continuously fed at a flow rate of 3 ml min^{-1} maintained through a peristaltic pump, corresponding to a hydraulic retention time of 80 min (unless otherwise specified). The external resistance of both the top and bottom reactors was set to maintain an operating voltage ~ 0.9 V during normal operation. The reactor was operated for a total of 365 days. For the first 100 days the reactor was operated at 5.9 gL^{-1} acetate and 80 mM PBS at different HRTs to determine the optimal operating conditions at higher substrate concentration. For the next 115 days, the reactor was operated at different substrate concentrations and different HRTs to further examine the effect of operational conditions on MFC performance. For the remaining 150 days, the reactor was operated at 1 gL^{-1} acetate and 10 mM PBS at an HRT of 25 minutes to determine performance and stability at lower substrate and buffer concentration. Total stack voltage as well as the voltage of individual MFCs were monitored using a multichannel data acquisition system (2700, Keithly, USA).

4.3 RESULTS & DISCUSSION

4.3.1 Start-up of the iCiS CEA-MFC

During start-up, the resistance of the Stack A and Stack B were controlled separately and set at 1000 ohms to facilitate growth of the biofilm. The voltage of Stack A (bottom) rapidly reached a maximum of 1.8 V within 3 days of operation (Figure 4.2 a). During this period, voltage of individual MFCs of Stack A were similar, ranging from maximum values between 0.56 V to 0.6 V during the first 3 days, with a variability of less than 7% between MFCs (Figure 4.2 b). The resistance of Stack A, controlled using a variable resistor, was then set to maintain an operating

voltage of ~ 1.5 V for another five days to further facilitate anodic biofilm development. In the following 18 days of operation, the resistance was incrementally decreased to achieve a higher power output and stabilized at an operating voltage of ~ 0.9 V corresponding to approximately 0.3 V per MFC in the series

Stable power output for Stack A reached a maximum of 3.5 Wm^{-2} after 18 days of operation (Figure 4.2 a), which was 6% higher than that previously obtained (3.3 W m^{-2}) in a significantly smaller CEA-MFC operated in batch mode [125]. This result indicates that power can be maintained during scale-up with a greater than 33-fold increase in total cathode surface area and greater than 20-fold increase in reactor volume. It should be noted that the result for the smaller scale CEA-MFC was obtained at a buffer concentration of 50 mM, which was lower than that used to obtain the result presented here (80 mM). However, previous results have shown that when buffer concentration was increased from 50 mM PBS to 100 mM PBS, in a similar smaller CEA-MFC operated under similar conditions, power density only increased 11% [124]. The result presented here is also similar to that obtained when platinum was used as the cathode catalyst in a smaller CEA-MFC operated under similar conditions [124]. By comparison, this represents an increase in cathode surface area by 140% with an increase in reactor volume by 700% without a loss in performance despite the use of low cost activated carbon as the catalyst.

The voltage of Stack B (top) reached a maximum value of ~ 1.57 V at 1000 ohms resistance after 7 days of operation, which was 9% lower and took twice as long as Stack A (Figure 4.3 a). The resistance of Stack B was then adjusted to maintain an

operating voltage of ~ 1.4 V for 5 days. During this start-up period voltage of individual MFCs of Stack B were highly variable, ranging from a low of 0.07 V to a high of 0.77 V (Figure 4.3 b). After this 12 day's operation, the resistance was gradually decreased until a total stack operating voltage of ~ 0.9V was achieved in approximately 20 days. However, voltage of individual MFCs remained significantly variable with 36% variability between cells. Furthermore, voltage of individual MFCs also varied between 0.25V and 0.36V. By comparison, Stack B took slightly longer to achieve a stable power output, reaching 2.2 Wm^{-2} after 20 days of operation, representing a power density 37% lower than Stack A (Figure 4.3 a). The slower start-up, lower maximum voltage and power density of Stack B compared to Stack A, and the highly variable voltage of individual MFCs of Stack B suggest that there may have been mass transfer limitations.

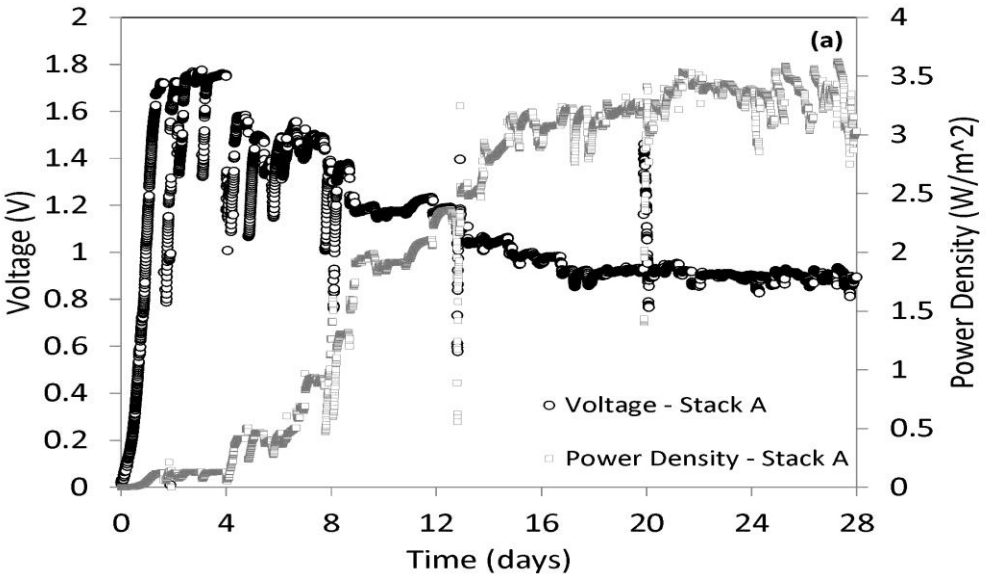

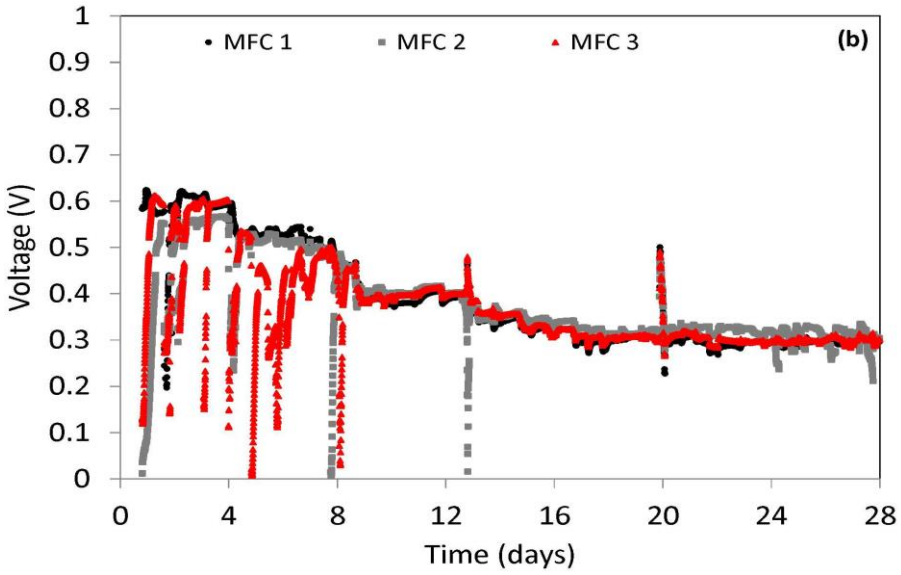

FIGURE 4.2: (a) Voltage and power as a function of time during start-up of Stack A; and (b) voltage of individual cells of Stack A.

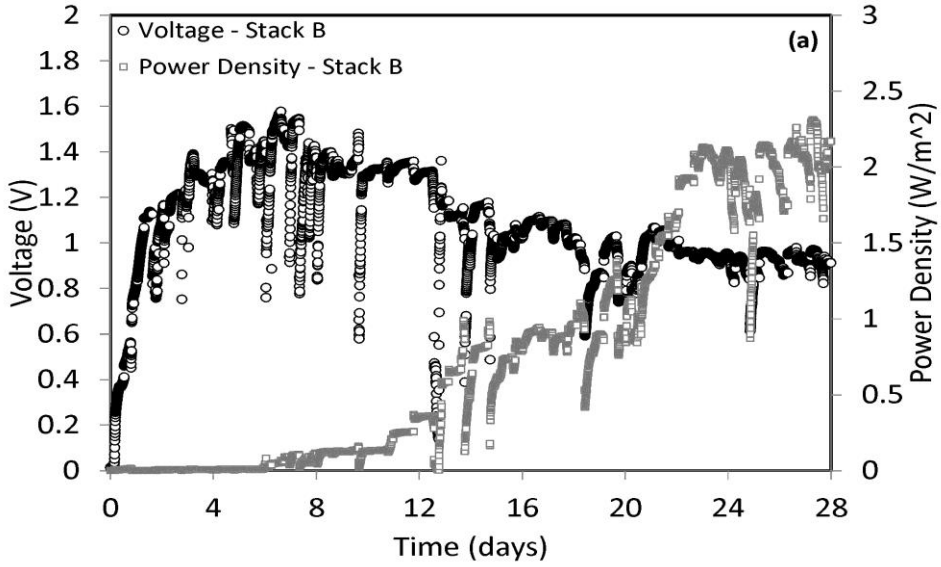

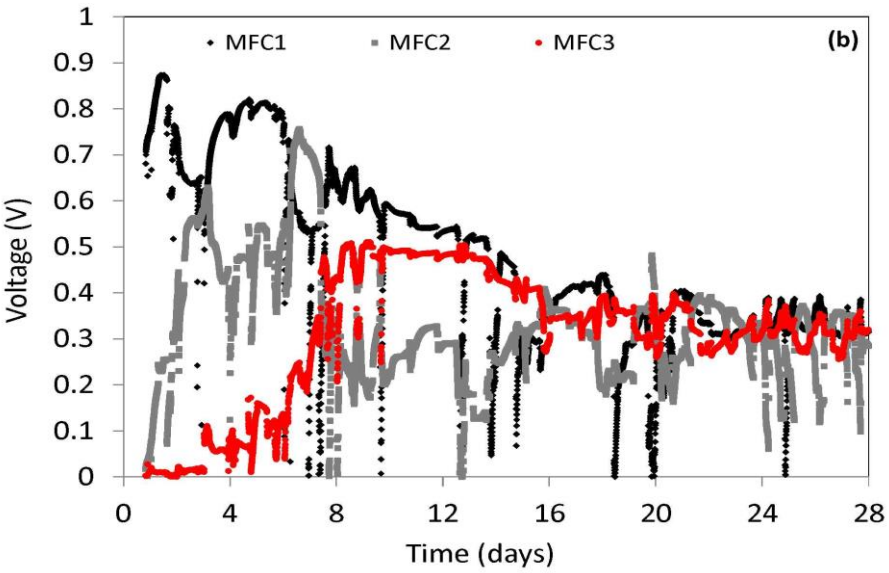

FIGURE 4.3:(a)Voltage and power as a function of time during start-up of Stack B; and (b) voltage of individual cells of Stack B.

4.3.2 Effect of the stack location on performance

Due to the higher performance and faster start-up of Stack A, and the highly variable voltage of Stack B during and after start-up, it was believed that reactor location may have led to the significantly different performance of the stacks. Therefore, after 28 days of operation, the reactor was flipped so that Stack A was operating as the top reactor and Stack B was operating as the bottom reactor. Voltage of individual MFCs of Stack A (initially the bottom reactor) were similar prior to flipping the reactor (Figure 4.4 a). However, variability in voltage between individual MFCs began to increase after the reactor was flipped, ranging from 0.23 V to 0.32 V, representing a 32% difference between individual MFCs (Figure 4.4 a). In contrast, voltage of individual MFCs of Stack B (initially the top reactor), prior to flipping, were highly variable (Figure 4.4 b). Once the reactors were flipped, variability in voltage decreased to only 7% between individual MFCs, ranging from

0.29 V to 0.31 V (Figure 4.4 b). Furthermore, the decreased voltage variability corresponded to an increase in power density of Stack B (Figure 4.4 c), which ultimately reached a maximum value of 3 Wm^{-2} after 40 days of operation. This represents a greater than 36% increase in power density when Stack B was operated as the bottom reactor compared to when operated as the top reactor, although it was 14% less than the maximum power achieved with Stack A before flipping. Flipping the reactors, however, had a detrimental effect on Stack A, as power density was decreased 28% to 2.5 Wm^{-2}.

The higher performance and stable voltage of Stack B when operated as the bottom reactor in combination with the decreased performance and variable voltage of Stack A after the reactors were flipped indicate that reactor location can significantly affect performance. The reduced performance when reactors are operated as the top reactor is likely due to mass transfer limitations and increased electrode spacing caused by gas being trapped within the CEA structure. Despite gas-venting slits in the anodes, when operated as the top reactor, gas is more likely to become trapped, as it will rise unless otherwise prevented. Both increased electrode spacing and mass transfer limitations; caused by gas build-up, result in increased internal resistance, which ultimately decreases performance. Distribution of trapped gas within the CEA structures would not be the same across the 3 MFCs connected in series. Gas could accumulate in one MFC faster and/or in larger quantities than in other MFCs in the series. As a result, internal resistance of individual MFCs will be different within the Stack, ultimately leading to the highly variable voltage observed when either Stack A or Stack B was operated as the top reactor. Differences in

internal resistance could also affect biofilm growth, limiting development during the critical start-up phase, ultimately effecting maximum power density achievable within a stack of MFCs

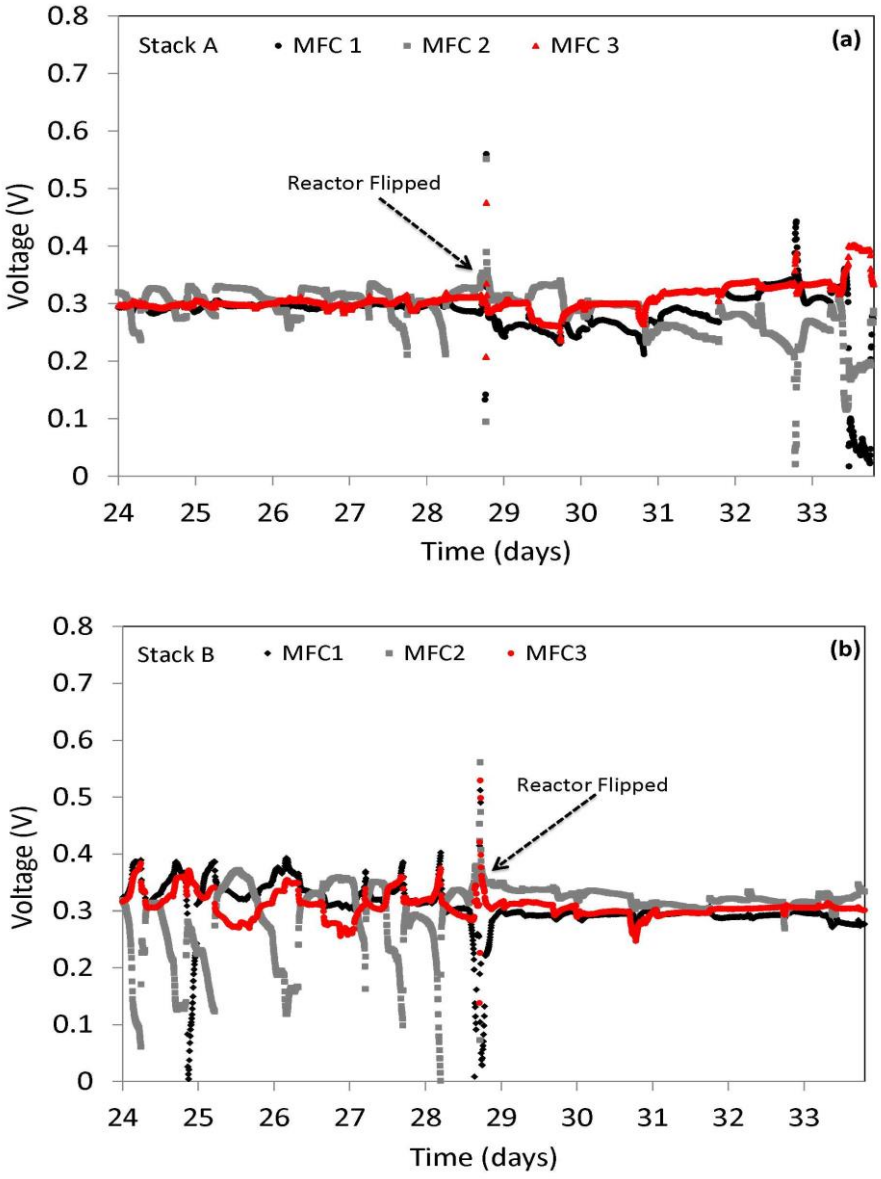

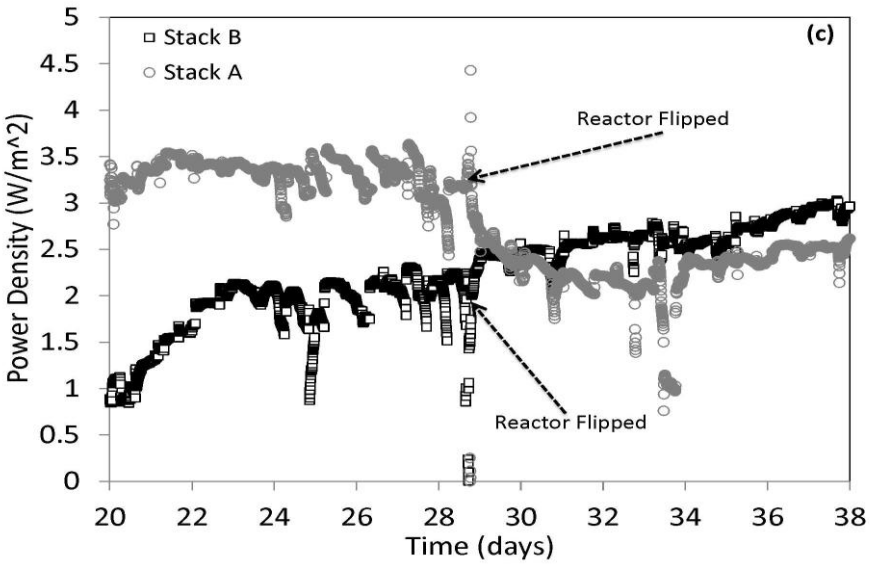

FIGURE 4.4: Performance of the reactor before and after flipping showing (a) voltage as a function of time for Stack A; (b) voltage as a function of time for Stack B; and (c) power as a function of time for both Stack A and Stack B.

4.3.3 Effects of operational conditions (HRT, substrate and buffer concentrations), on iCiS-MFC performance

At an acetate concentration of 5.9 g/L, decreasing HRT of Stack B from 240 min to 120 min resulted in an increase in power density by 6% from 2.56 to 2.71 Wm^{-2} (Figure 5 a). Further decreasing HRT from 120 min to 80 min resulted in a further increase in power density by 11% (3 Wm^{-2}). However, decreasing HRT from 80 to 60 min did not result in further increase in power density. A similar trend was observed for Stack A.

When the MFC stacks were operated at lower acetate concentration (1 g L^{-1}), power density decreased by more than 60% for both Stack A and Stack B. Decreasing HRT of Stack B from 80 min to 40 min resulted in an increase in power density by 21% from 0.55 Wm^{-2} to 0.67 Wm^{-2} (Figure 4.5 b). An additional decrease in HRT from 40 min to 25 min resulted in an additional increase in power density by 46%

(0.98 Wm^{-2}). However, further decreasing HRT from 25 to 20 min resulted in a decrease in power density by 12%. A similar trend was observed for Stack A.

The results at both high and low acetate concentration, presented here, indicate that at longer HRTs, substrate can become limiting when iCiS CEA-MFCs are operated hydraulically in series [80]. The decreased performance at the lowest HRTs tested (highest flow rates) was possibly due to the high hydrodynamic shear stress, which may result in younger and less diverse anodic biofilms, ultimately affecting performance [127]. Furthermore, significantly higher performance was achieved when the reactor was operated at the higher acetate concentration. Although this was also the case for a similar smaller CEA-MFC [124], it has not been shown to be the case for other MFC designs in which increasing acetate concentration beyond 1 gL^{-1} did not appreciably affect performance [26]. The high substrate utilization rate achieved in the CEA-MFCs was possible due to the development of a highly efficient anodic biofilm resulting from the lowered internal resistance of the iCiS CEA MFCs.

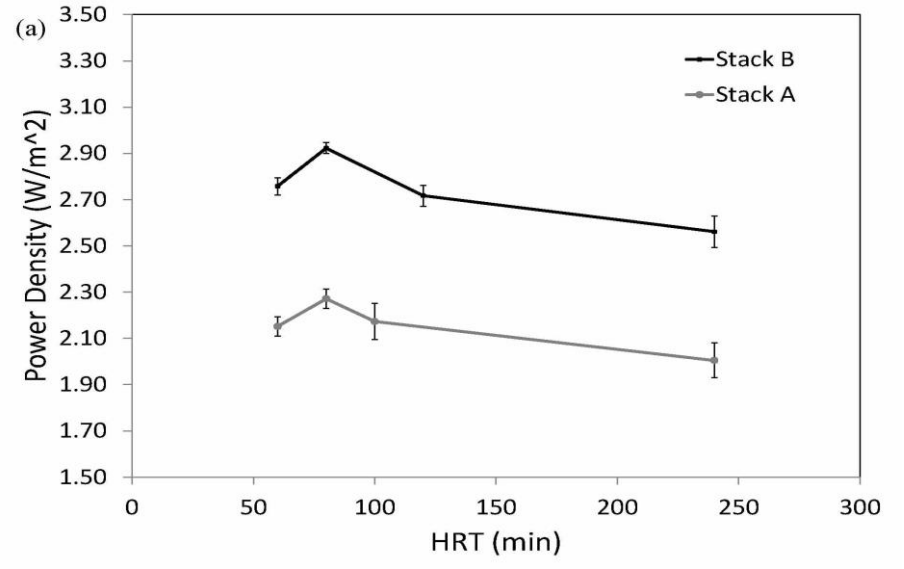

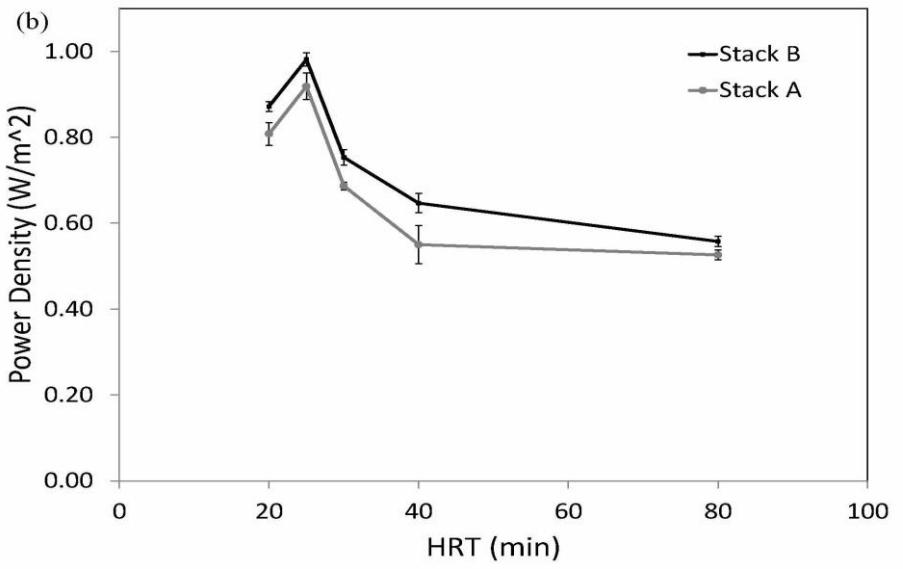

FIGURE 4.5: Power density as a function of HRT for (a) Stack A & B operated at higher acetate concentration (5.9 g L^{-1}); and (b) Stack A & B operated at lower acetate concentration (1 g L^{-1}).

It is well known that increasing buffer concentration can increase maximum power generation of MFCs [33]. However, addition of large quantities of buffers will likely be cost prohibitive for practical applications. To investigate how power generation of the newly developed system was affected by the buffer concentration, iCis-MFC stack were also operated under low buffer concentration (10 mM PBS). Results show that power reached a maximum of 1.5 Wm^{-2} at an acetate concentration of 5.9 g L^{-1} (Figure 4.6). This represents a 50% decrease in performance when buffer concentration is decreased from 80 mM PBS to 10 mM. When the substrate concentration decreased to 1 g L^{-1}, the power density further decreased to 0.5 Wm^{-2} and remained stable over the 150 days of operation. (Figure 4.7 a and b, Figure 4.8).

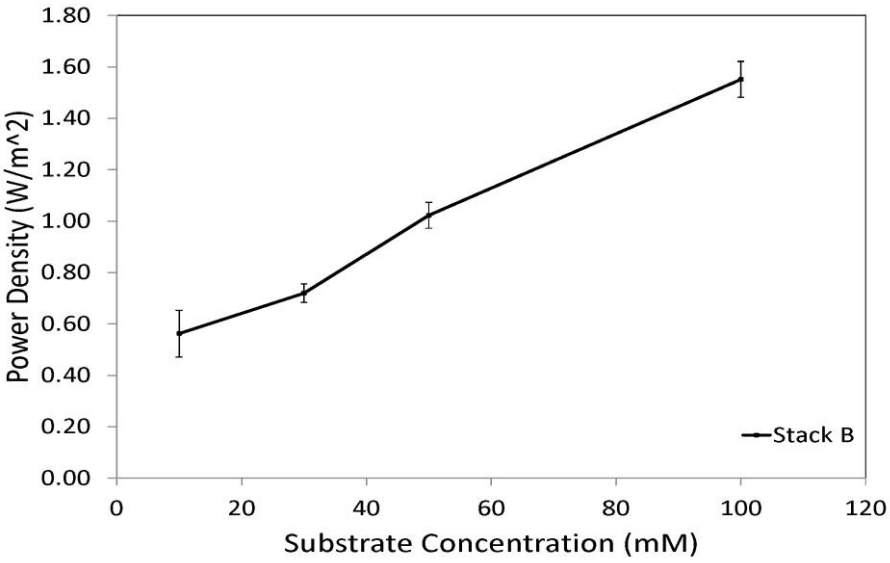

FIGURE 4.6: Power density as a function of substrate (acetate) concentration for Stack B operated at 10 mM PBS.

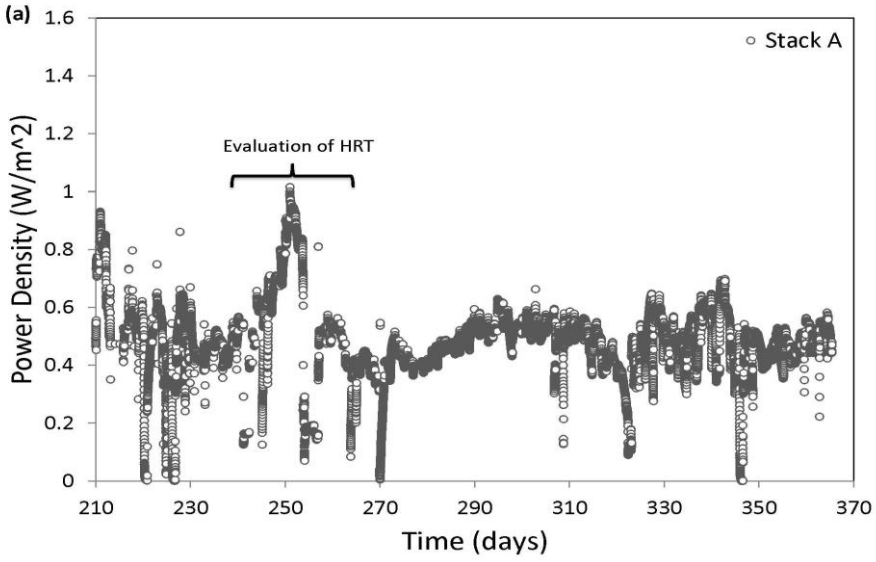

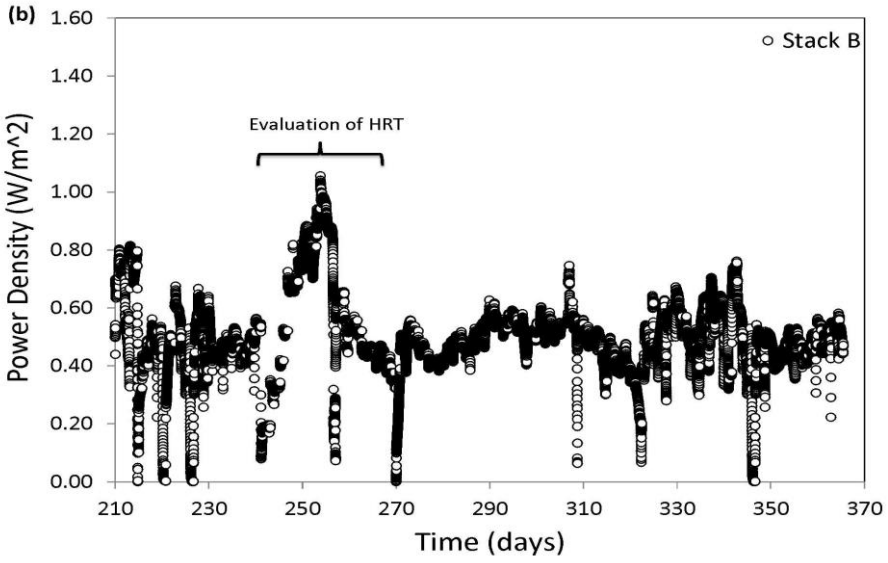

FIGURE 4.7: Power density as a function of time showing stable performance during the remaining ~150 days of operation at an acetate concentration of 1 g L^{-1} for (a) Stack A; and (b) Stack B.

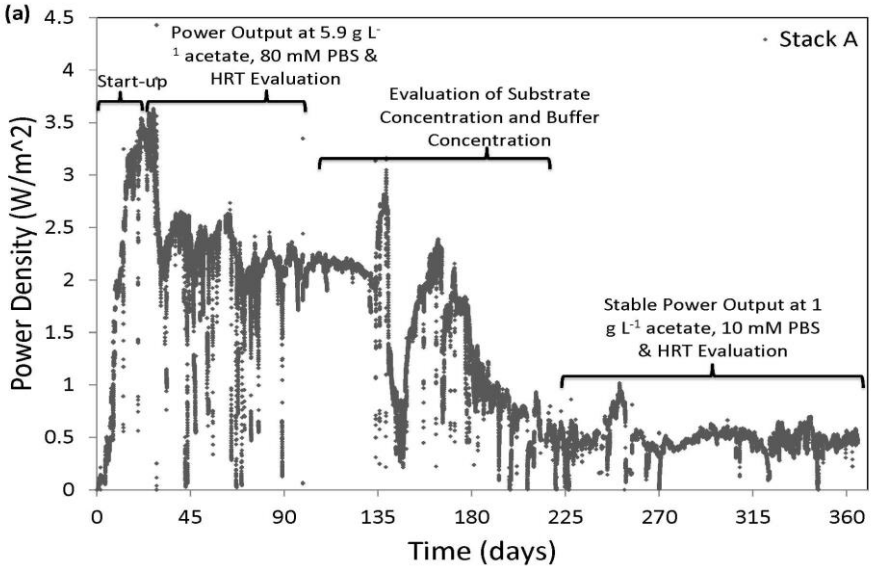

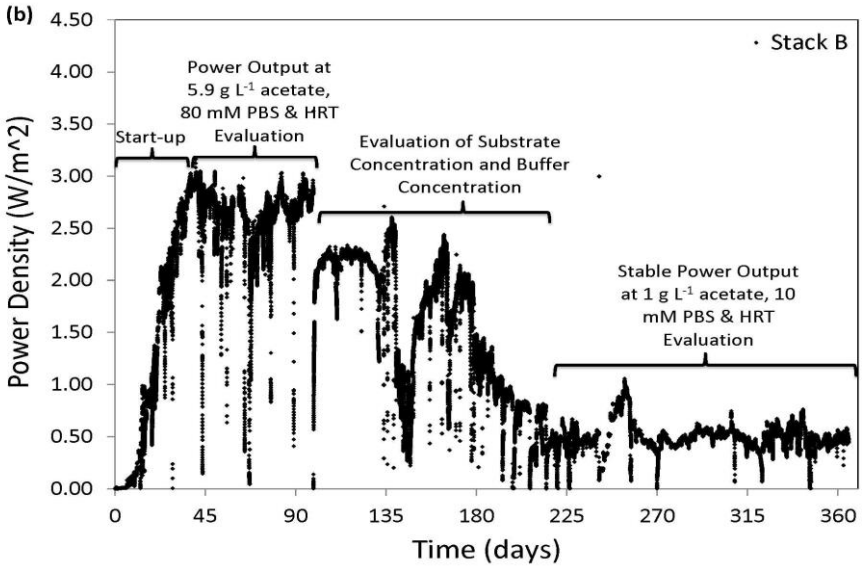

FIGURE 4.8: Power density as a function of time showing power output for (a) Stack A; and (b) Stack B during 365 days of operation

4.3.4 Implications for scale-up of MFC technology

Results presented here demonstrate that the iCiS CEA-MFCs can achieve a high stable power output of over 3 W/m^2 at an overall voltage output of 0.9 V. The high performance can be attributed to both the CEA structure and the design of internal series connection, which lead to lower internal resistance. The lowered internal resistance combined with the fact that the reactor was acclimated (first 100 days of operation) at the higher acetate concentration (5.9 gL^{-1}), may also have allowed a highly efficient anodic biofilm to develop. The internal series connection also alleviated the need for a current collector, resulting in low cost for fabrication. With this design, reactor size was increased significantly with no decrease in performance, as is typically the case when increasing MFC reactor size. These results clearly demonstrate the great potential of the iCiS CEA-MFCs design for scaling-up.

Lower performance when both stacks were operated as the top reactor suggests that trapped gas may be an issue during scale-up if the current operational mode is used. One alternative is to operate the reactor in a vertical orientation rather than the current horizontal orientation. Vertical orientation in combination with gas release mechanisms may prevent gas from becoming trapped between electrodes. The activated carbon/carbon cloth cathode used in this study is well suited for this type of operation, as it has shown high pressure tolerance [106,125]. Results presented here also indicate that a high degree of voltage variability between MFCs in a stack, during start-up, may lead to lower performance during the stable power output phase. Facilitating even biofilm growth during start-up phase seems crucial.

The high and low acetate concentrations tested in the reactor represent COD values of approximately 6000 mg L^{-1} COD and 500 mg L^{-1}COD, respectively, as representatives of typical food pressing wastewater and municipal wastewater. The significantly higher power density of the reactor at the higher acetate concentration suggests that treating wastewaters with higher COD values would be more appropriate for the iCiS CEA-MFC to balance the energy recovery and fabrication cost. Treating municipal wastewater may not justify the current expense of MFC technology, as adequate energy may not be generated. In addition, despite the low internal resistance caused by the internal series connection compared to reactors connected in series that don't contain this feature, low buffer concentration presents a significant challenges to performance. Further scaling up this reactor could be accomplished by increasing the number of MFCs connected in series as well as further increasing the size of each MFC. However, further investigation into scaling-

up the iCiS CEA-MFC design will ultimately determine any limitations with respect to size and reactor effectiveness for practical application.

5. Stability and Voltage Reversal /Recovery of Internally Connected in Series (iCiS) CEA-MFC Stacks

Anthony Janicek, Yanzhen Fan, and Hong Liu

ABSTRACT

Serial electrical connection of MFCs can result in unbalanced voltage between individual MFCs, which can lead to voltage reversal, causing decreased voltage and power output and electrode material deterioration. In this study, voltage reversal in newly designed iCiS-MFC stacks with metal mesh or carbon cloth as the cathode base material is examined. Serious corrosion was observed in the MFC stacks with the stainless steel cathode base material, which may have been caused and further worsened by repeated voltage reversal. Higher power output and stability was observed in the MFC stack using carbon cloth as the cathode base material. Conditions related to MFC continuous operation including pump stoppage, gas build-up within the reactor, and rapid decreases in external resistance at high current density, were also examined to determine their relation to voltage reversal and MFC performance. Although negative MFC voltages occurred in some MFCs and the total reactor voltage decreased 67 to 85% under these operational conditions, full recovery following voltage reversal was observed after normal operating conditions were restored in the MFC stacks. These results indicate that voltage reversal can be avoided through proper operation and design of MFC stacks and in the event voltage reversal occurs, full recovery is possible with the iCiS CEA-MFC.

5.1 INTRODUCTION

Microbial fuel cells (MFC), which can generate electricity from wastewater, have great potential as a means of converting renewable sources of waste into sustainable alternative energy. However, the operating voltage of a single MFC is still too low to be used in practical applications for energy generation. The open circuit voltage of an individual microbial fuel cell is around 0.8V while the operating voltage is only ~0.5V, due to electrochemical losses. As a result, it is necessary to connect multiple MFCs electrically in series to increase voltage. Connection of MFCs as stacks of individual MFCs allows for serial electrical connection and has shown to produce nearly additive voltage [84,87,128]. Series electrical connection of MFCs allows for useful voltages to be produced, which is a requirement for practical application of MFC technology to be realized.

While many different designs have been used and proposed for scale-up of MFC technology [80], cloth electrode assembly (CEA)-MFCs have shown to produce high power with high treatment efficiency [124]. To demonstrate the potential of the CEA-MFC design for scaling up, an internally connected in series (iCiS) CEA-MFC stack was developed that achieved a maximum power density of 3.5 Wm^{-2} [129]. In this design, MFCs were connected electrically in series by connecting the anode of one MFC to the cathode of the adjacent MFC by using a single piece of carbon cloth [129]. This internal electrical connection reduces ohmic losses by eliminating the contact resistance when connecting MFCs electrically in series.

When connected electrically in series, unbalanced voltage between individual MFCs often occurs. If the imbalance in voltage is large enough, a phenomenon

known as voltage reversal can occur under certain conditions. This phenomenon results in one of the electrodes switching polarity, either becoming more positive (in the case of the anode) or more negative (in the case of the cathode) than the other electrode. The ultimate effect of voltage reversal is reduced power and voltage output. Voltage reversal has been shown to occur in chemical fuel cells as a result of fuel starvation, fuel crossover, and impedance differences [88–92]. In MFCs, voltage reversal has been attributed to causes such as mass transfer and catalytic limitations of the biofilm [84], membrane polarization or deformation [58,130], ohmic losses due to ion cross conduction [85,131–133], and cathodic limitations [58]. In all cases, voltage reversal results from an imbalance in voltage between cells, which is due to differences in internal resistance of individual cells.

The effects and extent of voltage reversal on reactor performance of the iCiS CEA-MFC stack are not well understood. However, in chemical fuel cells, voltage reversal is known to have deleterious effects. For example, voltage reversal has been shown to lead to deterioration of both the anode and cathodes due to chemical degradation of electrode materials. Performance degradation occurs as a result of catalyst dissolution and/or agglomeration and carbon support material corrosion due to potentials applied to electrodes during reversal [88–92,134–137]. Oxidation of carbon based support materials typically occurs on the anode in chemical fuel cells due to the presence of a chemical catalyst and oxygen under certain conditions [138]. Oxidation of carbon support materials is less favorable in MFCs due to a lack of chemical catalyst on the anode and a lower level of oxygen in the anode chamber compared to chemical fuel cells. However, in MFCs, when using carbon based

support materials for the anode or cathode, if electrode potential and surface area are high enough and there is sufficient oxygen present, the possibility for carbon oxidation exists.

Perhaps the most significant effect of voltage reversal on MFCs will be on the cathode when cathode base materials consist of metal mesh or metal foam. Metal base materials made from nickel or stainless steel have been used as base materials for activated carbon cathodes used in MFCs [38–43,45,52,53,55,139]. Recent studies have shown that oxidation of both stainless steel and nickel base materials can occur in MFCs [54,56,106]. Oxidation of metal base materials used in MFCs is thermodynamically more favorable at more negative cathode potentials [56,114]. During voltage reversal, cathode potentials can drop significantly, becoming negative [58]. However, despite the probability of cathodes reaching negative potentials and the possibility for oxidation of metal based supporting materials, the effect of voltage reversal on these materials has not yet been examined in MFCs.

In this study, MFC stacks, each consisting of 4 internally serially connected CEA-MFCs, were constructed to investigate the power/voltage production of the stacks and the imbalanced voltage output of individual cells under hydraulically serially connected condition. The effects of voltage reversal on the oxidation of cathode base material (stainless steel mesh and carbon cloth) are analyzed. Extreme operational conditions were also created to investigate the factors causing voltage reversal in the MFC stack and the strategies to avoid voltage reversal in the CEA-MFC stacks were discussed.

5.2 EXPERIMENTAL

5.2.1 MFC stack construction

The iCiS CEA-MFC stacks were constructed based on a similar design described previously [129]. The anode chamber contained 4 openings measuring 30 cm by 5 cm by 1 cm for a total of volume of 150 ml per CEA-MFC. The effective surface area of each CEA-MFC was 120 cm^2 due to a supportive cross bar across the center of the frame to allow the plates to be sandwiched together. In addition, perforated spacers were included in the anode chamber to facilitate hydraulic mixing and to ensure CEAs were sandwiched together. Cathodes were made from carbon cloth (CCP, fuelcellearth.com) or stainless steel mesh (mcmaster-carr.com) while anodes were made only of carbon cloth. Carbon cloth cathodes were constructed as previously described with an activated carbon loading of 17.5 mg cm^{-2} [106]. Metal mesh based cathodes were constructed similarly to that previously described except that the PTFE concentration was increased by 40% in order to adhere the catalyst to the mesh through a rolling procedure, without pressing, as it was previously shown that pressing may have led to corrosion of the metal base material [106]. To create the internal electrical connection of the stainless steel based MFCs, a portion of the stainless steel cathode was overlapped with the adjacent carbon cloth anode. Pressure was applied to the overlapping area through bolting the external PVC frames together, ultimately resulting in the internal electrical connection. Reactors containing carbon cloth cathodes were designated as CC while those containing stainless steel were designated SS. The 4 MFCs on the top of the iCiS-MFC are designated as T1-T4 and the 4 MFCs on the bottom are designated as B1-B4 (Figure

5.1). A non-woven fabric layer was sandwiched between the anode and cathode of each CEA-MFC as previously described [124].

5.2.2 MFC operation

The MFC stacks were inoculated with a mixed bacterial culture as previously described [124]. Unless otherwise specified, acetate (5.9 g/L) was used as the substrate and the medium solution contained the following (per liter): NH_4Cl, 1.5 g; KCl, 0.13 g; $NaH_2PO_4 \bullet H_2O$, 5.84 g; $Na_2HPO_4 \bullet 7H_2O$, 15.5 g; and mineral (12.5 ml) and vitamin (12.5 ml) solutions as reported [126]. The MFC experiments were operated at 32 ± 1°C in a temperature controlled chamber. The reactor was operated hydraulically in series. The reactors were initially operated in batch mode to facilitate start-up of the reactor. The system was switched to the continuous flow mode after two days as the power output started to increase significantly. Then the CEA-MFCs were continuously fed at a flow rate of 8 ml min^{-1} maintained through a peristaltic pump, corresponding to a hydraulic retention time of 1 hr. The external resistance of both the top and bottom reactors was set to maintain an operating voltage of ~ 2 V for each MFC stack during start-up and ~ 1.2 V during normal operation. MFC reactors were operated for 22 days before switching to other operational conditions as described below. The reactor was equipped with gas venting ports at the effluent of each anode chamber. However, periodically, gas that had accumulated within the reactor was removed through priming of the pump (operating at a higher flow rate) for a short period of time, typically less than 1 minute.

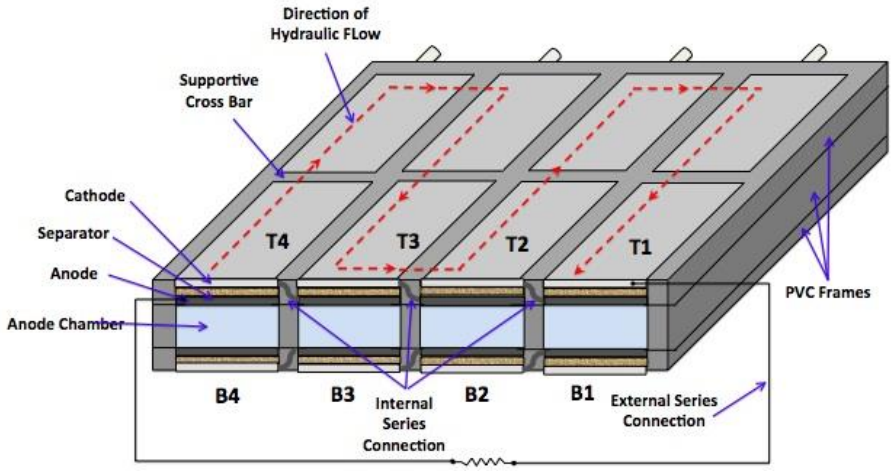

FIGURE 5.1: Schematic of the internally connected in series (iCiS) CEA-MFC reactor showing a cross-section of the reactor, 3 PVC frames, external and internal connections, direction of hydraulic flow, and individual MFC labeling for both the Top and Bottom reactor.

5.2.3 Investigate the effect of operational conditions on voltage reversal

Following stable power output, the CC reactor was used to investigate the three operational conditions that may lead to voltage reversal in the MFC stack reactor. For the first set of experiments, pumps were stopped for 8 hours to determine the effect on reactor performance and possible connection to voltage reversal. The second set of experiments involved gas buildup in the reactor. During both start-up and normal operation, a small amount of gas build-up was noticed in the reactor, which required infrequent priming of the pump to remove the gas. To determine the effect that gas buildup had on reactor performance and potential to cause voltage reversal, gas was allowed to accumulate in the reactor over a 30-hour period. The composition of the gas was also measured through collection of gas exiting the reactor in a 250 ml sample bottle. The gas composition was measured according to a previous procedure [124] . In the third set of experiments, external

resistance was initially decreased ~ 75% from 12 ohms to 3 ohms for both the top and bottom MFC stack to determine the effect on reactor operation and possible connection to voltage reversal. To investigate the effect of cross-conductance, in a later experiment, the external resistance was reduced for the bottom reactor only.

5.3 RESULTS & DISCUSSION

5.3.1 Voltage and power production by CEA-MFC stack with SS cathodes

During start-up, the external resistance of both the top and bottom reactors was adjusted to maintain an operating voltage of ~ 2 V. Although voltage stabilized after 16 days for the SS reactors, during start-up, voltages of individual cells were highly variable ranging from as much as -0.47 V to +0.9 V for the SS-B reactor and -0.55V to 0.6 V for the SS-T reactor (Figure 5.2 a and b). Negative cell voltages can result in negative potentials applied to the cathode during voltage reversal although the individual electrode potential was not measured in this study. It is also possible that individual MFCs with lower positive cell voltages also experienced negative cathode potentials.

Noticeable corrosion appeared on the surface of cathodes containing stainless steel mesh after only 2 days of operation with corrosion continuing to worsen over the duration of the 16 day start-up period (Figure 5.3). The cause of corrosion was likely due to the high negative electrode potentials of the cathodes caused by voltage reversal during reactor start-up. Based on the potential-pH diagram for iron [140], the theoretical range at which dissolution of iron into solution is favored at neutral pH is between 0V and -0.6V (vs. SHE). Although the potential could be affected by

other species in solution, it shows that corrosion can occur at potentials seen by MFC cathodes during voltage reversal [58].

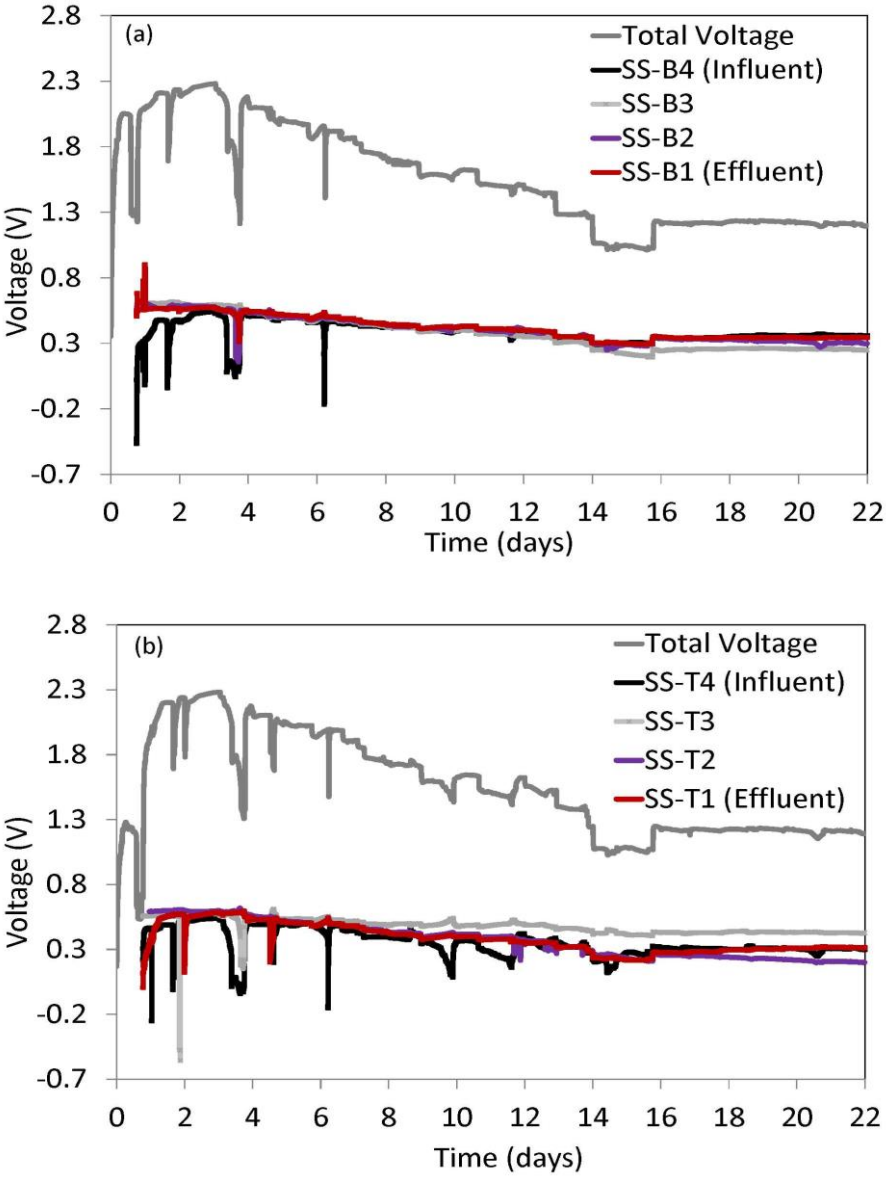

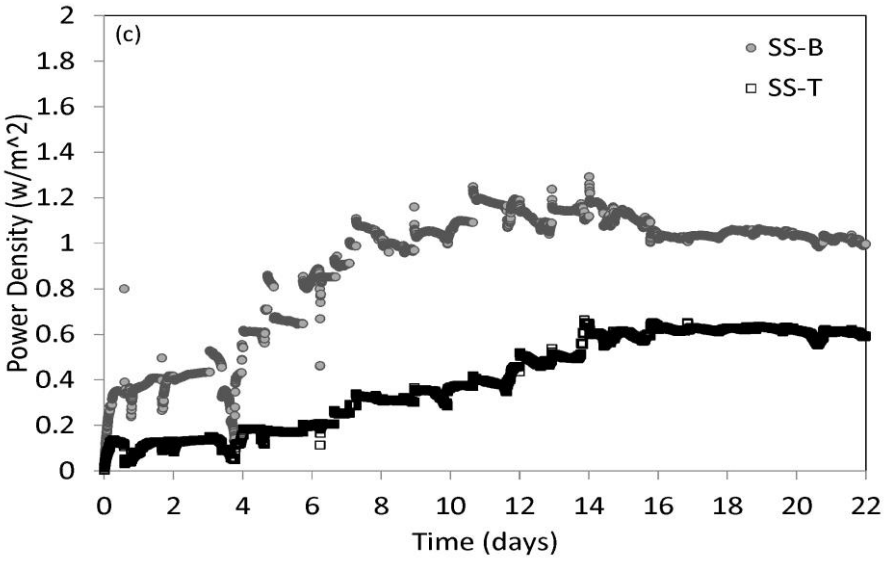

FIGURE 5.2: (a) Voltage as a function of time for the CEA-MFC stack with activated carbon/stainless steel mesh cathodes for the bottom reactor; (b) Voltage as a function of time for the CEA-MFC stack with activated carbon/stainless steel mesh cathodes for the top reactor; and (c) Power density as a function of time for the top and bottom reactors of the CEA-MFC reactor with activated carbon /stainless steel mesh cathodes.

(a)

(b)

(c)

FIGURE 5.3: Photographs showing (a) corrosion of stainless steel mesh cathodes of the top reactor; and (b) and (c) close-up of corrosion shown in (a) indicating holes in the cathodes caused by severe corrosion.

Total voltage during stable power output for both the SS-B and SS-T reactors, remained ~ 1.2 V (Figure 5.2 a and b). During stable power output, voltages between individual cells for the SS reactors were highly variable with a 33% difference between cells for the SS-B reactor, ranging from 0.25 to 0.35 V (Figure 5.2 a) and a 71% difference between cells for the SS-T reactor, ranging from 0.2 V to 0.42 V (Figure 5.2 b). Variability in voltages between individual cells of the SS reactors during stable power output was likely caused by voltage reversal during start-up.

Differences in potentials applied to the anode biofilms may have led to differences in biofilm development leading to imbalances in operating voltages produced by individual cells in the reactor. Furthermore, corrosion of support materials, resulting from voltage reversal during start-up, likely led to the variable voltages between individual cells during stable power output.

Maximum power reached ~ 1.0 and ~ 0.6 W m^{-2} for the SS-B and SS-T reactors, respectively (Figure 5.2 c). In our previous work, electrochemical evaluation showed that activated carbon cathodes containing stainless steel mesh as the base material was similar to cathodes containing carbon cloth [106]. However, in that study power output in MFCs was lower for cathodes containing stainless steel mesh. The lower power output was attributed to corrosion of the stainless steel base material, due in part to the pressing procedure used to fix the catalyst to the base material. In this study the catalyst was rolled onto the stainless steel base material, rather than pressed, in an attempt to prevent damage caused by the pressing procedure and subsequent corrosion of the base material. Studies using rolling methods to apply the catalyst to the base material reported in the literature did not result in observed corrosion of the base material [45,52,139,141]. The electrochemical performance of the SS mesh cathode prepared using the new procedure was similar to the cathode prepared using the former procedure (Figure 5.4). Despite the new preparation procedure, corrosion still occurred on the surface of cathodes containing stainless steel mesh base material. Differences in the extent of corrosion between the top and bottom reactor are likely responsible for the 40% lower power of the top reactor compared to the bottom reactor.

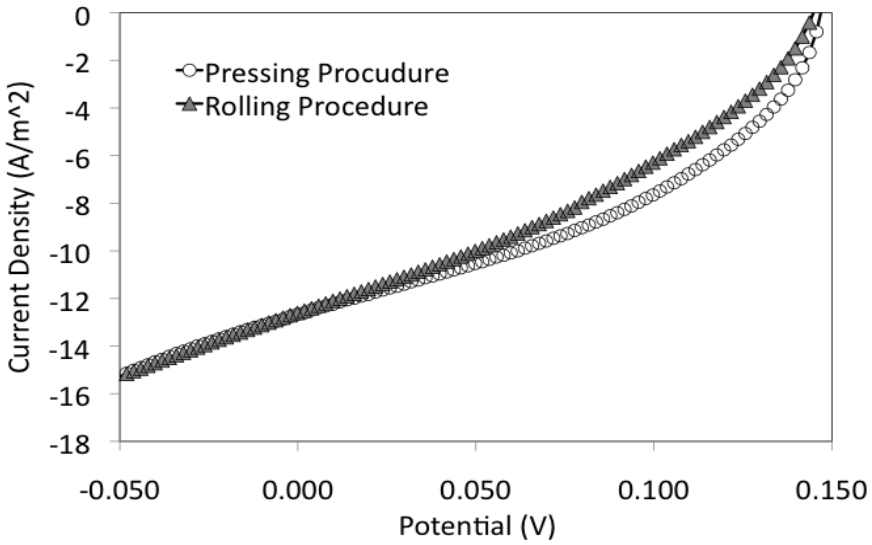

FIGURE 5.4: Current density as a function of potential for the activated carbon cathode containing metal mesh base material showing the performance of the two different preparation procedures.

5.3.2 Voltage and power production by CEA-MFC stack with CC cathodes

During start-up of the CEA-MFC stack with carbon cloth cathodes, voltages of individual cells were also variable ranging from as much as -0.6 V to +0.42 V for the CC-B and -0.6 V to + 0.55 V for the CC-T. However, voltage stabilized after 8 days of operation, which is much faster than that of the MFC stack with SS cathodes (Figure 5.5 a and b). During stable power output, total voltage for both CC-B and CC-T remained ~ 1.2 V (Figure 5.5 a and b). Voltage between individual cells of the CC reactors was less variable than that of the SS reactor. For the CC-T reactor, voltages were only 10% different, varying over the range of 0.27 V to 0.3 V (Figure 5 b) while individual cell voltages between the CC-B reactor were slightly more variable with a 26% difference, ranging from 0.26 V to 0.34 V (Figure 5 a). Similar to the SS reactors, variability in voltages between individual cells of the CC MFC

stack was likely caused by voltage reversal. Applied potentials experienced by the biofilm during start-up likely resulted in differences in performance between MFCs, ultimately resulting in the variation in voltage output.

The CC-T and CC-B reactors reached a stable power output of ~ 2.4 Wm^{-2} after 8 days of operation, which was 140 to 300% higher and two times faster than the SS reactors (Figure 5.5 c). No corrosion was observed on the cathodes of the CC reactors, which demonstrates the stability of carbon fiber based base materials. Carbon support material corrosion was shown to be negligible in chemical fuel cells at potentials less than + 1.1 V (vs RHE), although presence of precious metal catalysts can reduce the corrosion onset potential to as low as +0.55 V (vs RHE) [92]. Further protection is provided by water oxidation, which is thermodynamically more favorable than oxidation of carbon support materials, unless current densities cannot be sustained by water electrolysis alone. As a result, corrosion of carbon fiber support materials is not likely at the potentials experienced by electrodes during voltage reversal in MFCs. For this reason, the remainder of the experiments were carried out with the CC reactor to determine the operational causes and extent of voltage reversal in the CEA-MFC stack.

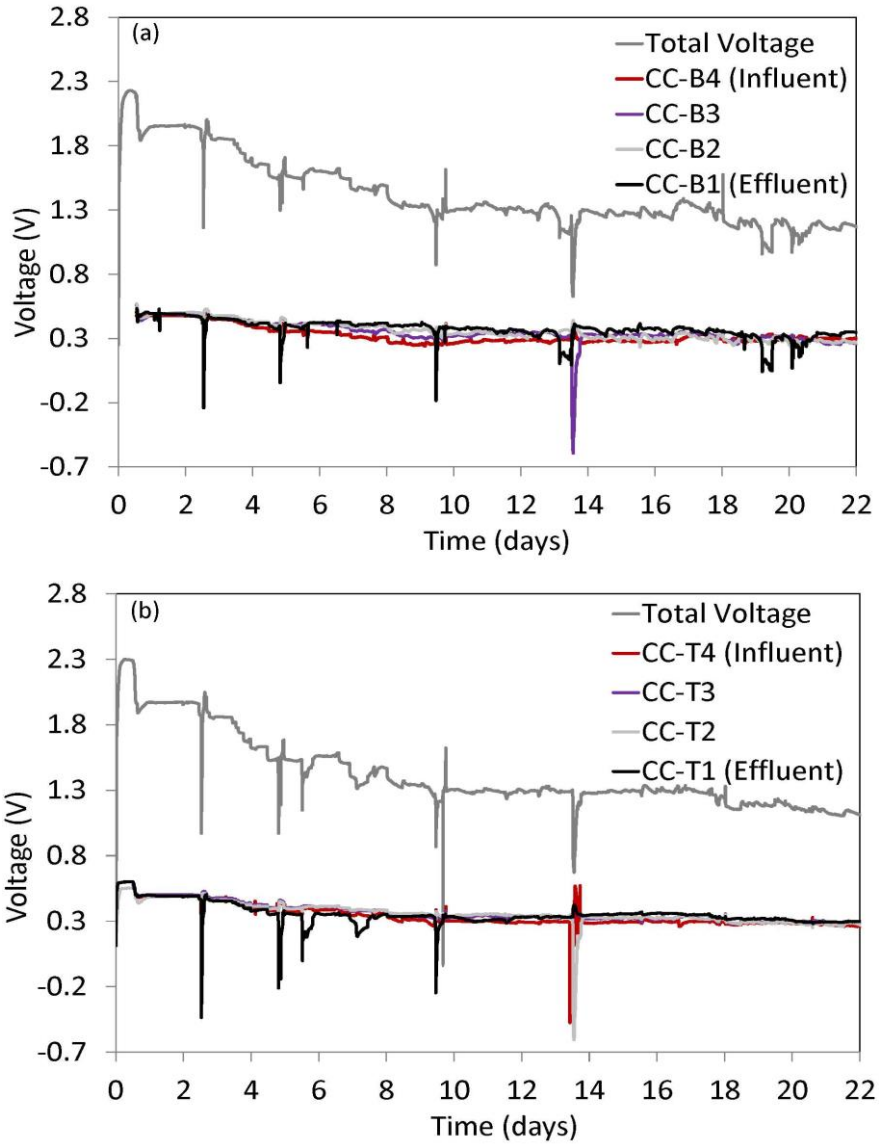
(a)
Total Voltage
CC-B4 (Influent)
CC-B3
CC-B2
CC-B1 (Effluent)
Voltage (V)
2.8
2.3
1.8
1.3
0.8
0.3
-0.2
-0.7
0
2
4
6
8
10
12
14
16
18
20
22
Time (days)
(b)
Total Voltage
CC-T4 (Influent)
CC-T3
CC-T2
CC-T1 (Effluent)
Voltage (V)
Time (days)

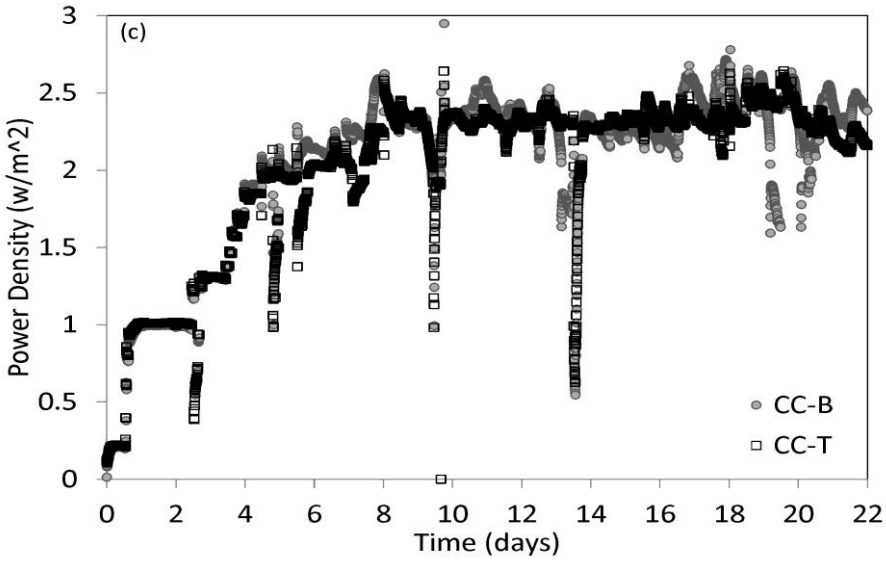

FIGURE 5.5: (a) Voltage as a function of time for the CEA-MFC stack with activated carbon/carbon cloth cathodes for the bottom reactor; (b) Voltage as a function of time for the CEA-MFC stack with activated carbon/carbon cloth cathodes for the top reactor; and (c) Power density as a function of time for the top and bottom reactors of the CEA-MFC reactor with activated carbon /carbon cloth cathodes.

5.3.3 Voltage reversal caused by Pump Stoppage

Pump stoppage may lead to fuel starvation due to decreased substrate concentrations over time, as fresh substrate is not entering the reactor. Reversal may first occur in the cells with the lowest substrate concentration. Figure 5.6 illustrates that the overall and individual cell voltages begin to drop approximately 4.7 hours into the 8-hour stoppage period. For the individual cell voltages, a cascading effect of declining voltages is observed, with individual cell voltages reaching as low as -0.65 V. This result would be expected as the substrate concentration in the effluent would be lowest and therefore is more likely to experience a decrease in voltage first, followed by the preceding cell, continuing in this manner back to the influent cell for the series. The imbalance in cell voltages between cells was possibly due to fuel

starvation and/or mass transfer limitations as with the pump stopped, there is not sufficient mixing or fresh influent delivered to bacterial cells. A similar trend was observed previously when two cells, operated in batch mode, were connected electrically in series and one cell was intentionally starved of substrate [87]. The cascading effect of voltage reversal shown in Figure 5.6 a suggests that voltage reversal as a result of pump stoppage in the iCiS CEA-MFC is a dynamic phenomenon. Voltage recovery of a reversed cell corresponds to reversal of an adjacent cell, which can continue through the series of internally connected MFCs. This likely occurs because fuel starvation leads to decreased microbial activity resulting in an increased anode potential and eventually voltage reversal. For example, as shown in Figure 5.7, the anode of the reversed cell is electrically connected to the cathode of an adjacent cell (anode of T3 connected to cathode of T2 in Figure 5.7 a). As a result, the cathode potential (cathode of T2) begins to decrease due to decreased oxygen reduction resulting from the decreased microbial activity of the reversed anode (anode of T3) it is electrically connected to. Eventually, the cell adjacent (T2) to the reversed cell (T3) experiences voltage reversal (Figure 5.7 b) due to the decreasing cathode potential. When this occurs, the lower potential of the cathode (T3) decreases the potential of the anode (T2) it is electrically connected to which results in charging and subsequent re-reversal of the original cell (i.e., the cell voltage of T3 cell becomes positive again). The overall effect of voltage reversal due to pump stoppage was a drop in total voltage of the top reactor by 85% from 1.2 V to 0.18 V.

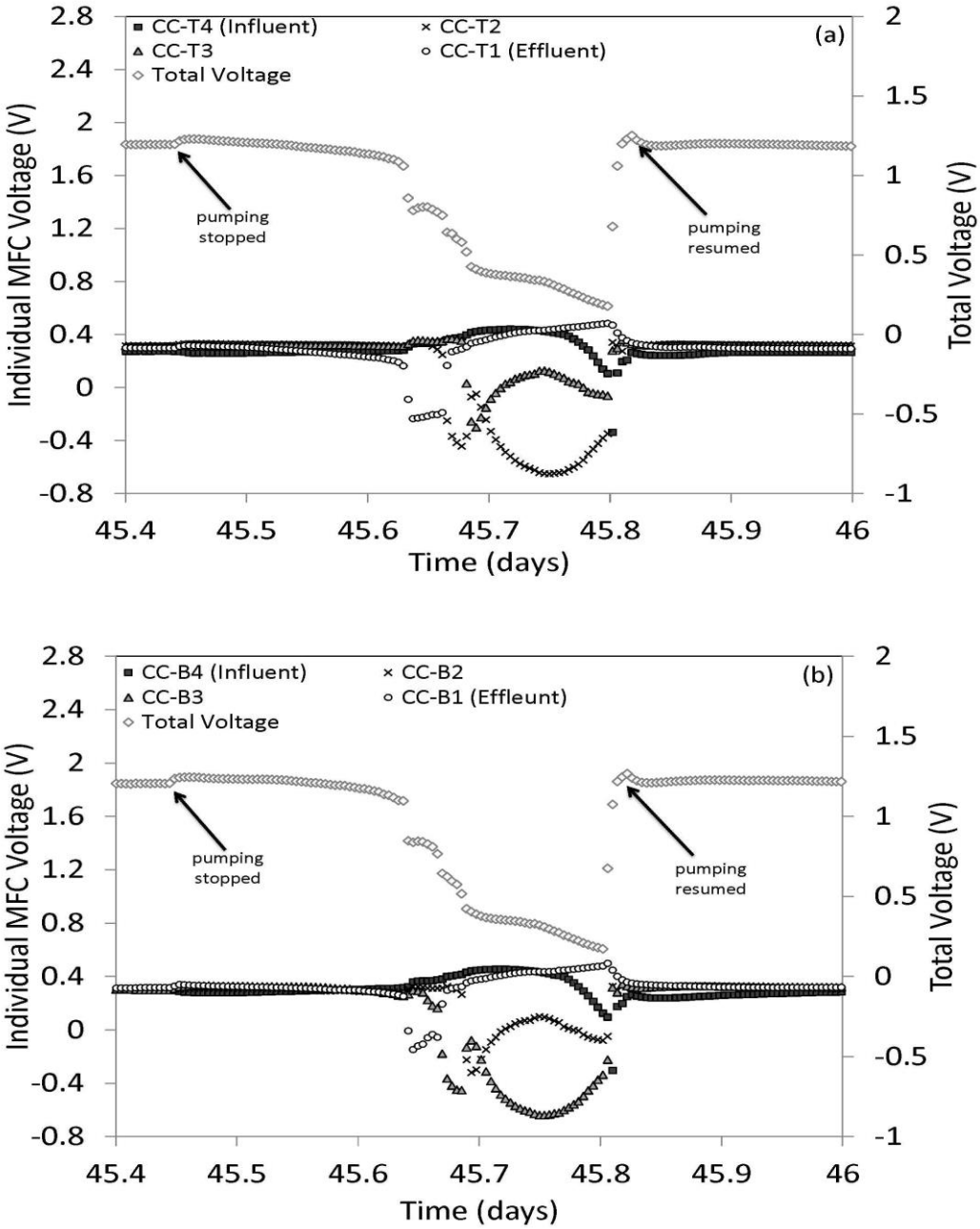

FIGURE 5.6: Total voltage and individual MFC voltage as a function of time for (a) the top reactor; and (b) the bottom reactor showing voltage reversal during the 8 hour period when the pump was stopped.

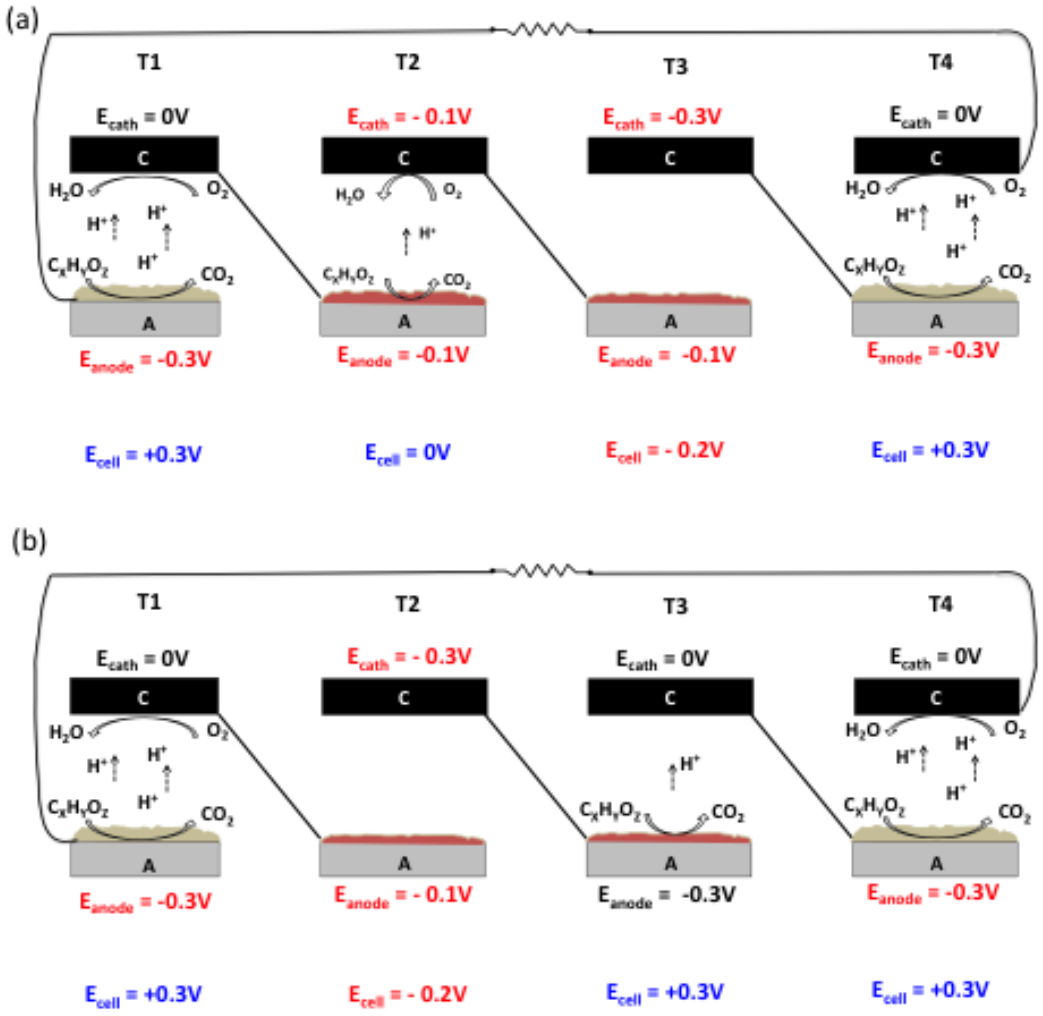

FIGURE 5.7: (a) Schematic showing voltage reversal in MFC T3 leading to decreased cathode potential of T2 due to the reduced biofilm activity on the anode of T3. Reduced cathode potential of T2 leads to increased anode potential of T2 as biofilm activity of T2 anode begins to decrease; and (b) MFC T2 eventually experiences voltage reversal as T2 cathode potential decreases and T2 anode potential increases. The decreased cathode potential of T2 decreases the anode potential of T3 eventually leading to voltage re-reversal of MFC T3 (i.e., the MFC voltage becomes positive again).

Individual cell voltages of the bottom reactor reached as low as -0.63 V. However, the voltage reversal sequence did not follow the cascading effect as that observed in the top reactor. It can be seen from Figure 5.6 b that the order of voltage

reversal in the individual cells was as follows: B1 (effluent), followed by B3, then B2, with a decrease in B4 (influent) but no reversal for the 8 hour duration of the test. It is possible that B3 experienced a greater internal resistance change than B2 after pump stoppage due to separator deformation and/or air trapped between the electrodes in addition to fuel starvation. The total effect of voltage reversal on reactor performance was a drop in total voltage by more than 85% from 1.2 V to 0.17 V. Once the pump was restarted, voltage returned to 1.2 V, for both the top and bottom reactor, indicating complete recovery.

5.3.4 Voltage reversal caused by gas accumulation in the reactor

The MFCs were previously operated with gas venting ports at the effluent end of each anode chamber to avoid biogas buildup. To investigate the impact of potential gas accumulation on voltage reversal, gas was allowed to build-up in the reactor. Voltages were monitored to determine when voltage reversal began. Following a period of voltage reversal, gas was primed out of the reactor and the composition measured as 71.33% N_2 and 28.67% CO_2. The presence of CO_2 indicated that gas build-up in the reactor could be attributed to microbial metabolism. After 30 hours of operation, individual cell voltages dropped more than 4-fold to below -0.9 V in individual cells of the bottom and top reactor (Figure 5.8). Gas build-up likely occurred within the anode chamber on the surface of the anodes as well as becoming trapped between the separator and electrodes. Trapped gas between the separator and electrodes may increase the internal resistance of some cells leading to an imbalance in voltage between cells in the reactor [124]. Gas build-up on the surface of the

anode in the anode chamber may also contribute to voltage reversal by limiting mass transfer of substrate to the biofilm thus producing a similar phenomenon to that caused by fuel starvation, leading to an increased anode potential [87]. It would be expected that gas accumulation would affect the top reactor more than the bottom reactor. However, this was not the case, both reactors were effected equally by the gas build-up. This was likely due to hydraulically dead spaces within the reactor caused by the addition of the perforated spacers. Although one purpose of the spacer was to increase mixing, this may not have been the case. The effect on performance likely caused by the spacers may also be, in part, the reason for the slightly lower power production compared to that previously reported for a similar iCiS CEA-MFC reactor [129]. Although, in the previous case a higher catalyst loading was used, which would also contribute to the higher performance of that reactor compared to the one presented here.

In addition, it can be seen from Figure 5.8 that there was a second reversal event. The second voltage reversal was likely caused by trapped gas becoming dislodged, moving through the reactor, and then becoming trapped again. Gas can also become trapped in the reactor when flow rates are not sufficient to move air through the reactor or if the flow rate is not sufficient enough to prevent dead spaces within the anode chambers. The overall effect of voltage reversal was a drop in total voltage of the bottom reactor by 67%, from 1.2 V to 0.4 V, and a drop by nearly 73% from 1.2 V to 0.33 V for the top reactor (Figure 5.8). While it's not clear which gas trapping mechanism is dominant in the present reactor, complete voltage recovery occurred once gas build-up was primed through the reactor, suggesting that voltage

reversal caused by gas build up might be avoided through proper design and operation of MFC reactors.

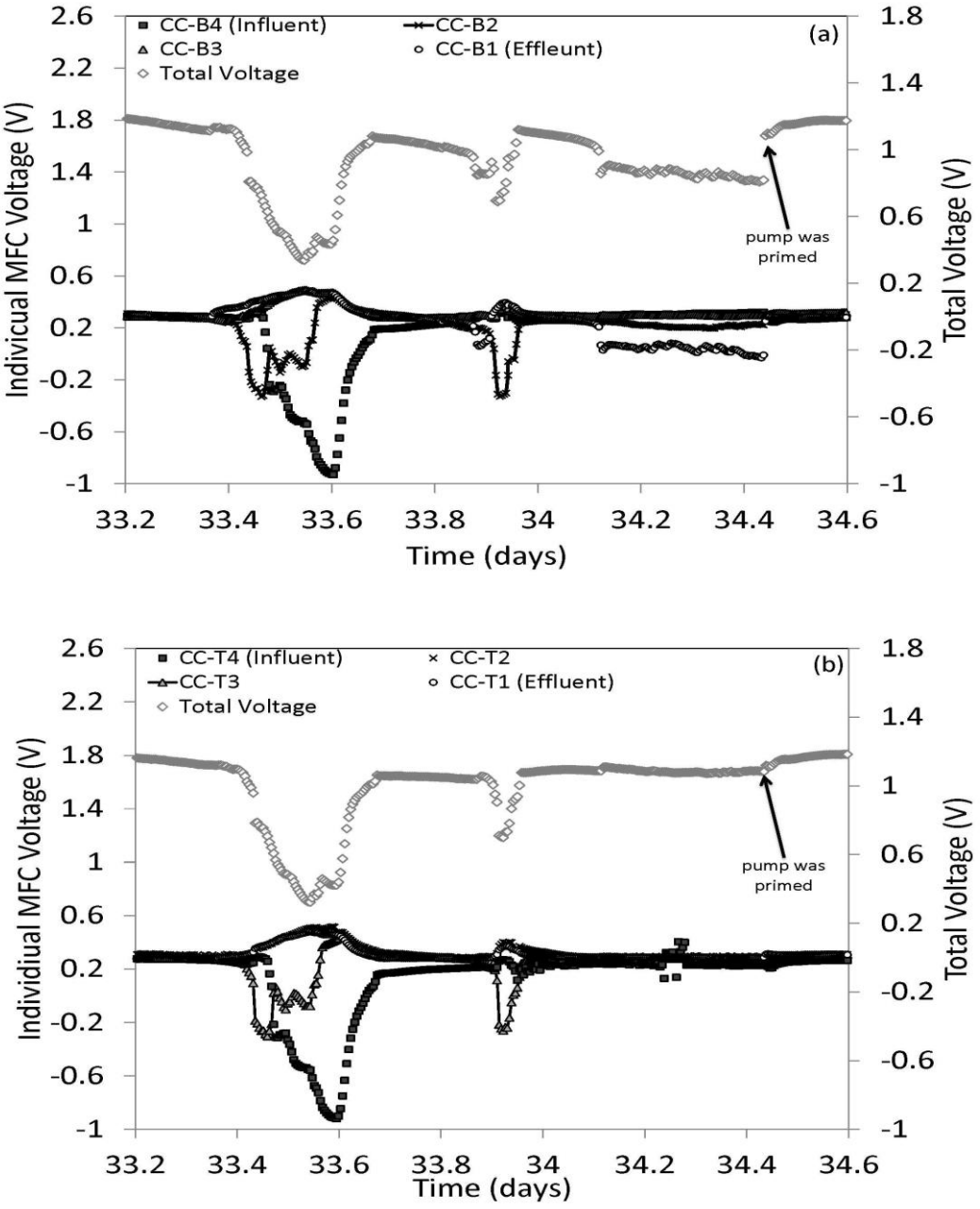

FIGURE 5.8: Total voltage and individual MFC voltage as a function of time for (a) the bottom reactor; and (b) the top reactor during voltage reversal caused by gas build-up in the reactor.

5.3.5 Voltage reversal caused by large decreases in external resistance at higher current densities

External resistance is typically adjusted to facilitate the growth and maturation of anodic biofilm and to maximize the power output. Previous results operating individual MFCs have shown that large decreases in external resistance can result in significant voltage drop due to power overshoot [142,143]. Power overshoot caused by large decreases in external resistance can lead to performance loss during start-up as well as during normal operation. Significant decreases in external resistance can lead to mass transfer limitations at both the anode and cathode due to insufficient reactants. Results show that with large decreases in external resistance by more than 75%, voltage reversal occurs instantly. Individual cells of the bottom reactor reached as low as -0.43 V while cells of the top reactor reached as low as -0.35 V (Figure 5.9). Due to the fact that the external resistance connection was between the effluent and influent cells, reversal occurred first in the influent cell followed by the effluent cell. The cause of reversal is likely due to mass transfer limitations of the biofilm created by the decrease in external resistance. If the decrease in external resistance is large enough, the biofilm lacks the catalytic ability to keep up with the demand [84]. As a result of lowered catalytic activity on both the anode and cathode, the potential of the anode becomes more positive while the potential of the cathode becomes more negative eventually leading to voltage reversal. Although voltages of both the bottom and top MFC stacks dropped by more than 75% as a result of reversal (Figure 5.9), they returned to 1.2 V once external resistance was returned to the pre-reversal value.

When external resistance of only the bottom MFC stack was decrease by 75%,

voltage reversal occurred only in the bottom reactor with the top reactor remaining largely unaffected (Figure 5.10). The decrease in total voltage of the bottom reactor was similar to the decrease observed when external resistance was decrease for both the top and bottom reactor. Ionic cross-conductance which results in reduced power and voltage has been shown to occur in electrically serially connected MFCs with a shared anode chamber [29,131]. However, it is likely that the spacing between anodes of the top and bottom reactor is large enough to prevent cross conductance, which could occur as a result of the difference in potential between the reversed anode and the opposite anode if the anodes shared the same chamber with smaller spacing. The voltage returned to 1.2 V when external resistance of the bottom reactor was increased to the pre-reversal value, indicating complete recovery following voltage reversal over a four-hour period. However, longer durations of voltage reversal may cause damage to the biofilm resulting in incomplete recovery of voltage or total loss of voltage. Further investigation is needed to determine the length of time a biofilm can sustain the effects of voltage reversal.

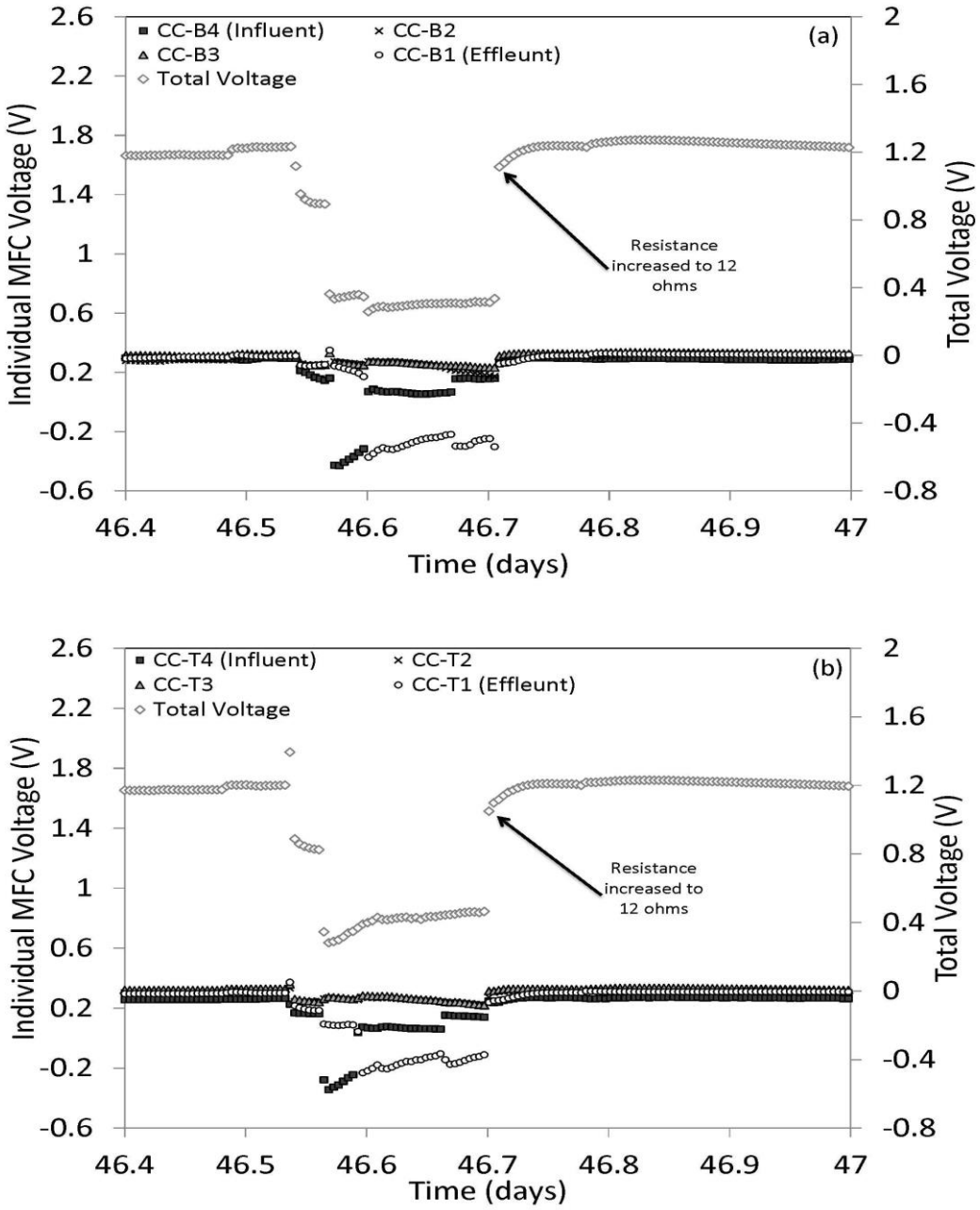

FIGURE 5.9: Total voltage and individual MFC voltage as a function of time for (a) the bottom reactor; and (b) the top reactor during voltage reversal caused by a 75% decrease in external resistance form 12 ohms to 3 ohms of both the top and bottom reactor.

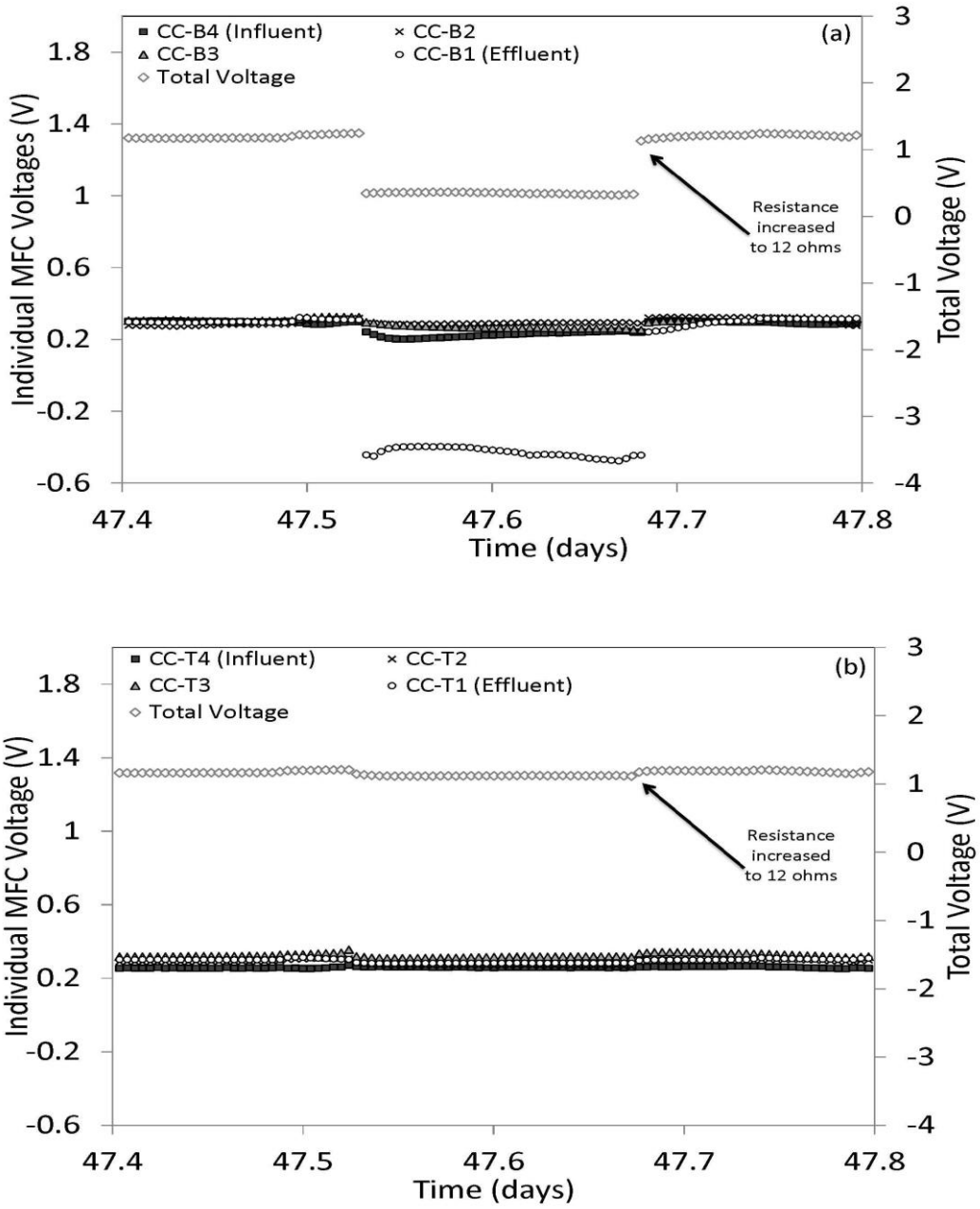

FIGURE 5. 10: Total voltage and individual MFC voltage as a function of time for (a) the bottom reactor; and (b) the top reactor during voltage reversal caused by a 75% decrease in external resistance from 12 ohms to 3 ohms of the bottom reactor only.

5.3.6 Implications for MFC design and operation

Voltage reversal will occur during practical application as a result of differences in internal resistance between cells when MFCs are connected in series. The differences in internal resistance led to voltage imbalance, which ultimately led to voltage reversal between cells in the series. Voltage reversal induced corrosion of stainless steel base materials indicate that cathodes containing metal base materials are likely not suitable for use in MFCs connected electrically in series. This limits the use of cathodes containing metal base materials to only certain applications. On the other hand, carbon cloth based cathodes were unaffected by voltage reversal, further demonstrating the potential of this material for use as a base material in cathodes for scaling-up MFC technology.

The full recovery of iCiS CEA-MFC stacks containing carbon cloth cathodes following voltage reversal demonstrates the great potential of this design for MFC applications in which series electrical connection is needed to increase voltage. In spite of the fact that the voltage reversal of iCiS CEA-MFC stacks only occurred under extreme operational conditions in this study, the potential for voltage reversal always exists when MFCs are connected electrically in series. Finding ways to prevent or lesson the effects of voltage reversal is key for useful voltages to be produced during practical application of MFC technology.

Various power management methods have been proposed to circumvent voltage reversal in MFCs. However, use of power management systems such as diodes connected in between individual cells in the series [121], DC/DC converters to

increase voltage [119,123,144,145], and using MFCs to charge capacitors in parallel and discharge capacitors in series [122] may result in significant voltage losses of 40-60% [119,121–123,144,145]. In the absence of efficient external power management systems, a general strategy to prevent or lesson the severity of voltage reversal is to minimize the differences in internal resistance between cells connected in series. Since electrode and separator materials are typically the same for all the cells, the biofilm may have the greatest impact on internal resistance differences, if the individual cells are assembled properly. Differences in performance of the biofilm between cells can be caused by different operational conditions within individual cells, for example, low substrate concentration in one cell. Differences in biofilm performance between cells can also result from differences arising during start-up of MFCs [146]. As a result, strict control of conditions during start-up would lead to more uniform biofilm performance between different MFCs. One method is to set the potential of the anode. Previous studies have shown the beneficial effects for facilitating growth and maturation of the biofilm by setting the anode potential [146–150].

In the present study, voltage reversal caused by operational conditions led to a significant reduction in total voltage and high negative voltages of individual MFCs connected in series. The results indicate that properly controlling operating conditions is also an effective way of avoiding voltage reversal in the iCiS CEA-MFC. Other approaches to reduce the possibility of voltage reversal may include (1) designing electrode materials with high capacitance to increase their tolerance to current

changes[151–156] and (2) Setting the potential of the anode to facilitate uniform growth of anodic biofilms during start-up[146–150].

6. CONCLUSION & FUTURE WORK

6.1 CONCLUSION

6.1.1 Cathode development and optimization

In the first part of this work, a high performing and stable cathode was developed for use in scaling-up MFCs. Both metal and carbon based materials were evaluated and compared as base materials for MFC cathodes. The study was conducted using carbon cloth and several finer stainless steel mesh sizes. Electrochemical testing results showed that cathodes containing the finest metal mesh size outperformed more coarse mesh sizes as well as cathodes containing carbon cloth. However, operation of cathodes in MFCs showed that cathodes containing carbon cloth as the base material outperformed cathodes containing all different mesh sizes. The lower performance in MFCs of the cathodes containing metal base materials was attributed to corrosion of the stainless steel mesh. It was determined that corrosion of stainless steel mesh likely occurred, at least in part, due to the pressing procedure used to fix the catalyst to the base material. This result suggests that metal based supporting materials may be limited to certain applications. As mentioned in Chapter 2, the majority of MFC studies reported in the literature use metal base materials as the supporting material for activated carbon cathodes. As a result, the work presented here has significant implications for the future direction of cathode development in the field of MFC research.

The use of inexpensive activated carbon as a catalyst for MFC cathodes was a breakthrough in MFC research, as it increased the economic feasibility of scaling-up MFC technology. As mentioned in Chapter 3, previous attempts to correlate the

physical and chemical properties of activated carbon with performance yielded contradictory results. As a result, activated carbon powders made from bamboo, peat, coal, coconut, and hardwood sources were characterized in terms of their surface area, pore size distribution, surface chemistry, and conductivity to better understand the linkages between the physical properties of activated carbon and their electrochemical performance with carbon cloth as the base material. This is the first time conductivity of activated carbon has been linked to performance of MFC cathodes. The results indicated that higher proportion of micorpore surface area/volume, higher conductivity, and lower C/O ratio all contributed to the higher performance. Based off of this analysis, a cathode containing the highest performing activated carbon as the catalyst was developed and optimized.

The bamboo-based AC demonstrated the highest potential for use as a catalyst for carbon cloth based cathodes, reaching -10.6 A m^{-2} and -11.27 A m^{-2} at 0V during electrochemical testing with loading of 25mg cm^{-2} and 50mg cm^{-2}, respectively. The results demonstrated for the first time the high performance of activated carbon containing bamboo as the source material as a catalyst for MFC cathodes. Furthermore, the loading required to achieve the high electrochemical performance is lower than that typically used with activated carbons based from other source materials. To further develop the cathode for use in scaling-up MFCs, the hydrostatic pressure tolerance as well as the performance and stability while operating in MFCs were evaluated. The maximum power density reached 3.3 Wm^{-2} in CEA-MFCs and 2.6 Wm^{-2} in cube-MFCs, which are much higher than that typically reported for single-chamber MFCs. In addition, the hydrostatic pressure tolerance of the bamboo-

based AC carbon cloth cathode is greater than 1.8 m, allowing for a more versatile cathode, suitable for use in many different reactor design configurations.

6.1.2 Scaled-up MFC design and operation

In the second part of this work, performance and stability of the activated carbon cathode containing carbon cloth as the base material was evaluated at a larger scale and over the long-term (one year). A novel internally connected in series scaled-up CEA-MFC design was used to evaluate the cathode. The new CEA-MFC design was also simultaneously evaluated to determine reactor performance at larger scales under various operating conditions. Scale-up of MFCs is typically done by increasing MFC size or connecting multiple MFCs into stacks. The iCiS design is ideally suited for both of these scale-up approaches. The internal series electrical connection alleviated the need for current collectors, which would normally be required when increasing electrode size and connecting MFCs into stacks, as was done here. The lack of a current collector also reduced the cost of fabrication, which increases the overall economic feasibility of MFC technology for practical application. Finally, different operational conditions, such as HRT as well as substrate and buffer concentration, were examined to determine the most appropriate operational mode to maximize power in the reactor.

Maximum power density reached as high as 3.5 W m^{-2}, which is 6% higher than that reported for a similar smaller CEA-MFC, indicating that power can be maintained during scale-up with a greater than 33-fold increase in total cathode surface area and greater than 20-fold increase in reactor volume. Evaluation of different operational conditions showed that higher substrate concentration (COD =

6000 mg L^{-1}), at shorter HRTs (1.33 hours), led to the highest power generation. The high performance could be attributed to both the CEA structure and the design of internal series connection, which lead to lower internal resistance. The lowered internal resistance combined with the fact that the reactor was acclimated (first 100 days of operation) at the higher acetate concentration (5.9 gL^{-1}), may also have allowed a highly efficient anodic biofilm to develop. In addition, relatively low performance when operated at low substrate concentration (COD = 500 mg/L) and low buffer concentration (10 mM PBS) suggests that the reactor may be more ideally suited to treat high strength (COD) industrial wastewaters such as brewery or food processing wastewaters. With this design, reactor size was increased significantly with no decrease in performance, as is typically the case when increasing MFC reactor size. Furthermore, results demonstrated that when activated carbon/carbon cloth cathodes are used in iCiS CEA-MFCs, stable power can be produced over long-term operation, making this design ideal for scaling-up MFC technology.

When MFCs are connected electrically in series, voltage reversal can occur, ultimately reducing performance. As a result, the effect of voltage reversal on reactor performance and cathode stability was evaluated when activated carbon cathodes containing carbon cloth or stainless steel mesh as the base material were used in an iCiS CEA-MFC reactor. To further investigate the voltage reversal phenomenon, different conditions occurring during continuous operation that could lead to voltage reversal were also examined and discussed. Full recovery following voltage reversal indicated that MFCs containing activated carbon cathodes with carbon cloth as the base material were unaffected by voltage reversal.

Power production when activated carbon/carbon cloth cathodes were used was as much as 300% higher than that achieved with reactors containing stainless steel mesh as the base material. Lower power production of the reactors containing metal mesh as the base material was a result of the corrosion that likely occurred from high negative potentials (> -0.6 V) during voltage reversal. In Chapter 2, the onset of corrosion on cathodes containing stainless steel mesh as the base material was largely attributed to the pressing procedure used to prepare the cathode. However, despite a new preparation procedure that alleviated the need for pressing the catalyst onto the base material, corrosion still occurred on the cathode with stainless steel mesh as the base material. This result indicates that cathodes containing metal base materials may not be suitable for use in MFCs connected electrically in series, which limits their use for scaling-up MFC technology.

Voltage reversal was caused by three conditions occurring during operation: (1) gas build-up within the reactor; (2) pump stoppage; and (3) large decreases in external resistance at higher current density. The results indicated that negative MFC voltages occurred in only some of the MFCs connected electrically in series. However, the total stack voltage could be decreased 67 to 85% as a result of voltage reversal caused by these operational conditions. Full recovery following voltage reversal was observed in all cases after normal operating conditions were restored in the MFC stacks. These results suggest that voltage reversal can be avoided through proper operation and design of MFC stacks and in the event voltage reversal occurs, full recovery is possible with the iCiS CEA-MFC.

6.2 FUTURE WORK

6.2.1 Further cathode development

Although results presented here indicate the high stability of carbon cloth as the base material for activated carbon cathodes, results presented in the chemical fuel cell literature suggest that corrosion and catalyst agglomeration/dissolution can occur at certain potentials depending on operational conditions and the type of catalyst used. As a result, further work is needed to determine under what operating conditions and applied potentials corrosion of the activated carbon/carbon cloth cathode will occur, if at all. In addition, based on the current design, further increases in reactor size will lead to increases in cathode size. Increased cathode size will lead to increases in ohmic resistance. Consequently, it will be necessary to determine at which point electrode size becomes the limiting factor to performance. In order to further reduce costs, which will increase the economic feasibility for practical application of MFC technology, lower-cost conductive carbon fiber based materials should be examined as base materials for MFC cathodes. Finally, the characteristics of activated carbon that effect performance in MFCs are determined from both the type of source material used as well as the process used to prepare the activated carbon. Future work regarding activated carbon catalysts should focus on determining how preparation temperature and activation process affect key characteristics of activated carbon related to performance as MFC cathodes.

6.2.2 Reactor design and operation

To further increase performance of the iCiS CEA-MFC, the reactor design should be modified so that the cathodes can be operated vertically. Vertical operation, in combination with proper gas ventilation, will ensure gas build-up does not occur within the CEA structure, ultimately resulting in similar power between stacks of the iCiS CEA-MFC reactor. In addition, results presented here suggest that variability in voltage and power production between MFCs connected electrically in series may have resulted from differences in biofilm development between individual MFCs in the series. Further work is needed to confirm if this is indeed the case. Controlling conditions during biofilm development by setting the anode potential during reactor start-up will likely decrease the differences between individual MFCs connected electrically in series, ultimately resulting in similar performance between MFCs. Similar performance between individual MFCs connected electrically in series will reduce voltage imbalances, thereby maximizing performance and reducing the risk of voltage reversal.

In spite of the fact that voltage reversal of iCiS CEA-MFC stacks only occurred under extreme operational conditions in this study, the potential for voltage reversal always exists when MFCs are connected electrically in series. Finding ways to prevent or lesson the effects of voltage reversal is key for useful voltages to be produced during practical application of MFC technology. Novel electrode materials with high capacitance, to increase their tolerance to changes in current, should be designed and evaluated in the iCiS CEA-MFC. Furthermore, in order to minimize the effect of detrimental operating conditions during larger-scale power generation, iCiS

CEA-MFC connection type should be investigated to optimize performance. For example, different combinations of parallel and series electrical connection should be evaluated to determine the optimum connection type to maximize voltage, current, and power production. In addition, under different connection schemes, both series and parallel hydraulic flow through individual stacks and between stacks should be examined to determine how flow regime and different operational conditions under these flow regimes affect performance. Further scaling up this reactor could be accomplished by increasing the number of MFCs connected in series as well as further increasing the size of each MFC. Future investigation into scaling-up the iCiS CEA-MFC design will ultimately determine any limitations with respect to size and reactor effectiveness for practical application.

The performance of the iCiS CEA-MFC stacks should be evaluated using real wastewaters. High COD strength wastewaters such as brewery and food processing waste streams should be the initial targets. As mentioned in Chapter 4, most MFC studies reported in the literature achieved high power at low substrate (1 gL^{-1} acetate) concentration. However, this was not the case here in which a relatively low power density was achieved at low substrate concentration compared to that achieved at higher concentrations. The reactor used here was acclimated at higher substrate concentration (5.9 gL-1 acetate) for the first 100 days of operation, possibly resulting in an anodic biofilm more suited to this concentration. This may be, in part, the reason for the relatively low performance achieved at the lower substrate concentration. As a result, future work should investigate acclimating the iCiS CEA-

MFC reactor with lower substrate concentrations to determine if performance can be improved.

Finally, real waste streams may contain organic material that is not as readily degradable as the relatively simple substrate (acetate) used here. In addition, real waste streams may not contain all the nutrients required for bacterial growth. As a result, it will be necessary to determine the effect that these factors have on performance of the iCiS CEA-MFC reactor. Furthermore, real waste streams often have low conductivity and buffer capacity. The relatively low performance of the iCiS CEA-MFC reactor when operated at low buffer concentration suggest that solution conductivity and buffer capacity may present an issue during scale-up of this design. Although this problem is not unique to the iCiS CEA-MFC design, it is one that may need to be overcome. Results of the work outlined above will be key in moving MFC technology towards practical application.

7. BIBLIOGRAPHY

[1] FOOD AND AGRICULTURE ORGANIZATION OF THE UNITED NATIONS, Coping with water scarcity An action framework for agriculture and food security, United Nations, 2012.

[2] UN WWAP, The World Water Development Report 1: Water for People, Water for Life., United Nations World Water Assessment Programme, Paris, France, 2003.

[3] Corcoran, E, Nellemann, C., Baker, E., Bos, R., Osbonr, D., Savelli, H. (eds), Sick Water? The central role of wastewater treatment management in sustainable development., United Nations Environment Programme, 2010.

[4] ASCE, 2013 Report Card for Ammericas Infrastructure, American Society for Civil Engineers, 2013. WWW.INFRASTRUCTUREREPORTCARD.ORG.

[5] EPA Office of Water, Wastewater Management Fact Sheet, Energy Conservation, U.S. Environmental Protection Agency, 2006.

[6] T.P. Curtis, Low-Energy Wastewater Treatment: Strategies and Technologies, in: R. Mitchell, J.-D. Gu (Eds.), Environ. Microbiol., John Wiley & Sons, Inc., 2010: pp. 301–318. http://onlinelibrary.wiley.com/doi/10.1002/9780470495117.ch13/summary (accessed July 16, 2013).

[7] U.S. Energy Information Administration, Electric Power Annual 2012, U.S Department of Energy, 2013. http://www.eia.gov/electricity/annual/pdf/epa.pdf (accessed January 24, 2015).

[8] WERF, Energy Production and Efficiency Research-The Roadmap to Net-Zero Energy, Water Environment Research Foundation, 2011. www.werf.org.

[9] P.L. McCarty, J. Bae, J. Kim, Domestic Wastewater Treatment as a Net Energy Producer–Can This be Achieved?, Environ. Sci. Technol. 45 (2011) 7100–7106. doi:10.1021/es2014264.

[10] H. Liu, R. Ramnarayanan, B.E. Logan, Production of Electricity during Wastewater Treatment Using a Single Chamber Microbial Fuel Cell, Environ. Sci. Technol. 38 (2004) 2281–2285. doi:10.1021/es034923g.

[11] M.C. Potter, Electrical Effects Accompanying the Decomposition of Organic Compounds, Proc. R. Soc. Lond. B Biol. Sci. 84 (1911) 260–276. doi:10.1098/rspb.1911.0073.

[12] B.E. Logan, Scaling up microbial fuel cells and other bioelectrochemical systems, Appl. Microbiol. Biotechnol. 85 (2010) 1665–1671.

[13] K. Rabaey, G. Lissens, S.D. Siciliano, W. Verstraete, A microbial fuel cell capable of converting glucose to electricity at high rate and efficiency, Biotechnol. Lett. 25 (2003) 1531–1535.

[14] Y. Fan, H. Hu, H. Liu, Enhanced Coulombic efficiency and power density of air-cathode microbial fuel cells with an improved cell configuration, J. Power Sources. 171 (2007) 348–354. doi:10.1016/j.jpowsour.2007.06.220.

[15] B. Logan, S. Cheng, V. Watson, G. Estadt, Graphite Fiber Brush Anodes for Increased Power Production in Air-Cathode Microbial Fuel Cells, Environ. Sci. Technol. 41 (2007) 3341–3346. doi:10.1021/es062644y.

[16] B.E. Logan, Exoelectrogenic bacteria that power microbial fuel cells, Nat. Rev. Microbiol. 7 (2009) 375–381. doi:10.1038/nrmicro2113.
[17] K. Carns, BRINGING ENERGY EFFICIENCY TO THE WATER AND WASTEWATER INDUSTRY: HOW DO WE GET THERE?, Proc. Water Environ. Fed. 2005 (2005) 7650–7659. doi:10.2175/193864705783813728.
[18] D.A. Lashof, D.R. Ahuja, Relative contributions of greenhouse gas emissions to global warming, Nature. 344 (1990) 529–531. doi:10.1038/344529a0.
[19] Gao, N., Lesnik, K.L., Bermek, H., Liu, H., Microbial Fuel Cells: From Fundamentals to Wastewater Treatment Applications, In Press, n.d.
[20] K. Rabaey, Bioelectrochemical Systems: From Extracellular Electron Transfer to Biotechnological Application, IWA Publishing, 2010.
[21] H. Liu, H. Hu, J. Chignell, Y. Fan, Microbial electrolysis: novel technology for hydrogen production from biomass, Biofuels. 1 (2010) 129–142. doi:10.4155/bfs.09.9.
[22] D.R. Lovley, Powering microbes with electricity: direct electron transfer from electrodes to microbes, Environ. Microbiol. Rep. 3 (2011) 27–35. doi:10.1111/j.1758-2229.2010.00211.x.
[23] S. Jung, J.M. Regan, Comparison of anode bacterial communities and performance in microbial fuel cells with different electron donors, Appl. Microbiol. Biotechnol. 77 (2007) 393–402. doi:10.1007/s00253-007-1162-y.
[24] K.L. Lesnik, H. Liu, Establishing a core microbiome in acetate-fed microbial fuel cells, Appl. Microbiol. Biotechnol. 98 (2014) 4187–4196. doi:10.1007/s00253-013-5502-9.
[25] J. Wei, P. Liang, X. Huang, Recent progress in electrodes for microbial fuel cells, Bioresour. Technol. 102 (2011) 9335–9344. doi:10.1016/j.biortech.2011.07.019.
[26] S. Cheng, B.E. Logan, Increasing power generation for scaling up single-chamber air cathode microbial fuel cells, Bioresour. Technol. 102 (2011) 4468–4473. doi:10.1016/j.biortech.2010.12.104.
[27] J.R. Kim, J. Rodríguez, F.R. Hawkes, R.M. Dinsdale, A.J. Guwy, G.C. Premier, Increasing power recovery and organic removal efficiency using extended longitudinal tubular microbial fuel cell (MFC) reactors, Energy Environ. Sci. 4 (2011) 459–465. doi:10.1039/C0EE00073F.
[28] A. Gálvez, J. Greenman, I. Ieropoulos, Landfill leachate treatment with microbial fuel cells; scale-up through plurality, Bioresour. Technol. 100 (2009) 5085–5091. doi:10.1016/j.biortech.2009.05.061.
[29] L. Zhuang, Y. Zheng, S. Zhou, Y. Yuan, H. Yuan, Y. Chen, Scalable microbial fuel cell (MFC) stack for continuous real wastewater treatment, Bioresour. Technol. 106 (2012) 82–88. doi:10.1016/j.biortech.2011.11.019.
[30] L. Zhuang, Y. Yuan, Y. Wang, S. Zhou, Long-term evaluation of a 10-liter serpentine-type microbial fuel cell stack treating brewery wastewater, Bioresour. Technol. 123 (2012) 406–412. doi:10.1016/j.biortech.2012.07.038.
[31] P. Liang, M. Fan, X. Cao, X. Huang, Evaluation of applied cathode potential to enhance biocathode in microbial fuel cells, J. Chem. Technol. Biotechnol. 84 (2009) 794–799. doi:10.1002/jctb.2114.

[32] H. Liu, S. Cheng, L. Huang, B.E. Logan, Scale-up of membrane-free single-chamber microbial fuel cells, J. Power Sources. 179 (2008) 274–279. doi:10.1016/j.jpowsour.2007.12.120.
[33] H. Liu, S. Cheng, B.E. Logan, Power Generation in Fed-Batch Microbial Fuel Cells as a Function of Ionic Strength, Temperature, and Reactor Configuration, Environ. Sci. Technol. 39 (2005) 5488–5493. doi:10.1021/es050316c.
[34] D. Jiang, M. Curtis, E. Troop, K. Scheible, J. McGrath, B. Hu, et al., A pilot-scale study on utilizing multi-anode/cathode microbial fuel cells (MAC MFCs) to enhance the power production in wastewater treatment, Int. J. Hydrog. Energy. 36 (2011) 876–884. doi:10.1016/j.ijhydene.2010.08.074.
[35] P. Clauwaert, S. Mulenga, P. Aelterman, W. Verstraete, Litre-scale microbial fuel cells operated in a complete loop, Appl. Microbiol. Biotechnol. 83 (2009) 241–247. doi:10.1007/s00253-009-1876-0.
[36] Y. Fan, S.-K. Han, H. Liu, Improved performance of CEA microbial fuel cells with increased reactor size, Energy Environ. Sci. 5 (2012) 8273. doi:10.1039/c2ee21964f.
[37] H. Dong, H. Yu, X. Wang, Q. Zhou, J. Feng, A novel structure of scalable air-cathode without Nafion and Pt by rolling activated carbon and PTFE as catalyst layer in microbial fuel cells, Water Res. 46 (2012) 5777–5787. doi:10.1016/j.watres.2012.08.005.
[38] X. Zhang, X. Xia, I. Ivanov, X. Huang, B.E. Logan, Enhanced Activated Carbon Cathode Performance for Microbial Fuel Cell by Blending Carbon Black, Environ. Sci. Technol. (2014). doi:10.1021/es405029y.
[39] F. Zhang, D. Pant, B.E. Logan, Long-term performance of activated carbon air cathodes with different diffusion layer porosities in microbial fuel cells, Biosens. Bioelectron. 30 (2011) 49–55. doi:10.1016/j.bios.2011.08.025.
[40] F. Zhang, S. Cheng, D. Pant, G.V. Bogaert, B.E. Logan, Power generation using an activated carbon and metal mesh cathode in a microbial fuel cell, Electrochem. Commun. 11 (2009) 2177–2179. doi:10.1016/j.elecom.2009.09.024.
[41] D. Pant, G. Van Bogaert, M. De Smet, L. Diels, K. Vanbroekhoven, Use of novel permeable membrane and air cathodes in acetate microbial fuel cells, Electrochimica Acta. 55 (2010) 7710–7716. doi:10.1016/j.electacta.2009.11.086.
[42] S. Cheng, J. Wu, Air-cathode preparation with activated carbon as catalyst, PTFE as binder and nickel foam as current collector for microbial fuel cells, Bioelectrochemistry. 92 (2013) 22–26. doi:10.1016/j.bioelechem.2013.03.001.
[43] B. Wei, J.C. Tokash, G. Chen, M.A. Hickner, B.E. Logan, Development and evaluation of carbon and binder loading in low-cost activated carbon cathodes for air-cathode microbial fuel cells, RSC Adv. 2 (2012) 12751–12758. doi:10.1039/C2RA21572A.
[44] V.J. Watson, C. Nieto Delgado, B.E. Logan, Influence of Chemical and Physical Properties of Activated Carbon Powders on Oxygen Reduction and Microbial Fuel Cell Performance, Environ. Sci. Technol. 47 (2013) 6704–6710. doi:10.1021/es401722j.

[45] H. Dong, H. Yu, X. Wang, Catalysis kinetics and porous analysis of rolling activated carbon-PTFE air-cathode in microbial fuel cells, Environ. Sci. Technol. 46 (2012) 13009–13015. doi:10.1021/es303619a.
[46] S. Cheng, H. Liu, B.E. Logan, Power Densities Using Different Cathode Catalysts (Pt and CoTMPP) and Polymer Binders (Nafion and PTFE) in Single Chamber Microbial Fuel Cells, Environ. Sci. Technol. 40 (2006) 364–369. doi:10.1021/es0512071.
[47] F. Zhang, G. Chen, M.A. Hickner, B.E. Logan, Novel anti-flooding poly(dimethylsiloxane) (PDMS) catalyst binder for microbial fuel cell cathodes, J. Power Sources. 218 (2012) 100–105. doi:10.1016/j.jpowsour.2012.06.088.
[48] F. Zhang, T. Saito, S. Cheng, M.A. Hickner, B.E. Logan, Microbial Fuel Cell Cathodes With Poly(dimethylsiloxane) Diffusion Layers Constructed around Stainless Steel Mesh Current Collectors, Environ. Sci. Technol. 44 (2010) 1490–1495. doi:10.1021/es903009d.
[49] Z. Luo, Z. Zhang, W. Wang, W. Liu, Q. Xue, Various curing conditions for controlling PTFE micro/nano-fiber texture of a bionic superhydrophobic coating surface, Mater. Chem. Phys. 119 (2010) 40–47. doi:10.1016/j.matchemphys.2009.07.039.
[50] Z. Li, L. Yao, L. Kong, H. Liu, Electricity generation using a baffled microbial fuel cell convenient for stacking, Bioresour. Technol. 99 (2008) 1650–1655. doi:10.1016/j.biortech.2007.04.003.
[51] Q. Deng, X. Li, J. Zuo, A. Ling, B.E. Logan, Power generation using an activated carbon fiber felt cathode in an upflow microbial fuel cell, J. Power Sources. 195 (2010) 1130–1135.
[52] H. Dong, H. Yu, H. Yu, N. Gao, X. Wang, Enhanced performance of activated carbon–polytetrafluoroethylene air-cathode by avoidance of sintering on catalyst layer in microbial fuel cells, J. Power Sources. 232 (2013) 132–138. doi:10.1016/j.jpowsour.2013.01.036.
[53] X. Wang, C. Feng, N. Ding, qingrui zhang, N. Li, X. Li, et al., Accelerated OH- Transport in Activated Carbon Air-cathode by Modification of Quaternary Ammonium for Microbial Fuel Cells, Environ. Sci. Technol. (2014). doi:10.1021/es5002506.
[54] X. Wang, N. Gao, Q. Zhou, H. Dong, H. Yu, Y. Feng, Acidic and alkaline pretreatments of activated carbon and their effects on the performance of air-cathodes in microbial fuel cells, Bioresour. Technol. 144 (2013) 632–636. doi:10.1016/j.biortech.2013.07.022.
[55] X. Xia, F. Zhang, X. Zhang, P. Liang, X. Huang, B.E. Logan, Use of Pyrolyzed Iron Ethylenediaminetetraacetic Acid Modified Activated Carbon as Air–Cathode Catalyst in Microbial Fuel Cells, ACS Appl. Mater. Interfaces. 5 (2013) 7862–7866. doi:10.1021/am4018225.
[56] J. Liu, Y. Feng, X. Wang, Q. Yang, X. Shi, Y. Qu, et al., The effect of water proofing on the performance of nickel foam cathode in microbial fuel cells, J. Power Sources. 198 (2012) 100–104. doi:10.1016/j.jpowsour.2011.09.078.

[57] S. Cheng, Y. Ye, W. Ding, B. Pan, Enhancing power generation of scale-up microbial fuel cells by optimizing the leading-out terminal of anode, J. Power Sources. 248 (2014) 931–938. doi:10.1016/j.jpowsour.2013.10.014.
[58] A. Dekker, A.T. Heijne, M. Saakes, H.V.M. Hamelers, C.J.N. Buisman, Analysis and Improvement of a Scaled-Up and Stacked Microbial Fuel Cell, Environ. Sci. Technol. 43 (2009) 9038–9042. doi:10.1021/es901939r.
[59] W.-W. Li, G.-P. Sheng, X.-W. Liu, H.-Q. Yu, Recent advances in the separators for microbial fuel cells, Bioresour. Technol. 102 (2011) 244–252. doi:10.1016/j.biortech.2010.03.090.
[60] F. Zhang, Z. Ge, J. Grimaud, J. Hurst, Z. He, In situ investigation of tubular microbial fuel cells deployed in an aeration tank at a municipal wastewater treatment plant, Bioresour. Technol. 136 (2013) 316–321. doi:10.1016/j.biortech.2013.02.107.
[61] X. Zhang, S. Cheng, X. Huang, B.E. Logan, The use of nylon and glass fiber filter separators with different pore sizes in air-cathode single-chamber microbial fuel cells, Energy Environ. Sci. 3 (2010) 659–664. doi:10.1039/B927151A.
[62] Y. Fan, E. Sharbrough, H. Liu, Quantification of the Internal Resistance Distribution of Microbial Fuel Cells, Environ. Sci. Technol. 42 (2008) 8101–8107. doi:10.1021/es801229j.
[63] H. Liu, B.E. Logan, Electricity Generation Using an Air-Cathode Single Chamber Microbial Fuel Cell in the Presence and Absence of a Proton Exchange Membrane, Environ. Sci. Technol. 38 (2004) 4040–4046. doi:10.1021/es0499344.
[64] S. Cheng, H. Liu, B.E. Logan, Increased Power Generation in a Continuous Flow MFC with Advective Flow through the Porous Anode and Reduced Electrode Spacing, Environ. Sci. Technol. 40 (2006) 2426–2432. doi:10.1021/es051652w.
[65] K. Rabaey, N. Boon, S.D. Siciliano, M. Verhaege, W. Verstraete, Biofuel Cells Select for Microbial Consortia That Self-Mediate Electron Transfer, Appl. Environ. Microbiol. 70 (2004) 5373–5382. doi:10.1128/AEM.70.9.5373-5382.2004.
[66] D.R. Bond, D.R. Lovley, Electricity Production by Geobacter sulfurreducens Attached to Electrodes, Appl. Environ. Microbiol. 69 (2003) 1548–1555. doi:10.1128/AEM.69.3.1548-1555.2003.
[67] F. Zhang, Z. Ge, J. Grimaud, J. Hurst, Z. He, Long-Term Performance of Liter-Scale Microbial Fuel Cells Treating Primary Effluent Installed in a Municipal Wastewater Treatment Facility, Environ. Sci. Technol. 47 (2013) 4941–4948. doi:10.1021/es400631r.
[68] K. Scott, C. Murano, G. Rimbu, A tubular microbial fuel cell, J. Appl. Electrochem. 37 (2007) 1063–1068. doi:10.1007/s10800-007-9355-8.
[69] O. Bretschger, MODULAR ENERGY RECOVERING WATER TREATMENT DEVICES, United States Patent Application 20130137000

Kind Code: A1,

2013. http://www.freepatentsonline.com/y2013/0137000.html (accessed July 16, 2013).
[70] O. Lefebvre, Y. Shen, Z. Tan, A. Uzabiaga, I.S. Chang, H.Y. Ng, Full-loop operation and cathodic acidification of a microbial fuel cell operated on domestic wastewater, Bioresour. Technol. 102 (2011) 5841–5848. doi:10.1016/j.biortech.2011.02.098.
[71] Z. Ge, F. Zhang, J. Grimaud, J. Hurst, Z. He, Long-term investigation of microbial fuel cells treating primary sludge or digested sludge, Bioresour. Technol. 136 (2013) 509–514. doi:10.1016/j.biortech.2013.03.016.
[72] Y. Fan, H. Hu, H. Liu, Sustainable Power Generation in Microbial Fuel Cells Using Bicarbonate Buffer and Proton Transfer Mechanisms, Environ. Sci. Technol. 41 (2007) 8154–8158. doi:10.1021/es071739c.
[73] L. Zhuang, S. Zhou, Substrate cross-conduction effect on the performance of serially connected microbial fuel cell stack, Electrochem. Commun. 11 (2009) 937–940. doi:10.1016/j.elecom.2009.02.027.
[74] L. Zhuang, S. Zhou, Y. Wang, C. Liu, S. Geng, Membrane-less cloth cathode assembly (CCA) for scalable microbial fuel cells, Biosens. Bioelectron. 24 (2009) 3652–3656. doi:10.1016/j.bios.2009.05.032.
[75] F. Zhang, K.S. Jacobson, P. Torres, Z. He, Effects of anolyte recirculation rates and catholytes on electricity generation in a litre-scale upflow microbial fuel cell, Energy Environ. Sci. 3 (2010) 1347–1352. doi:10.1039/C001201G.
[76] J.R. Kim, G.C. Premier, F.R. Hawkes, J. Rodríguez, R.M. Dinsdale, A.J. Guwy, Modular tubular microbial fuel cells for energy recovery during sucrose wastewater treatment at low organic loading rate, Bioresour. Technol. 101 (2010) 1190–1198. doi:10.1016/j.biortech.2009.09.023.
[77] J.R. Kim, G.C. Premier, F.R. Hawkes, R.M. Dinsdale, A.J. Guwy, Development of a tubular microbial fuel cell (MFC) employing a membrane electrode assembly cathode, J. Power Sources. 187 (2009) 393–399. doi:10.1016/j.jpowsour.2008.11.020.
[78] Keller, Jurg, Rabaey, Korneel, Experiences from MFC pilot plant operations, in: Microb. Fuel Cells-First Int. Symp., Pennsylvania, US, 2008.
[79] D. Jiang, B. Li, Granular activated carbon single-chamber microbial fuel cells (GAC-SCMFCs): a design suitable for large-scale wastewater treatment processes, Biochem. Eng. J. 47 (2009) 31–37.
[80] A. Janicek, Y. Fan, H. Liu, Design of microbial fuel cells for practical application: a review and analysis of scale-up studies, Biofuels. 5 (2014) 79–92. doi:10.4155/bfs.13.69.
[81] S. You, Q. Zhao, J. Zhang, J. Jiang, C. Wan, M. Du, et al., A graphite-granule membrane-less tubular air-cathode microbial fuel cell for power generation under continuously operational conditions, J. Power Sources. 173 (2007) 172–177. doi:10.1016/j.jpowsour.2007.07.063.
[82] A. Ter Heijne, F. Liu, L.S. van Rijnsoever, M. Saakes, H.V.M. Hamelers, C.J.N. Buisman, Performance of a scaled-up Microbial Fuel Cell with iron reduction as the cathode reaction, J. Power Sources. 196 (2011) 7572–7577. doi:10.1016/j.jpowsour.2011.04.034.

[83] A. ter Heijne, H.V.M. Hamelers, M. Saakes, C.J.N. Buisman, Performance of non-porous graphite and titanium-based anodes in microbial fuel cells, Electrochimica Acta. 53 (2008) 5697–5703. doi:10.1016/j.electacta.2008.03.032.
[84] P. Aelterman, K. Rabaey, H.T. Pham, N. Boon, W. Verstraete, Continuous Electricity Generation at High Voltages and Currents Using Stacked Microbial Fuel Cells, Environ. Sci. Technol. 40 (2006) 3388–3394. doi:10.1021/es0525511.
[85] I. Ieropoulos, J. Greenman, C. Melhuish, Microbial fuel cells based on carbon veil electrodes: Stack configuration and scalability, Int. J. Energy Res. 32 (2008) 1228–1240. doi:10.1002/er.1419.
[86] A. Gurung, S.-E. Oh, The Performance of Serially and Parallelly Connected Microbial Fuel Cells, Energy Sources Part Recovery Util. Environ. Eff. 34 (2012) 1591–1598. doi:10.1080/15567036.2011.629277.
[87] S.-E. Oh, B.E. Logan, Voltage reversal during microbial fuel cell stack operation, J. Power Sources. 167 (2007) 11–17. doi:10.1016/j.jpowsour.2007.02.016.
[88] A. Taniguchi, T. Akita, K. Yasuda, Y. Miyazaki, Analysis of electrocatalyst degradation in PEMFC caused by cell reversal during fuel starvation, J. Power Sources. 130 (2004) 42–49. doi:10.1016/j.jpowsour.2003.12.035.
[89] M.A. Travassos, V.V. Lopes, R.A. Silva, A.Q. Novais, C.M. Rangel, Assessing cell polarity reversal degradation phenomena in PEM fuel cells by electrochemical impedance spectroscopy, Int. J. Hydrog. Energy. (n.d.). doi:10.1016/j.ijhydene.2013.01.132.
[90] H. Lee, H. Song, J. Kim, Effect of Reverse Voltage on Proton Exchange Membrane Fuel Cell Performance, in: 1st Int. Forum Strateg. Technol., 2006: pp. 205–208. doi:10.1109/IFOST.2006.312286.
[91] P. Ferreira-Aparicio, A.M. Chaparro, B. Gallardo, M.A. Folgado, L. Daza, Anode Degradation Effects in PEMFC Stacks by Localized Fuel Starvation, ECS Trans. 26 (2010) 257–265. doi:10.1149/1.3428996.
[92] J. Wu, X.Z. Yuan, J.J. Martin, H. Wang, J. Zhang, J. Shen, et al., A review of PEM fuel cell durability: Degradation mechanisms and mitigation strategies, J. Power Sources. 184 (2008) 104–119. doi:10.1016/j.jpowsour.2008.06.006.
[93] S. Hays, F. Zhang, B.E. Logan, Performance of two different types of anodes in membrane electrode assembly microbial fuel cells for power generation from domestic wastewater, J. Power Sources. 196 (2011) 8293–8300. doi:10.1016/j.jpowsour.2011.06.027.
[94] A.J. Hutchinson, J.C. Tokash, B.E. Logan, Analysis of carbon fiber brush loading in anodes on startup and performance of microbial fuel cells, J. Power Sources. 196 (2011) 9213–9219. doi:10.1016/j.jpowsour.2011.07.040.
[95] Y. Ahn, B.E. Logan, Effectiveness of domestic wastewater treatment using microbial fuel cells at ambient and mesophilic temperatures, Bioresour. Technol. 101 (2010) 469–475. doi:10.1016/j.biortech.2009.07.039.
[96] X. Zhang, S. Cheng, X. Huang, B.E. Logan, Improved performance of single-chamber microbial fuel cells through control of membrane deformation, Biosens. Bioelectron. 25 (2010) 1825–1828. doi:10.1016/j.bios.2009.11.018.

[97] G.G. kumar, V.G.S. Sarathi, K.S. Nahm, Recent advances and challenges in the anode architecture and their modifications for the applications of microbial fuel cells, Biosens. Bioelectron. 43 (2013) 461–475. doi:10.1016/j.bios.2012.12.048.
[98] M. Ghasemi, W.R.W. Daud, S.H.A. Hassan, S.-E. Oh, M. Ismail, M. Rahimnejad, et al., Nano-structured carbon as electrode material in microbial fuel cells: A comprehensive review, J. Alloys Compd. 580 (2013) 245–255. doi:10.1016/j.jallcom.2013.05.094.
[99] P. Morgan, Carbon fibers and their composites, Taylor & Francis, Boca Raton, 2005.
[100] B. Min, B.E. Logan, Continuous Electricity Generation from Domestic Wastewater and Organic Substrates in a Flat Plate Microbial Fuel Cell, Environ. Sci. Technol. 38 (2004) 5809–5814. doi:10.1021/es0491026.
[101] F. Zhang, M.D. Merrill, J.C. Tokash, T. Saito, S. Cheng, M.A. Hickner, et al., Mesh optimization for microbial fuel cell cathodes constructed around stainless steel mesh current collectors, J. Power Sources. 196 (2011) 1097–1102. doi:10.1016/j.jpowsour.2010.08.011.
[102] S. Cheng, H. Liu, B.E. Logan, Increased performance of single-chamber microbial fuel cells using an improved cathode structure, Electrochem. Commun. 8 (2006) 489–494. doi:10.1016/j.elecom.2006.01.010.
[103] H. Liu, S. Cheng, B.E. Logan, Production of Electricity from Acetate or Butyrate Using a Single-Chamber Microbial Fuel Cell, Environ. Sci. Technol. 39 (2005) 658–662. doi:10.1021/es048927c.
[104] Y. Zuo, B.E. Logan, Power generation in MFCs with architectures based on tubular cathodes or fully tubular reactors, Water Sci. Technol. J. Int. Assoc. Water Pollut. Res. 64 (2011) 2253–2258. doi:10.2166/wst.2011.429.
[105] P.D. Kiely, G. Rader, J.M. Regan, B.E. Logan, Long-term cathode performance and the microbial communities that develop in microbial fuel cells fed different fermentation endproducts, Bioresour. Technol. 102 (2011) 361–366. doi:10.1016/j.biortech.2010.05.017.
[106] Janicek, A., Fan, Y., Liu, H., Performance and Stability of Different Cathode Base Materials for Use in Microbial Fuel Cells, J. Power Sources. Accepted Manuscript-Article in Press (2015). doi:doi:10.1016/j.jpowsour.2015.01.098.
[107] S. Basu, Recent Trends in Fuel Cell Science and Technology, Springer, 2007.
[108] S. Litster, G. McLean, PEM fuel cell electrodes, J. Power Sources. 130 (2004) 61–76. doi:10.1016/j.jpowsour.2003.12.055.
[109] S. Brunauer, P.H. Emmett, E. Teller, Adsorption of Gases in Multimolecular Layers, J. Am. Chem. Soc. 60 (1938) 309–319. doi:10.1021/ja01269a023.
[110] S.J. Gregg, K.S.W. Sing, Adsorption, surface area, and porosity, Academic Press, 1991.
[111] B.C. Moore, F.S. Cannon, J.A. Westrick, D.H. Metz, C.A. Shrive, J. DeMarco, et al., Changes in GAC pore structure during full-scale water treatment at Cincinnati: a comparison between virgin and thermally reactivated GAC, Carbon. 39 (2001) 789–807. doi:10.1016/S0008-6223(00)00097-X.

[112] S. Hajizadeh, H. Kirsebom, B. Mattiasson, Characterization of macroporous carbon-cryostructured particle gel, an adsorbent for small organic molecules, Soft Matter. 6 (2010) 5562–5569. doi:10.1039/C0SM00311E.
[113] R. Yan, T. Chin, Y.L. Ng, H. Duan, D.T. Liang, J.H. Tay, Influence of Surface Properties on the Mechanism of H2S Removal by Alkaline Activated Carbons, Environ. Sci. Technol. 38 (2003) 316–323. doi:10.1021/es0303992.
[114] A.J. Bard, L.R. Faulkner, Electrochemical Methods: Fundamentals and Applications, Wiley, 2000.
[115] V.J. Watson, C. Nieto Delgado, B.E. Logan, Improvement of activated carbons as oxygen reduction catalysts in neutral solutions by ammonia gas treatment and their performance in microbial fuel cells, J. Power Sources. 242 (2013) 756–761. doi:10.1016/j.jpowsour.2013.05.135.
[116] I. Ieropoulos, J. Greenman, C. Melhuish, Microbial fuel cells based on carbon veil electrodes: Stack configuration and scalability, Int. J. Energy Res. 32 (2008) 1228–1240. doi:10.1002/er.1419.
[117] H.-Y. Wang, A. Bernarda, C.-Y. Huang, D.-J. Lee, J.-S. Chang, Micro-sized microbial fuel cell: a mini-review, Bioresour. Technol. 102 (2011) 235–243. doi:10.1016/j.biortech.2010.07.007.
[118] A. Gurung, J. Kim, S. Jung, B.-H. Jeon, J.E. Yang, S.-E. Oh, Effects of substrate concentrations on performance of serially connected microbial fuel cells (MFCs) operated in a continuous mode, Biotechnol. Lett. 34 (2012) 1833–1839. doi:10.1007/s10529-012-0979-3.
[119] C. Donovan, A. Dewan, H. Peng, D. Heo, H. Beyenal, Power management system for a 2.5 W remote sensor powered by a sediment microbial fuel cell, J. Power Sources. 196 (2011) 1171–1177. doi:10.1016/j.jpowsour.2010.08.099.
[120] S.-E. Adami, N. Degrenne, W. Haboubi, H. Takhedmit, D. Labrousse, F. Costa, et al., Ultra-Low Power, Low Voltage, Self-Powered Resonant DC–DC Converter for Energy Harvesting, J. Low Power Electron. 9 (2013) 103–117. doi:10.1166/jolpe.2013.1245.
[121] N.W. Zhu, X. Chen, L.X. Tu, P.X. Wu, Z. Dang, Voltage Reversal during Stacking Microbial Fuel Cells with or without Diodes, Adv. Mater. Res. 396-398 (2011) 188–193. doi:10.4028/www.scientific.net/AMR.396-398.188.
[122] Y. Kim, M.C. Hatzell, A.J. Hutchinson, B.E. Logan, Capturing power at higher voltages from arrays of microbial fuel cells without voltage reversal, Energy Environ. Sci. 4 (2011) 4662–4667. doi:10.1039/C1EE02451E.
[123] P.K. Wu, J.C. Biffinger, L.A. Fitzgerald, B.R. Ringeisen, A low power DC/DC booster circuit designed for microbial fuel cells, Process Biochem. 47 (2012) 1620–1626. doi:10.1016/j.procbio.2011.06.003.
[124] Y. Fan, S.-K. Han, H. Liu, Improved performance of CEA microbial fuel cells with increased reactor size, Energy Environ. Sci. 5 (2012) 8273–8280. doi:10.1039/C2EE21964F.
[125] Janicek, A., Gao, N., Fan, Y., Liu, H., High Power Generation and Pressure Tolerance of an Activated Carbon/Carbon Cloth Cathode for Microbial Fuel Cells, Submitt. Environ. Sci. Technol. (n.d.).

[126] D.R. Lovley, E.J.P. Phillips, Novel Mode of Microbial Energy Metabolism: Organic Carbon Oxidation Coupled to Dissimilatory Reduction of Iron or Manganese, Appl. Environ. Microbiol. 54 (1988) 1472–1480.
[127] A. Rochex, J.-J. Godon, N. Bernet, R. Escudié, Role of shear stress on composition, diversity and dynamics of biofilm bacterial communities, Water Res. 42 (2008) 4915–4922. doi:10.1016/j.watres.2008.09.015.
[128] Shin, Seung-Hun, Choi, Youngjin, Na, Sun-Hee, Jung, Seunho, Kim, Sunghyun, Development of Bipolar Plate Stack Type Microbial Fuel Cells, Bull Korean Chem Soc. 27 (2006) 281–285.
[129] Janicek, A., Fan, Y., Liu, H., Stable and High Voltage and Power Output of CEA-MFCs Internally Connected in Series (iCiS), Submitt. Energy Environ. Sci. (n.d.).
[130] I. Ieropoulos, J. Greenman, C. Melhuish, Improved energy output levels from small-scale Microbial Fuel Cells, Bioelectrochemistry. 78 (2010) 44–50. doi:10.1016/j.bioelechem.2009.05.009.
[131] L. Zhuang, S. Zhou, Substrate cross-conduction effect on the performance of serially connected microbial fuel cell stack, Electrochem. Commun. 11 (2009) 937–940. doi:10.1016/j.elecom.2009.02.027.
[132] J. Winfield, I. Ieropoulos, J. Greenman, Investigating a cascade of seven hydraulically connected microbial fuel cells, Bioresour. Technol. 110 (2012) 245–250. doi:10.1016/j.biortech.2012.01.095.
[133] B. Wang, J.-I. Han, A single chamber stackable microbial fuel cell with air cathode, Biotechnol. Lett. 31 (2009) 387–393. doi:10.1007/s10529-008-9877-0.
[134] F.S. Saleh, E.B. Easton, Diagnosing Degradation within PEM Fuel Cell Catalyst Layers Using Electrochemical Impedance Spectroscopy, J. Electrochem. Soc. 159 (2012) B546–B553. doi:10.1149/2.098205jes.
[135] S. Maass, F. Finsterwalder, G. Frank, R. Hartmann, C. Merten, Carbon support oxidation in PEM fuel cell cathodes, J. Power Sources. 176 (2008) 444–451. doi:10.1016/j.jpowsour.2007.08.053.
[136] S.D. Knights, J.L. Taylor, D.P. Wilkinson, D.S. Wainwright, Fuel cell anode structures for voltage reversal tolerance, US6517962 B1, 2003.
[137] K.H. Kangasniemi, D.A. Condit, T.D. Jarvi, Characterization of Vulcan Electrochemically Oxidized under Simulated PEM Fuel Cell Conditions, J. Electrochem. Soc. 151 (2004) E125–E132. doi:10.1149/1.1649756.
[138] Lu, Z., Yan, L., Mao, Z., Zhuge, W., Zhang, Y., Wang, L., Behavior of PEMFC in starvation, J. Power Sources. 157 (2006) 166–176. doi:doi:10.1016/j.jpowsour.2005.08.006.
[139] H. Dong, H. Yu, X. Wang, Q. Zhou, J. Feng, A novel structure of scalable air-cathode without Nafion and Pt by rolling activated carbon and PTFE as catalyst layer in microbial fuel cells, Water Res. 46 (2012) 5777–5787. doi:10.1016/j.watres.2012.08.005.
[140] S.K. Sharma, Green Corrosion Chemistry and Engineering: Opportunities and Challenges, John Wiley & Sons, 2011.
[141] He, Liu, Jia, Li, Da, Wang, Haiman, Qu, Youpeng, Wang, Xin, et al., The electrochemical behavior of three air cathodes for microbial electrochemical

system (MES) under meter scale water pressure, J. Power Sources. 267 (2014) 219–226.
[142] J. Winfield, I. Ieropoulos, J. Greenman, J. Dennis, The overshoot phenomenon as a function of internal resistance in microbial fuel cells, Bioelectrochemistry. 81 (2011) 22–27. doi:10.1016/j.bioelechem.2011.01.001.
[143] X. Zhu, J.C. Tokash, Y. Hong, B.E. Logan, Controlling the occurrence of power overshoot by adapting microbial fuel cells to high anode potentials, Bioelectrochemistry. 90 (2013) 30–35. doi:10.1016/j.bioelechem.2012.10.004.
[144] A. Dewan, C. Donovan, D. Heo, H. Beyenal, Evaluating the performance of microbial fuel cells powering electronic devices, J. Power Sources. 195 (2010) 90–96. doi:10.1016/j.jpowsour.2009.07.001.
[145] C. Donovan, A. Dewan, D. Heo, H. Beyenal, Batteryless, Wireless Sensor Powered by a Sediment Microbial Fuel Cell, Environ. Sci. Technol. 42 (2008) 8591–8596. doi:10.1021/es801763g.
[146] H.C. Boghani, J.R. Kim, R.M. Dinsdale, A.J. Guwy, G.C. Premier, Control of power sourced from a microbial fuel cell reduces its start-up time and increases bioelectrochemical activity, Bioresour. Technol. 140 (2013) 277–285. doi:10.1016/j.biortech.2013.04.087.
[147] P. Aelterman, S. Freguia, J. Keller, W. Verstraete, K. Rabaey, The anode potential regulates bacterial activity in microbial fuel cells, Appl. Microbiol. Biotechnol. 78 (2008) 409–418. doi:10.1007/s00253-007-1327-8.
[148] D.A. Finkelstein, L.M. Tender, J.G. Zeikus, Effect of Electrode Potential on Electrode-Reducing Microbiota, Environ. Sci. Technol. 40 (2006) 6990–6995. doi:10.1021/es061146m.
[149] X. Wang, Y. Feng, N. Ren, H. Wang, H. Lee, N. Li, et al., Accelerated start-up of two-chambered microbial fuel cells: Effect of anodic positive poised potential, Electrochimica Acta. 54 (2009) 1109–1114. doi:10.1016/j.electacta.2008.07.085.
[150] F. Zhang, X. Xia, Y. Luo, D. Sun, D.F. Call, B.E. Logan, Improving startup performance with carbon mesh anodes in separator electrode assembly microbial fuel cells, Bioresour. Technol. 133 (2013) 74–81. doi:10.1016/j.biortech.2013.01.036.
[151] A. Deeke, T.H.J.A. Sleutels, H.V.M. Hamelers, C.J.N. Buisman, Capacitive Bioanodes Enable Renewable Energy Storage in Microbial Fuel Cells, Environ. Sci. Technol. 46 (2012) 3554–3560. doi:10.1021/es204126r.
[152] A. Deeke, T.H.J.A. Sleutels, A.T. Heijne, H.V.M. Hamelers, C.J.N. Buisman, Influence of the thickness of the capacitive layer on the performance of bioanodes in Microbial Fuel Cells, J. Power Sources. 243 (2013) 611–616. doi:10.1016/j.jpowsour.2013.05.195.
[153] C. Feng, Z. Lv, X. Yang, C. Wei, Anode modification with capacitive materials for a microbial fuel cell: an increase in transient power or stationary power, Phys. Chem. Chem. Phys. (2014). doi:10.1039/C4CP00923A.
[154] Z. Lv, D. Xie, F. Li, Y. Hu, C. Wei, C. Feng, Microbial fuel cell as a biocapacitor by using pseudo-capacitive anode materials, J. Power Sources. 246 (2014) 642–649. doi:10.1016/j.jpowsour.2013.08.014.

[155] X. Peng, H. Yu, H. Yu, X. Wang, Lack of anodic capacitance causes power overshoot in microbial fuel cells, Bioresour. Technol. 138 (2013) 353–358. doi:10.1016/j.biortech.2013.03.187.
[156] X. Peng, H. Yu, X. Wang, Q. Zhou, S. Zhang, L. Geng, et al., Enhanced performance and capacitance behavior of anode by rolling Fe3O4 into activated carbon in microbial fuel cells, Bioresour. Technol. 121 (2012) 450–453. doi:10.1016/j.biortech.2012.06.021.

8. **APPENDIX**: Design of Microbial Fuel Cells: A review and analysis of scale-up studies

Review

Design of microbial fuel cells for practical application: a review and analysis of scale-up studies

Biofuels (2014) 5(1), 79–92

Anthony Janicek, Yanzen Fan & Hong Liu*

There has been substantial progress towards scale-up and practical application of microbial fuel cell (MFC) technology in the last decade. Studies regarding this progress have been reported ranging from 1 to 1000 l, consisting of short-term laboratory-scale experiments, to long-term *in situ* pilot-scale investigations. Despite this fact, a successful demonstration has yet to be shown. This suggests that advances made at the milliliter-scale have not been translated, or are not transferrable, to larger scales, implying a lack of understanding on how to progress from the milliliter-scale to larger scales. This review compiles 18 separate studies, the majority of scale-up efforts (liter-scale and greater) to date, thoroughly reviewing and analyzing aspects of design in relation to performance and the potential for success. Key factors affecting the MFC performance are highlighted. A future perspective on scaling-up MFCs for practical wastewater treatment is also provided.

As the global population increases, the demand for water also increases. In the last century, water use has been growing at a rate more than double that of population increase [1]. This increase in water use has led to an increase in wastewater generated and, ultimately, an increase in the demand for treatment. As a result, current wastewater treatment technologies presently consume approximately 3% of the electricity generated in developed countries [2,3]. With an ever-increasing population and a finite supply of water, finding more efficient and cost-effective means of treating wastewater has become extremely important. Developing new treatment technologies that will offset this high-energy cost is necessary to maintain both water and energy security.

Microbial fuel cell (MFC) technology has the potential to revolutionize wastewater treatment in both industrialized and developing nations by becoming a net energy producer [4,5]. Through the use of exoelectrogenic bacteria, MFC technology releases the energy contained in wastewater while simultaneously treating it. This process occurs when bacteria growing on the anode oxidize organic matter contained in the wastewater and transfer the electrons to the anode. A current is produced when electrons flow from the anode to the cathode through an external circuit. At the cathode, the electrons reduce an electron acceptor, typically oxygen, ultimately forming a reduced compound such as water.

In order for practical applications to be realized, MFCs need to have the capability to treat large quantities of wastewater. Many MFC systems have been developed with liquid volumes of a few milliliters to several hundred milliliters. Recent advances in materials as well as reactor configurations have led to a growing number of scale-up studies, ranging from 1 to several hundred liters, with a few attempts at pilot-scale MFC systems. Moving this technology from the laboratory-scale to pilot scale brings it one step closer to the realization of practical application.

There are several recent reviews that have focused on electrodes summarizing materials, performance, cost, application range and surface modification methods [6–8]. Recent advances in separator materials comparing performance based on oxygen, substrate and proton transfer efficiencies, as well as the effect on **internal resistance**, power density and coulombic efficiency, have also been examined [9]. Another recent review has provided a brief overview of scale-up efforts ranging from the milliliter to the liter scale, and detailed the impacts of operational

Biological & Ecological Engineering, Oregon State University, Corvallis, OR 97333, USA
*Author for correspondence: Tel.: +1 541 737 6309; E-mail: liuh@engr.orst.edu

FUTURE SCIENCE

10.4155/BFS.13.69 ISSN 1759-7269

Key terms

Microbial fuel cell: Type of biological fuel cell in which bacteria growing on the anode oxidize organic matter and generates electricity.

Internal resistance: Electrochemical resistance associated with reactions and transport processes occurring with the anode, cathode, membrane and electrolyte.

conditions such as pH, temperature, organic load, feed rate and shear stress on MFC performance [10]. However, in general, these reviews have focused on the advances made at the milliliter scale and how these advances relate to scale-up, while only describing a few attempts at the liter scale or greater. Based on advances made at the milliliter scale, design recommendations and guidelines were provided, suggesting ways in which scale-up should proceed for practical application. Although recently there have been several attempts at scaling up, a successful demonstration has yet to be shown. This suggests that advances made at the milliliter scale have not been translated, or are not transferable, to larger scales, implying a lack of understanding on how to progress from the milliliter to larger scales. At this stage in MFC development, it is important to identify reasons why attempts at scale-up have not been successful. As a result, an in-depth critical analysis of these larger-scale MFC studies is needed. This review compiles 18 separate studies, the majority of scale-up efforts (liter scale and greater) to date, consisting of laboratory as well as practical application efforts, thoroughly reviewing and analyzing aspects of design in relation to performance and the potential for success. In this review, we will provide an overview of the different types of MFC configurations used during scale-up and focus the discussion on scale-up studies (over 1 l scale) to date for practical wastewater treatment.

MFC designs used in scale-up studies

While many different MFC designs have been used in the laboratory such as single and dual chamber cube and cylindrical type reactors [11–14], dual chambered H-cell reactors [14], plate and tube shaped reactors [13,15,16], the majority of scale-up studies use reactors that are tubular or flat-plate in design [13,17–26,101] **(Figures 1–3)**.

Scaled-up, tube shaped configurations typically consist of a tubular anode surrounded by a separator to electrically isolate the anode from the cathode. The tubular shape of the reactor is typically a product of the cylindrical structural material used. For example, scaled-up reactors have been designed using supporting materials such as polyvinyl chloride [19–22,27–29], polypropylene [17,30,31], cylindrical bottles [13], measuring cylinders [18], nylon tubing [23] and a cation exchange membrane formed into a tube [26]. Anodes in these reactors consist of a cylindrical brush (graphite or carbon fiber) **(Figure 1)**, granular material (granular activated carbon or graphite granules) or a flat electrode, made of some type of conductive fabric (carbon cloth, felt or veil) formed into a cylinder **(Figure 2 & Tables 1 & 2)**. The anodes, or anode chamber, are then wrapped by some type of membrane or separator material to electrically isolate the anode from the cathode **(Tables 1 & 2)**. The cathode is then wrapped around the separator. Cathodes consisting of base materials, such as carbon cloth, carbon fiber or carbon veil, and containing platinum, manganese (IV) oxide, or activated carbon as the catalyst, have been reported in the literature **(Tables 1 & 2)**. Only three studies report using a biologically catalyzed cathode [23,32,101], one of which used graphite fiber brush cathodes, the only such design reported. Depending on type of membrane or separator material used, the electrode/membrane or electrode/separator structure has been termed a membrane electrode assembly [31], a membrane cathode assembly [19] or a cloth cathode assembly [20]. The configuration can also be reversed with a cylindrical anode chamber surrounding a cathode tube [23]. Relatively few tubular designs have been reported that use no separator [13,24,33].

Most tubular designs reported were operated in continuous flow mode. As a result, further scale-up can be achieved by connecting additional tubular MFC modules together in series by extending the length of the tube, forming an MFC stack [20]. It is believed that the tubular design allows for near optimal cross-sectional dimensions to be maintained during scale-up [17,23,30,34]. As a result, minimal dead space is likely to occur in the reactor, thereby creating near plug-flow conditions, allowing for a sufficiently mixed, relatively steady-state flow regime [17].

Fewer studies have been reported on flat-plate designs than on tubular designs [13,16,35–38] **(Figure 3)**. Flat-plate configurations typically consist of rectangular anode chambers with some type of a membrane or separator material sandwiched between the anode and cathode. The supporting structural material is typically Plexiglass® or some other type of easily machineable plastic [16,35–39]. The anodes and cathodes in these designs have been made of granular graphite (anode only), carbon felt, carbon paper and titanium plates/mesh **(Tables 1 & 2)**. Both chemical and biological catalysts have been used to catalyze the reaction at the cathode **(Tables 1 & 2)**. One flat-plate design was similar to the bipolar plate design used in proton exchange membrane fuel cells [36,37]. The key feature of the flat plat design is that the distance between the anode and cathode is minimized, thereby increasing ionic diffusion rates and reducing internal resistance compared with other designs in which electrode spacing is larger [15,40,41]. As with tubular designs, most flat-plate designs were operated in continuous flow mode **(Tables 1 & 2)**, and individual flat plat modules can be connected to form larger MFC stacks during scale-up [35,36].

For both tubular and flat-plate designs, arrangements consisting of multiple individual MFCs can be operated hydraulically in series or hydraulically in parallel. When hydraulically connected in series, influent flows sequentially through each MFC module while parallel connection results in each module receiving the same influent. Similarly, multiple MFCs can be electrically connected in series to increase voltage or in parallel to increase current [42–45].

Factors affecting performance related to reactor design

▪ Electrode spacing

In many MFC systems, the electrolyte resistance contributes significantly to the internal resistance. While not the only limiting factor, high electrolyte resistance will ultimately restrict the maximum power achievable for a given design [46]. Reducing electrolyte resistance can be achieved either by reducing electrode spacing or increasing the conductivity of the solution. Increasing conductivity would likely require the addition of chemical buffers, which would be cost prohibitive for scaled-up practical applications. As a result, reducing electrode spacing is the most effective way to decrease the internal resistance and increase the power attainable in a given design [11,40,41,46–48]. To illustrate the importance of electrode spacing, a calculation can be made based on methods outlined by Fan *et al.* [46]. The internal resistance for an MFC can be calculated as:

$$R_{int} = R_c + R_a + R_e + R_m$$

Equation 1

where R_c, R_a, R_e and R_m are the resistance of the cathode, anode, electrolyte and membrane, respectively, and R_e is given by:

$$R_e = La/S_r C_e$$

Equation 2

where R_e is a function of the distance between anode and cathode (L), the cross-sectional area of the reactor (S_r) and the concentration of the charge transfer electrolyte (C_e), and a is a constant [46]. Using **Equations 1 & 2**, and assuming an operating voltage of 0.3 V for a membrane-less configuration ($R_m = 0$), the power can be calculated and compared at different electrode spacings. For an MFC with an electrode area equal to 7 cm^2, a buffer concentration of 50 mM, and using typical values for the anode and cathode resistance [46], the internal resistance and power density at an electrode distance

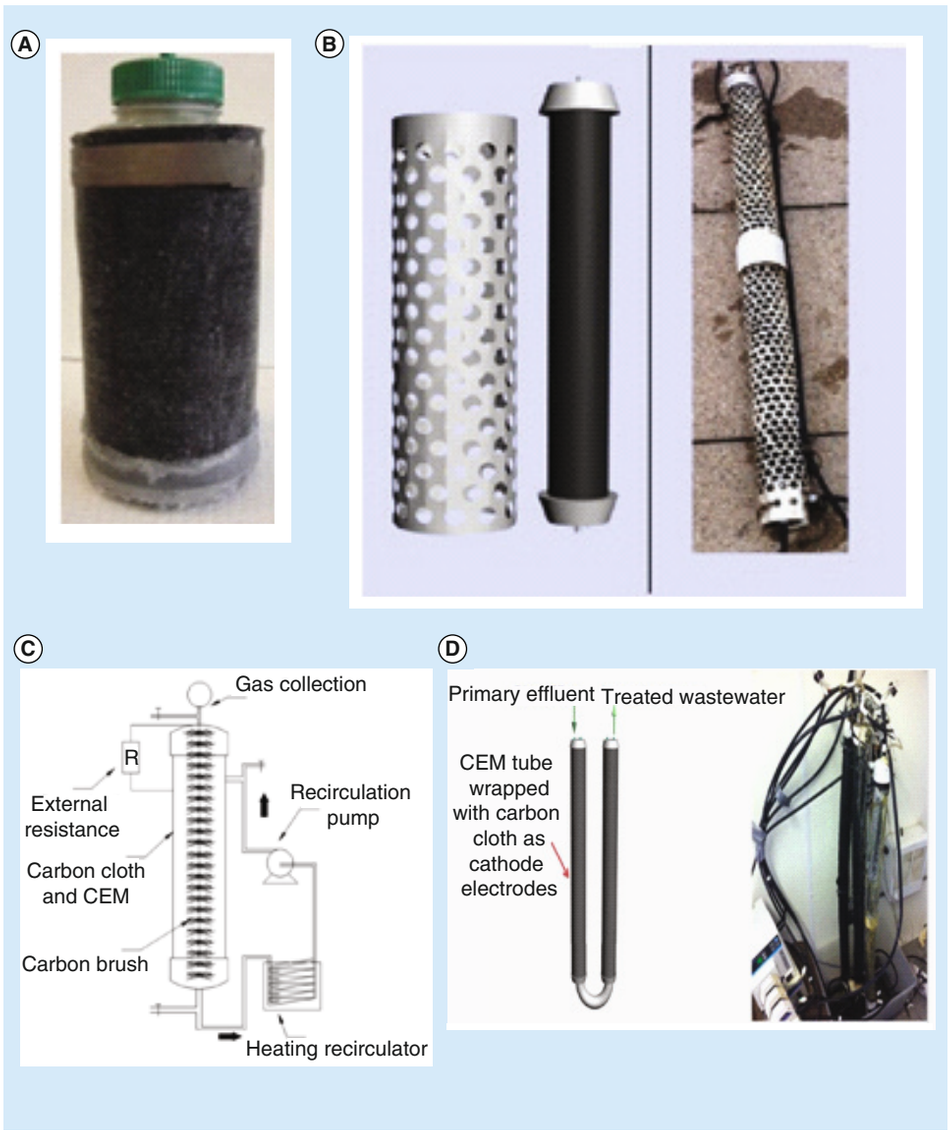

Figure 1. Tubular brush anode reactors. (A) Cylindrical bottle batch reactor; **(B)** perforated PVC brush anode reactor; **(C)** cation exchange membrane brush anode reactor; **(D)** u-shaped tubular brush anode reactor.
CEM: Cation exchange membrane; R: Resistor.
(A) Adapted from [13].
(B) Adapted from [22].
(C) Adapted from [26].
(D) Adapted with permission from [21] © American Chemical Scoiety (2013).

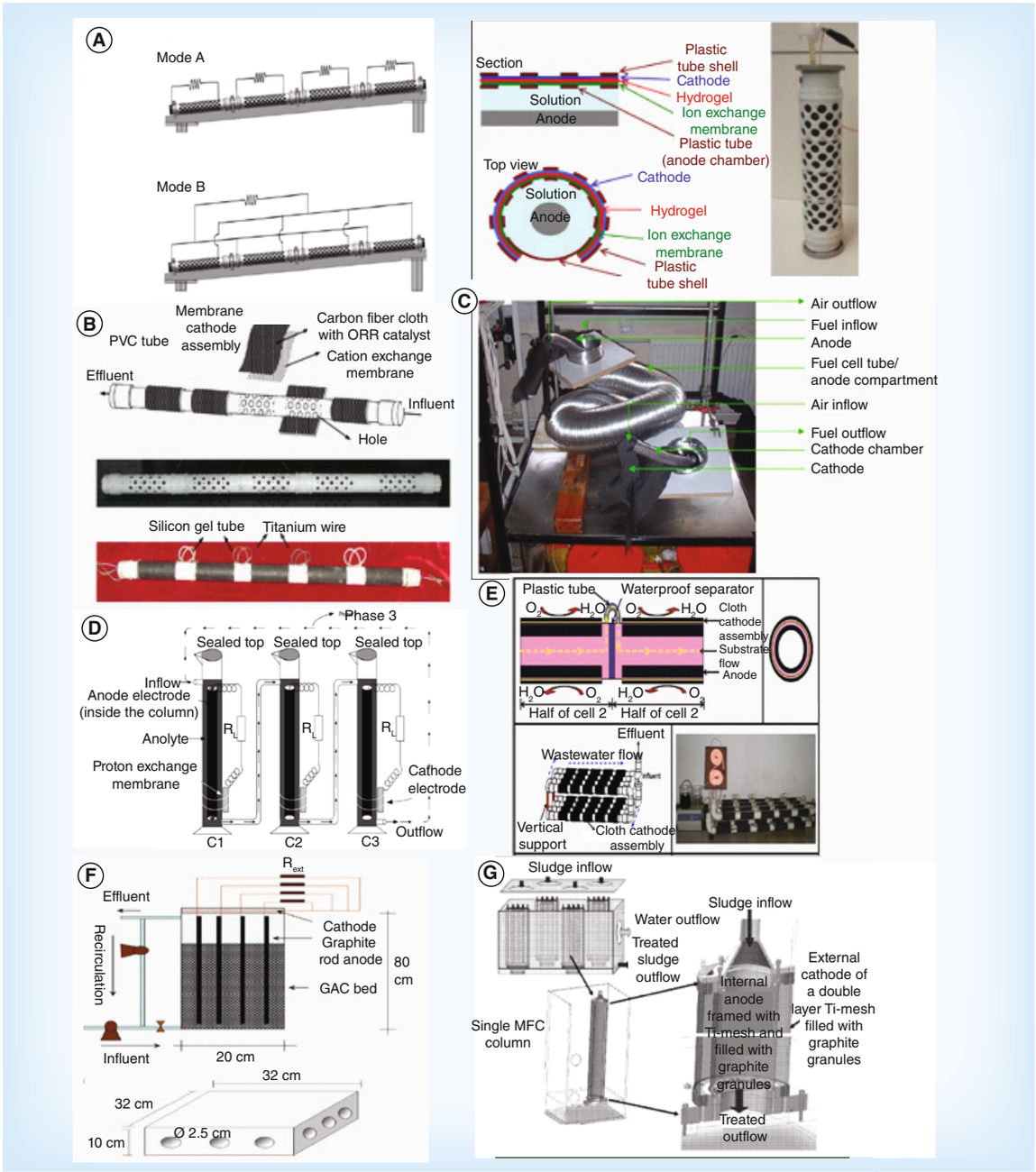

Figure 2. Tubular reactors with sandwiched membrane/electrode structures. (A) Longitudinal modular tubular reactor with membrane electrode assembly; **(B)** tubular stack reactor made with membrane cathode assembly; **(C)** inner cathode tubular reactor; **(D)** tubular column reactor; **(E)** tubular stack reactor made with membrane cathode assembly; **(F)** multi anode/cathode reactor; **(G)** tubular reactor with granular graphite anode/cathode chambers. C: Column; GAC: Granular activated carbon; MFC: Microbial fuel cell; ORR: Oxygen reduction reaction; R: Resistor.
(A) Adapted from [32]; and with permission from [17] © Royal Society of Chemistry (2011).
(B) Adapted from [19].
(C) Apated with permission from [23] © Springer Science and Business Media (2007).
(D) Adapted from [18].
(E) Adapted from [20].
(F) Adapted from [24].
(G) Adapted from [101].

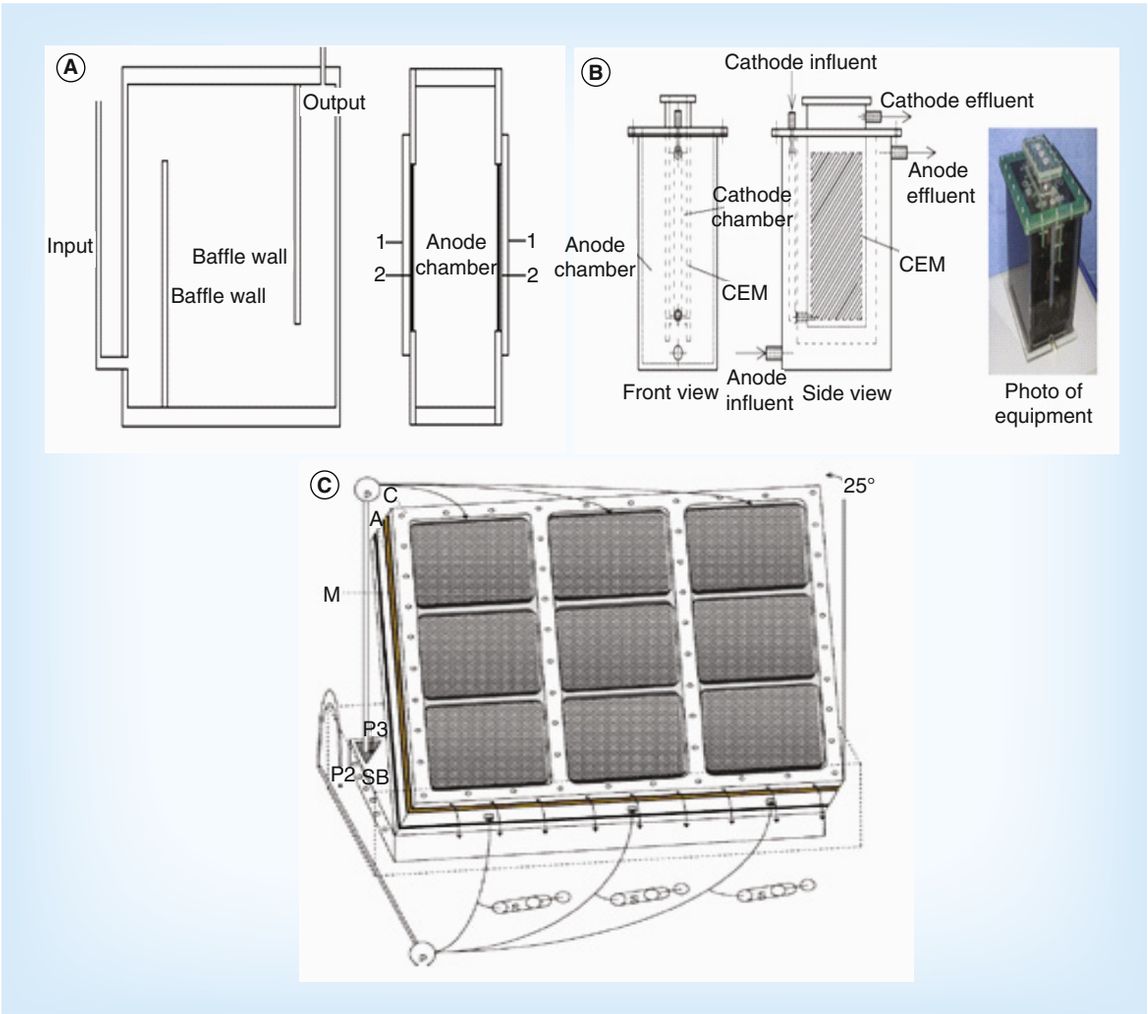

Figure 3. Flat-plate reactors. (A) Baffled flat-plate reactor; **(B)** inner cathode flat-plate reactor; **(C)** flat-plate stack reactor.
A: Anode; C: Cathode; CEM: Cation exchange membrane; M: Membrane.
(A) Adapted from [16].
(B) Adapted from [38].
(C) Adapted with permission from [35] © Springer Science and Business Media (2009).

of 1 cm are calculated as 142 Ω and 0.907 W m^{-2}, respectively.

Similarly, at a distance of 1 mm, power density can be calculated as 2.34 W m^{-2}. This represents a greater than 150% increase in power density by decreasing the electrode spacing from 1 cm to 1 mm. Similar increase in power density has been observed in our laboratory when electrode spacing is reduced from 1.7 cm for regular MFCs to approximately 1 mm for **cloth electrode assembly** MFCs. For systems that contain membranes, a significant increase in power density was demonstrated compared with other separator or separatorless systems when electrode spacing was reduced [40].

Electrode shape and orientation have the greatest effect on the minimum distance attainable in a given design. For the designs covered in this review, anode type dictated the minimum attainable electrode spacing. By nature of the cylindrical brush structure, reactor configurations using brush anodes had increased electrode spacing compared with flat-plate reactors and **tubular reactors** that did not use brush anodes **(Tables 1 & 2)**. This increased distance results in longer proton

Key terms

Cloth electrode assembly: Type of electrode configuration used in microbial fuel cells in which a separator made of cloth is sandwiched between the anode and cathode. This configuration allows the electrodes to be placed in close proximity.

Tubular reactors: Reactor configurations consisting of concentric cylindrical anode and cathode chambers separated by a membrane or separator material to electrically isolate the electrodes.

Table 1. Summary of design characteristics for reactors reported in the literature.

Volume (l)	Anode type	Cathode type	Separator/membrane	Specific area (m^2 m^{-3})	Figure	Ref.
1	Graphite fiber brush	Air cathode, carbon cloth with Pt	None	13	1A	[13]
~1	Carbon veil	Air, cathode, carbon cloth, 0.5 mg cm^{-2} Pt	CEM	43	2A	[17]
~1.5	Graphite felt	Air cathode, carbon fiber, MnO_2 catalyst	CEM	12.5	2B	[19]
2	Carbon brush	Carbon cloth with Pt/AC or AC only as catalyts	CEM or AEM	119.5	1B	[22]
2.5	Carbon cloth	Carbon cloth, biocathode	Perforated nylon tubing	40	2C	[23]
2.7	Carbon veil	Carbon veil	PEM	40	2D	[18]
2.7	Carbon veil	Carbon veil	PEM	40	2D	[18]
3.6	Carbon brush	Air cathode, carbon cloth with Pt catalyst	CEM	73.3	1C	[26]
4	Carbon brush	Carbon cloth with Pt/AC or AC only as catalyts	CEM	NA	1D	[21]
10	Graphite felt	GORE-TEX® cloth, conductive catalytic layer	Waterproof air-permeable layer, layer of GORE-TEX cloth	62	2E	[20]
20	Graphite rods, granular activated carbon	Air cathode, carbon cloth with Pt or MnO_2 as catalyst	None	0.3	2F	[24]
67	Graphite granules, titanium mesh	Graphite granules, titanium mesh	Nylon mesh	NA	2G	[101]
1.5		Air cathode, carbon paper, 0.5 mg/cm^2 Pt	PEM	21.3	3A	[16]
1.5		Air cathode, carbon paper, 0.5 mg/cm^2 Pt	PEM	NA	3A	[16]
3.5	Carbon felt	Carbon felt biocathode	CEM	5.6	3B	[38]
5	Titanium plate/mesh with mixed metal oxide coating	Titanium plate/mesh with mixed metal oxide coating and ferric iron	CEM	100	NA	[37]
7.5	Granular graphite	Carbon felt, biocathode	CEM	25.2	3C	[35]
20	Titanium plate/mesh with mixed metal oxide coating	Titanium plate/mesh with mixed metal oxide coating	CEM	100	NA	[36]

AC: Activated carbon; AEM: Anion exchange membrane; CEM: Cation exchange membrane; COD: Chemical oxygen demand; PEM: Proton exchange membrane.

diffusion times for areas of the brush located further away from the cathode, thereby increasing internal resistance and limiting power. Milliliter scale studies have shown that brush anodes are capable of achieving high power densities due to high electrode surface area and reduced effect of oxygen crossover from the cathode [48–50]. However, this was not the case for the reactors presented in this review. These reactors were larger in both length and diameter than similar smaller reactors. If brush diameter were left the same when scaling up from the smaller scale versions, electrode spacing would be increased, ultimately reducing power. Likewise, if brush diameter were increased, anode surface area would be increased compared with smaller

Table 2. Summary of operational and performance characteristics for reactors reported in the literature.

Volume (l)	Operational mode (batch/ continuous flow)	Substrate	Buffer/ amendments	Operation temperature (°C)	Hydraulic retention time	Total operation time	Power density $Wm^{-2}(Wm^{-3})$	Removal COD (%)	Organic loading rate (g COD l^{-1} d^{-1})	Organic removal rate (g COD l^{-1} d^{-1})	Figure	Ref.
1	Batch	Domestic WW	100 mM Buffer	30	NA	NA	0.33 (4.3)	NA	NA	NA	1A	[13]
~1	Continuous	Synthetic	50 mM Buffer	26 ± 2	28.4 h	10 months	0.13 (5.6)	43	0.8	0.34	2A	[17]
~1.5	Continuous	Swine WW	pH adjusted, conductivity increased	30	1.21 and 4.84 days	NA	0.175 (11)	77.10	4.9	3.78	2B	[19]
2	Continuous	Primary effluent	None	Not reported	11.1 h	400 days	(0.37 ± 0.31)	<53	0.1–1.3	0.053–0.7	1B	[22]
2.5	Batch	Manure slurry	None	Room temperature	NA	NA	0.03	NA	NA	NA	2C	[23]
2.7	Continuous	Landfill leachate	None	Not reported	~4.68 days	28 days	0.0018	31	4.17	1.29	2D	[18]
2.7	Batch	Landfill leachate	None	Not reported	4 days	28 days	NA	79	7.05	5.57	2D	[18]
3.6	Continuous	Sludge	50 mM Buffer	35	14 days	<500 days	0.130 (9.6)	~60	NA	NA	1C	[26]
4	Continuous	Primary effluent	None	-10–36	11 h	450 days	NA	>90	0.6	0.54	1D	[21]
10	Continuous	Brewery	None	30	2 days	180 days	0.093 (6)	86.40	1.06	0.92	2E	[20]
20	Continuous	Primary effluent	None	Room temperature	5–20 h	15 weeks	0.38 (0.2)	60–84	0.66	0.4–0.55	2F	[24]
67	Continuous	Raw sludge	None	Ambient temperature	NA	5 days	(0.5)	99.50	NA	NA	2G	[101]
1.5	Batch	Innoculated with sludge, fed synthetic	50 mM Buffer	30	91 h	NA	0.133 (2.02)	88	NA	NA	3A	[16]
1.5	Continuous	Innoculated with sludge, fed synthetic	50 mM Buffer	30	15.5 h	NA	0.108	NA	NA	NA	3A	[16]
3.5	Continuous	Synthetic	50 mM Buffer	Not reported	5.14	>40 days	0.77 (3.32)	~80	0.08–0.325	0.064–0.26	3B	[38]
5	Continuous	Synthetic	20 mM Buffer	30	~2.15 min	37 days	2 (200)	NA	NA	3	NA	[37]
7.5	Continuous	Synthetic	50 mM Buffer	Room temperature, ~22	6.2 h	Several days	(2–10)	69–97	0.32	0.22–0.31	3C	[35]
20	Continuous	Synthetic	20 mM Buffer	30	~7 min	>34 days	1.44 (144)	NA	NA	NA	NA	[36]

COD: Chemical oxygen demand; WW: Wastewater.

designs. It has been shown that increasing anode surface area with brush anode reactors at smaller scales increased power significantly, but with similar designs at larger scales, power was not significantly increased by increasing brush anode surface area [11,13,49]. Details regarding brush diameter were not provided for all designs described here so a comparison based on brush length and diameter between reactors, as well as with smaller reactors, is not possible.

In brush anode reactors, the centerline of the brush can be oriented parallel or perpendicular to the cathode. Although high power has been generated in both electrode orientations at smaller scales, larger reactors using brush anodes discussed in this review have the centerline of the cylindrical brush oriented parallel to the tubular structure with the membrane/cathode assembly wrapped around the entire circumference of the reactor, surrounding the entire anode [21,22,26]. However, the power obtained by these reactors (operated on wastewater) was lower than that achieved by a similar smaller scale reactor also treating wastewater [51], indicating that substrate composition may not be the sole reason for reduced performance (discussed below).

When brush anodes are used in flat-plate reactors, cathodes were placed on only one or two sides of the brush anodes, which results in an inefficient use of anode area compared with the tubular designs [11,13,48]. However, flat-plate reactors with brush anodes may have an advantage over tubular reactors with brush anodes if electrode spacing can be reduced. A smaller scale (14 ml) brush anode reactor was developed in which the brush, centerline oriented parallel to the cathode, was pressed against the separator of the membrane electrode assembly. This design formed a hemispherical brush anode shape, reducing the electrode distance by half [48]. This design has not been investigated at larger scales, but does hold promise due to the reduced electrode spacing compared with the tubular designs presented in this review. This design configuration could also be extended to tubular reactors through the use of multiple brush anodes or by using smaller diameter tubing, which would flatten the brush against the separator/membrane. Further investigation regarding brush anodes with respect to electrode orientation (parallel or perpendicular) as well as with respect to reactor type (tubular or flat-plate) is needed before any conclusion can be drawn regarding this aspect of design structure.

Regardless of the configuration, reactors containing brush anodes will always have greater electrode spacing compared with tubular reactors and flat-plate reactors that have electrodes pressed against a separator or membrane. Tubular reactors, described in this review, with sandwiched membrane electrode structures should have similar performance as flat-plate designs if electrode spacing is the same. However, several of these tubular reactors had perforated structural material (PVC or similar material) separating the anode from the membrane/cathode assembly [16–19,29,30]. Although this likely would not increase the electrode spacing significantly, the perforated nature of the design limits the available surface area of anode (discussed in further detail below). This, in conjunction with the increased spacing, could reduce performance significantly compared with flat-plate designs that do not contain this limiting structural feature.

In both tubular and plate reactors, electrode spacing is reduced furthest through the use of a separator material sandwiched between the anode and cathode. Most reactors listed in **Tables 1 & 2** used some type of separator, especially cation exchange membranes (~75%). However, the use of membranes (cation and proton exchange membranes) should be avoided if possible due to their high cost compared with separator materials and high area specific resistance [15,46]. Under proton-deficient conditions or neutral pH, proton carriers (commonly anions) are blocked by cation exchange membranes leading to high resistance and high cross membrane pH gradients [52]. Similarly, results based on separator materials have shown that internal resistance was increased due to decreased proton transport to the cathode due to the presence of the separator [53]. However, cloth separators have been shown to enhance coulombic efficiency by greatly reducing the oxygen diffusion rate while still maintaining high power densities, due to greatly reduced electrode spacing and much higher ion conductivity compared with other separator materials [40,53]. Although separator materials such as nylon mesh or perforated nylon tubing used in some reactors **(Tables 1 & 2)** may prevent contact between electrodes, the impermeable material ultimately reduces the available area of the electrodes, which ultimately reduces performance.

In membraneless configurations, oxygen diffusion through the cathode can reduce coulombic efficiency as well as potentially interfere with activity of anaerobic bacteria on the anode [40,41,47,54]. The effect of oxygen is further exacerbated when the anode is in close proximity to the cathode. As a result, separators are a critical component of design, allowing electrode spacing to be reduced as much as possible. It is important to select separators based on material type as well as mass transfer properties. Reactors described in this review using cation exchange membranes or other separator material would likely experience increased performance through the use of better separator materials **(Tables 1 & 2)**.

It should be noted that separators (or membranes) have been observed to deform in both smaller and larger scale flat-plate MFCs [36,55]. Separator deformation can decrease anode compartment volume, increase the spacing between electrodes, trapping gas and ultimately reducing performance. This problem is likely less common in smaller reactors due to the small electrode and separator sizes used. However, as reactor size increases, electrode and separator size will increase, which increases the chance for deformation. Supporting structures may need to be designed that maintain the electrode/separator structure while still maximizing the available area of the electrodes.

Tubular and flat-plate reactors reported in this review have used granular material in the anode and/or cathode compartments (Tables 1 & 2). Although these designs all use some type of current collector (graphite rods or titanium mesh), the contact resistance between the granular material and current collector is high. As a result, material with low conductivity such as granular activated carbon is not ideal. Materials with a higher conductivity, such as granular graphite, are better suited for these types of designs. In addition, tubular reactors using this material have very low performance, indicating that granular material may be, in part, the cause. However, other aspects of design likely contribute more to the decreased performance. For example, the low performance of one tubular configuration with large electrode spacing could be improved greatly, simply by decreasing the large distance between the anode and cathode [24].

▪ Surface area to volume ratio

Reducing electrode spacing can also reduce the surface area to volume ratio, depending on the configuration used. Size and effective electrode surface area will ultimately determine the maximum power attainable for a given design. Scaling-up typically results in an increase in electrode area. Depending on the type of electrode material used, larger electrode area can result in increased internal resistance due to the increased distance electrons travel through the material. It has been shown that although increasing anode surface area can increase power, it does not affect performance as much as increasing cathode surface area [11,13], which is currently the limiting factor with respect to performance. In particular, it is important to maintain **cathode specific surface area** (i.e., surface area to volume ratio) when scaling up, as volumetric power density is a function of this parameter. Cathode specific surface areas, for reactors described in this review, are presented in Tables 1 & 2. High specific surface area does not necessarily correspond to higher power densities. However, many other factors contribute to the performance of these reactors. Factors such as electrode spacing, anode surface area, separators, substrate and hydraulic retention time all play a role in determining power output. As a result, it is not possible to draw any conclusions based on this parameter. However, in more controlled experiments, higher cathode specific area led to higher volumetric power densities [13,15].

Key term

Cathode specific surface area: Ratio of cathode surface area to the volume of the reactor.

▪ Materials & structural supports

Some reactors contain surface modified electrodes to reduce the internal resistance by increasing surface area and conductivity [36,37,39]. Electrode surface modification of both the anode and cathode has shown to increase performance [7,56]. However, in the case of the two flat-plate reactors described here, titanium mesh was used as part of the modification. This type of electrode would likely be cost-prohibitive when produced at larger scales during scale-up. Similarly, most of the reactors described in this review use platinum to catalyze the reaction at the cathode. Precious metal catalysts and expensive materials should be avoided for scale-up application, as it is economically not feasible. This topic, as well as alternatives to precious metal catalysts, will not be covered further here as it has been covered in detail in other reviews [6,8].

In addition, structural supports used in some tubular reactors, such as PVC or polypropylene tubing, not only act to further separate electrodes but also reduce proton transfer, thereby increasing internal resistance. Using perforated piping as structural supports lowers the percentage of open area between the electrodes due to the perforations, reducing the area available for proton transfer, which ultimately reduces performance. This was likely the main reason for decreased performance when scaling up from a similar smaller version of the tubular brush anode reactors operated on wastewater described above. Similarly, another tubular design used a perforated pipe as the structural support for the membrane electrode assembly [22]. Although this supporting structure was on the exterior of the cathode and did not reduce the available area between the electrodes, oxygen availability to the cathode needed for the oxygen reduction reaction was likely limited due to the lower open area created by the perforated pipe. Structural supports should be chosen so that interference with necessary electrode interactions and processes is limited.

There are significantly more studies on scale-up of tubular designs compared with flat-plate reactor designs. As a result, the discussion has focused mainly on scale-up of tubular designs for practical application. Flat-plate designs have great potential for scale-up applications. The key attribute is minimized electrode spacing without a

reduction in available surface area from structural material. However, more studies are needed at larger scales before any conclusion can be drawn between tubular and flat-plate designs.

Factors affecting performance related to practical application

The compositions of real waste streams can have drastic impacts on performance during practical applications, ultimately determining reactor operation mode. Two-thirds of the reactors described here have reported results of operation on real waste streams. When comparing these reactors to reactors operated with synthetic wastewater, power is generally lower (Tables 1 & 2). This has also been shown for other smaller scale MFCs [57]. Most of the tubular designs in Tables 1 & 2 were operated on sludge or wastewater, while the flat-plate reactors were operated on buffered synthetic waste streams. This would in part account for the higher power generated by the flat-plate designs and highlights the need for the flat-plate design to be tested with real waste streams.

Scale-up studies presented here also indicate that certain operation modes may be more suitable for treating different types of waste during practical application. For example, in one larger scale reactor, treating landfill leachate in a loop operation and recycling the effluent back through the reactor continuously was more effective than treating it in a continuous flow mode [18]. The manner in which influent waste streams enter the reactor can also have an affect on the treatment of different types of waste streams. Connecting individual modules hydraulically in series will lead to different substrate concentrations and/or compositions compared with reactors fed hydraulically in parallel. When connected in series, each sequential reactor receives the effluent from the previous reactor. As different components of the waste stream are broken down, different substrates become available to microbes as the waste progresses through sequential cells in the reactor. Depending on waste strength and composition, hydraulic retention times may need to be adjusted to achieve desired performance [18,26].

In general, reactors operating on buffered real waste streams produce higher power densities than with unbuffered waste streams (Tables 1 & 2). Amendments to waste streams such as addition of buffers, pH adjustments [19,26,35], adjustments to increase conductivity [19] and addition of carbon sources [24] may be necessary to improve performance or reduce start-up times. These improvements will likely increase operating costs. Adjusting pH is common in many wastewater treatment plants so pH adjustment would be preferable to the addition of buffers. Recently, it has been suggested that enhanced production of self-produced bicarbonate buffer through the manipulation of retention time leads to a decrease in internal resistance, increasing power [15,52]. Although further work is needed, designing systems for use in treating high organic waste streams may reduce the need for pH adjustment.

Furthermore, certain types of waste streams can have a high inorganic composition. As shown with some reactors described in this review [24], high concentrations of calcium ions and decreased localized pH leads to deposits on the water-facing side of the cathode, again reducing long-term performance. In a different reactor, similar issues occurred when deposits of alkali salts occurred on the cathode surface when treating brewery wastewater [20]. Clogging due to wastewater composition or excess biofilm growth can also occur during *in situ* applications [21,22,32]. Clogging and excess biofilm growth have not been significant issues during shorter-term laboratory-scale experiments and will likely become a more important issue as studies run for longer terms. Clogging can be reduced through pretreatment of wastewaters, as well as through optimization of reactor design and operation, which is design specific. Excess biofilm growth can be controlled in part by modifying structural surfaces to prevent attachment. However, further research is needed in this area.

When comparisons are made within studies, higher organic loading rate results in higher power densities [17,19,24]. Of the studies reporting chemical oxygen demand (COD) removal efficiencies, more than half reported greater than 80% removal of COD. However, lower organic loading rates generally lead to higher COD removal rates. All of the reactors reporting high removal rates, in general, also had lower organic loading rates compared with reactors in which COD removal was not as efficient (Tables 1 & 2). Tables 1 & 2 shows that the addition of granular material to the anode (and cathode) chamber increases COD removal efficiency. Both reactors that contained granular material reported COD removal efficiencies above 80%. The increased surface area created by the material increases biofilm attachment and adsorption of pollutants, which leads to an increase in COD removal. Because granular material essentially acts as a filter, clogging due to wastewater composition or excess biofilm growth could occur, which would likely decrease performance. Based on other research [48], it would be expected that the reactors using brush anodes would have higher COD removal; however, this was not the case. The three reactors using brush anodes that reported organic removal rates, reported relatively low COD removal efficiencies ranging from 50 to 70% (Tables 1 & 2). Although one of the reactors reported COD removal at >90%, only 60–70% removal was related to the anode chamber and another 20–25% removal occurred as a result of aerobic processes from flowing wastewater over the cathode [21]. The hydraulic retention times (HRT) of these reactors

ranged from 11 h to 14 days. Higher removal efficiency is expected at longer HRTs, but this was not the case for the reactor with the 14-day HRT. The other two brush anode reactors used similar HRTs that were used with other designs and similar removal efficiencies resulted (Tables 1 & 2).

It would be expected that waste streams high in organic content would perform similarly to synthetic substrates with similar organic content. However, due to the complex nature of many waste streams, high concentrations as well as the presence of inhibitory compounds or heavy metals could ultimately limit performance. As a result, characterization is necessary before use in MFCs at the laboratory scale or larger. Characterization will also identify if pretreatment is necessary.

Conclusion

Several studies regarding scale-up have been reported in this review ranging from 1 to 1000 l, consisting of short-term, laboratory scale experiments to long-term, *in situ* pilot-scale investigations. Although there are more studies regarding tubular reactor designs compared with flat-plate designs, lessons can be drawn regarding both types of configurations. If brush anodes are to be used in either type of reactor, it is essential that electrode spacing be reduced in order to decrease internal resistance. Optimization of design factors such as brush length, diameter, orientation and number of brushes will likely further decrease the internal resistance and increase power. Furthermore, structural and supporting material used in reactors needs to be designed in such a way that it does not reduce mass transfer to and from electrode surfaces. Likewise, separator material should be permeable and used instead of expensive anion/cation exchange membranes. In certain designs, there may be a trade-off between high power and treatment capability. However, configurations that produce high power will likely have high treatment efficiency, as higher current indicates not only higher substrate conversion but increased treatment efficiency. Although granular material may be an effective means of increasing treatment, in designs presented to date it increases internal resistance and ultimately reduces power. If granular material is to be used, it should be conductive. Finally, fully characterizing waste streams will go a long way in determining the appropriateness of MFC technology for treating different wastes. For any type of design, a systematic progression from the laboratory scale to pilot-scale is needed to determine the effectiveness of a given design. This strategy will allow for identification of potential issues before larger scale applications are undertaken.

Future perspective

There has been substantial progress towards scale-up and practical application of MFC technology in the last decade. However, to date, there are still many obstacles to overcome. First and foremost, a successful pilot-scale study, demonstrating the feasibility MFC technology for practical application, is paramount. In the near future, a greater focus on scaling-up flat-plate designs will likely lead to significant advances in taking this technology from the laboratory to the pilot scale and beyond. Moreover, the longest study reported to date operated for only 1.25 years. Materials used in MFCs, mainly electrodes and separators, need to operate for longer lifetimes and have low cost in order to make MFC technology competitive with other waste-to-energy technologies.

Additionally, waste streams with high organic concentrations would likely generate higher performance and would therefore be the most suitable for energy generation. However, at higher organic loading rates, COD removal is typically lower. Designs in which several MFCs are stacked hydraulically in series would be required to ensure treatment demands are met. Cells at the end of the hydraulic stack would have a reduced power output due to the lower organic loadings and would be used mostly for polishing the effluent rather than power production. Although MFC technology has the potential to replace traditional treatment technologies, it may be better used in conjunction with current technologies such as aeration or anaerobic digestion. However, the most promising use for this technology is in decentralized industrial wastewater treatment. Treatment of certain industrial waste streams such as brewery or fruit processing streams, which can have high organic content and are typically less complex than municipal waste streams, may prove to be the most viable option for MFC technology.

For the MFC systems discussed in this manuscript, the overall power densities, based on both area and volume (Tables 1 & 2), are still too low to be competitive with current waste-to-energy technologies such as anaerobic digestion (~1 kW m^{-3}) [15,37]. The COD conversion rates are also lower than the typical conversion rates of anaerobic digester (~25 kg COD m^{-3} d^{-1}). However, the highest maximum power density achieved with a smaller milliliter-scale flat-plate MFC design was reported as over 2 kW m^{-3} with a conversion rate of over 90 g COD l^{-1} d^{-1} using a synthetic wastewater [15], indicating that if power could be maintained during scale-up, MFC technology would be competitive with anaerobic digestion on both an energy generating and a treatment efficiency basis.

Financial & competing interests disclosure

The authors would like to acknowledge support from the US National Science Foundation (Chemical, Biological, Environmental, and Transport Systems 0955124, Partnerships for Innovation 1312301; VA, USA) and Oregon Built Environment and Sustainable Technologies Center (OR, USA). The authors have no other relevant affiliations or financial involvement with any organization or entity with a financial interest in or financial conflict with the subject matter or materials discussed in the manuscript apart from those disclosed.

No writing assistance was utilized in the production of this manuscript.

Executive summary

Background

- Several studies regarding scale-up have been reported in this review ranging from 1 to 1000 l, from short-term laboratory scale experiments to long-term *in situ* pilot-scale investigations.

Microbial fuel cell designs used in scale-up studies

- Tubular reactor configurations and flat-plate reactor configurations are the two most common reactor designs used. More research has been done on tubular designs than on flat-plate designs.

Factors affecting performance related to reactor design

- Key issues dealing with electrode configurations such as spacing, shape and orientation, size and effective electrode surface area will ultimately determine the maximum power attainable for a given design.
- Many of the reactor designs used in scaled-up studies contain expensive membrane materials when there are less expensive and often better performing separator materials available.

Factors affecting performance related to practical application

- Compositions of real waste streams can have drastic impacts on performance during practical applications, ultimately determining operation mode.

Future perspective

- Overall power densities of scaled-up microbial fuel cells are still too low to be competitive with current waste-to-energy technologies.
- A greater focus on scaling-up flat-plate designs will likely lead to significant advances in taking this technology from the laboratory to the pilot scale and beyond.
- A successful pilot-scale study, demonstrating the feasibility of microbial fuel cell technology for practical application of wastewater treatment, is needed.

References

Papers of special note have been highlighted as:

- ▪ of interest

1 FAO. *Coping with Water Scarcity: an Action Framework for Agriculture and Food Security.* FAO, Rome, Italy (2012).

2 US EPA Office of Water. *Wastewater Management Fact Sheet, Energy Conservation.* US EPA, Washington, DC, USA (2006).

3 Curtis TP. Low-energy wastewater treatment: strategies and technologies. In: *Environmental Microbiology.* Mitchell R, Gu JD (Eds). John Wiley & Sons, Inc., NY, USA, 301–318 (2010).

4 McCarty PL, Bae J, Kim J. Domestic wastewater treatment as a net energy producer – can this be achieved? *Environ. Sci. Technol.* 45(17), 7100–7106 (2011).

5 Liu H, Ramnarayanan R, Logan BE. Production of electricity during wastewater treatment using a single chamber microbial fuel cell. *Environ. Sci. Technol.* 38(7), 2281–2285 (2004).

6 Wei J, Liang P, Huang X. Recent progress in electrodes for microbial fuel cells. *Bioresour. Technol.* 102(20), 9335–9344 (2011).

7 Kumar GG, Sarathi VGS, Nahm KS. Recent advances and challenges in the anode architecture and their modifications for the applications of microbial fuel cells. *Biosens. Bioelectron.* 43, 461–475 (2013).

8 Logan BE. Scaling up microbial fuel cells and other bioelectrochemical systems. *Appl. Microbiol. Biotechnol.* 85(6), 1665–1671 (2010).

9 Li W-W, Sheng G-P, Liu X-W, Yu H-Q. Recent advances in the separators for microbial fuel cells. *Bioresour. Technol.* 102(1), 244–252 (2011).

10 Oliveira VB, Simões M, Melo LF, Pinto AMFR. Overview on the developments of microbial fuel cells. *Biochem. Eng. J.* 73, 53–64 (2013).

11 Liu H, Cheng S, Huang L, Logan BE. Scale-up of membrane-free single-chamber microbial fuel cells. *J. Power Sources* 179(1), 274–279 (2008).

12 Rabaey K, Boon N, Siciliano SD, Verhaege M, Verstraete W. Biofuel cells select for microbial consortia that self-mediate electron transfer. *Appl. Environ. Microbiol.* 70(9), 5373–5382 (2004).

13 Cheng S, Logan BE. Increasing power generation for scaling up single-chamber air cathode microbial fuel cells. *Bioresour. Technol.* 102(6), 4468–4473 (2011).

14 Bond DR, Lovley DR. Electricity production by *Geobacter sulfurreducens* attached to electrodes. *Appl. Environ. Microbiol.* 69(3), 1548–1555 (2003).

15 Fan Y, Han S-K, Liu H. Improved performance of CEA microbial fuel cells with increased reactor size. *Energy Environ. Sci.* 5(8), 8273 (2012).

- ▪ **Demonstrates highest power density achieved to date in a microbial fuel cell.**

16 Li Z, Yao L, Kong L, Liu H. Electricity generation using a baffled microbial fuel cell convenient for stacking. *Bioresour. Technol.* 99(6), 1650–1655 (2008).

17 Kim JR, Rodríguez J, Hawkes FR, Dinsdale RM, Guwy AJ, Premier GC. Increasing power recovery and organic removal efficiency using

extended longitudinal tubular microbial fuel cell (MFC) reactors. *Energy Environ. Sci.* 4(2), 459–465 (2011).

18 Gálvez A, Greenman J, Ieropoulos I. Landfill leachate treatment with microbial fuel cells; scale-up through plurality. *Bioresour. Technol.* 100(21), 5085–5091 (2009).

19 Zhuang L, Zheng Y, Zhou S, Yuan Y, Yuan H, Chen Y. Scalable microbial fuel cell (MFC) stack for continuous real wastewater treatment. *Bioresour. Technol.* 106, 82–88 (2012).

- **Highest power density achieved in a scaled-up tubular reactor reported in this review.**

20 Zhuang L, Yuan Y, Wang Y, Zhou S. Long-term evaluation of a 10-liter serpentine-type microbial fuel cell stack treating brewery wastewater. *Bioresour. Technol.* 123, 406–412 (2012).

21 Zhang F, Ge Z, Grimaud J, Hurst J, He Z. Long-term performance of liter-scale microbial fuel cells treating primary effluent installed in a municipal wastewater treatment facility. *Environ. Sci. Technol.* 47(9), 4941–4948 (2013).

22 Zhang F, Ge Z, Grimaud J, Hurst J, He Z. *In situ* investigation of tubular microbial fuel cells deployed in an aeration tank at a municipal wastewater treatment plant. *Bioresour. Technol.* 136, 316–321 (2013).

23 Scott K, Murano C, Rimbu G. A tubular microbial fuel cell. *J. Appl. Electrochem.* 37(9), 1063–1068 (2007).

24 Jiang D, Curtis M, Troop E *et al.* A pilot-scale study on utilizing multi-anode/cathode microbial fuel cells (MAC MFCs) to enhance the power production in wastewater treatment. *Int. J. Hydrogen Energy* 36(1), 876–884 (2011).

25 Lefebvre O, Shen Y, Tan Z, Uzabiaga A, Chang IS, Ng HY. Full-loop operation and cathodic acidification of a microbial fuel cell operated on domestic wastewater. *Bioresour. Technol.* 102(10), 5841–5848 (2011)

26 Ge Z, Zhang F, Grimaud J, Hurst J, He Z. Long-term investigation of microbial fuel cells treating primary sludge or digested sludge. *Bioresour. Technol.* 136, 509–514 (2013).

27 Zhuang L, Zhou S. Substrate cross-conduction effect on the performance of serially connected microbial fuel cell stack. *Electrochem. Commun.* 11(5), 937–940 (2009).

28 Zhuang L, Zhou S, Wang Y, Liu C, Geng S. Membrane-less cloth cathode assembly (CCA) for scalable microbial fuel cells. *Biosens. Bioelectron.* 24(12), 3652–3656 (2009).

29 Zhang F, Jacobson KS, Torres P, He Z. Effects of anolyte recirculation rates and catholytes on electricity generation in a litre-scale upflow microbial fuel cell. *Energy Environ. Sci.* 3(9), 1347–1352 (2010).

30 Kim JR, Premier GC, Hawkes FR, Rodríguez J, Dinsdale RM, Guwy AJ. Modular tubular microbial fuel cells for energy recovery during sucrose wastewater treatment at low organic loading rate. *Bioresour. Technol.* 101(4), 1190–1198 (2010).

31 Kim JR, Premier GC, Hawkes FR, Dinsdale RM, Guwy AJ. Development of a tubular microbial fuel cell (MFC) employing a membrane electrode assembly cathode. *J. Power Sources* 187(2), 393–399 (2009).

32 Keller J, Rabaey K. Experiences from MFC pilot plant operations. Presented at: *Microbial Fuel Cells-First International Symposium*. PA, USA, 27–29 May 2008.

33 Jiang D, Li B. Granular activated carbon single-chamber microbial fuel cells (GAC-SCMFCs): a design suitable for large-scale wastewater treatment processes. *Biochem. Eng. J.* 47(1), 31–37 (2009).

34 You S, Zhao Q, Zhang J *et al.* A graphite-granule membrane-less tubular air-cathode microbial fuel cell for power generation under continuously operational conditions. *J. Power Sources* 173(1), 172–177 (2007).

35 Clauwaert P, Mulenga S, Aelterman P, Verstraete W. Litre-scale microbial fuel cells operated in a complete loop. *Appl. Microbiol. Biotechnol.* 83(2), 241–247 (2009).

36 Dekker A, Heijne AT, Saakes M, Hamelers HVM, Buisman CJN. Analysis and improvement of a scaled-up and stacked microbial fuel cell. *Environ. Sci. Technol.* 43(23), 9038–9042 (2009).

37 Ter Heijne A, Liu F, van Rijnsoever LS, Saakes M, Hamelers HVM, Buisman CJN. Performance of a scaled-up microbial fuel cell with iron reduction as the cathode reaction. *J. Power Sources*. 196(18), 7572–7577 (2011).

- **Highest power density achieved in a scaled-up flat-plate reactor reported in this review.**

38 Liang P, Fan M, Cao X, Huang X. Evaluation of applied cathode potential to enhance biocathode in microbial fuel cells. *J. Chem. Technol. Biotechnol.* 84(5), 794–799 (2009).

39 Ter Heijne A, Hamelers HVM, Saakes M, Buisman CJN. Performance of non-porous graphite and titanium-based anodes in microbial fuel cells. *Electrochim. Acta* 53(18), 5697–5703 (2008).

40 Fan Y, Hu H, Liu H. Enhanced Coulombic efficiency and power density of air-cathode microbial fuel cells with an improved cell configuration. *J. Power Sources* 171(2), 348–354 (2007).

- **Demonstrates enhanced coulombic efficiency and increased power density using a cloth electrode assembly containing an inexpensive separator material.**

41 Cheng S, Liu H, Logan BE. Increased power generation in a continuous flow MFC with advective flow through the porous anode and reduced electrode spacing. *Environ. Sci. Technol.* 40(7), 2426–2432 (2006).

42 Aelterman P, Rabaey K, Pham HT, Boon N, Verstraete W. Continuous electricity generation at high voltages and currents using stacked microbial fuel cells. *Environ. Sci. Technol.* 40(10), 3388–3394 (2006).

43 Ieropoulos I, Greenman J, Melhuish C. Microbial fuel cells based on carbon veil electrodes: stack configuration and scalability. *Int. J. Energy Res.* 32(13), 1228–1240 (2008).

44 Gurung A, Oh S-E. The performance of serially and parallelly connected microbial fuel cells. *Energ. Source. Part A* 34(17), 1591–1598 (2012).

45 Oh S-E, Logan BE. Voltage reversal during microbial fuel cell stack operation. *J. Power Sources* 167(1), 11–17 (2007).

46 Fan Y, Sharbrough E, Liu H. Quantification of the internal resistance distribution of microbial fuel cells. *Environ. Sci. Technol.* 42(21), 8101–8107 (2008).

- **Provides method for estimation of internal resistance and shows that decreasing electrode spacing can increase power significantly.**

47 Liu H, Cheng S, Logan BE. Power generation in fed-batch microbial fuel cells as a function of ionic strength, temperature, and reactor configuration. *Environ. Sci. Technol.* 39(14), 5488–5493 (2005).

48 Hays S, Zhang F, Logan BE. Performance of two different types of anodes in membrane electrode assembly microbial fuel cells for power generation from domestic wastewater. *J. Power Sources* 196(20), 8293–8300 (2011).

49 Logan B, Cheng S, Watson V, Estadt G. Graphite fiber brush anodes for increased power production in air-cathode microbial fuel cells. *Environ. Sci. Technol.* 41(9), 3341–3346 (2007).

50 Hutchinson AJ, Tokash JC, Logan BE. Analysis of carbon fiber brush loading in anodes on startup and performance of microbial fuel cells. *J. Power Sources* 196(22), 9213–9219 (2011).

51 Ahn Y, Logan BE. Effectiveness of domestic wastewater treatment using microbial fuel cells at ambient and mesophilic temperatures. *Bioresour. Technol.* 101(2), 469–475 (2010).

52 Fan Y, Hu H, Liu H. Sustainable power generation in microbial fuel cells using bicarbonate buffer and proton transfer mechanisms. *Environ. Sci. Technol.* 41(23), 8154–8158 (2007).

53 Zhang X, Cheng S, Huang X, Logan BE. The use of nylon and glass fiber filter separators with different pore sizes in air-cathode single-chamber microbial fuel cells. *Energy Environ. Sci.* 3(5), 659–664 (2010).

54 Liu H, Logan BE. Electricity generation using an air-cathode single chamber microbial fuel cell in the presence and absence of a proton exchange membrane. *Environ. Sci. Technol.* 38(14), 4040–4046 (2004).

55 Zhang X, Cheng S, Huang X, Logan BE. Improved performance of single-chamber microbial fuel cells through control of membrane deformation. *Biosens. Bioelectron.* 25(7), 1825–1828 (2010).

56 Ghasemi M, Daud WRW, Hassan SHA *et al.* Nano-structured carbon as electrode material in microbial fuel cells: a comprehensive review. *J. Alloys Compd.* 580, 245–255 (2013).

57 Pant D, Van Bogaert G, Diels L, Vanbroekhoven K. A review of the substrates used in microbial fuel cells (MFCs) for sustainable energy production. *Bioresour. Technol.* 101(6), 1533–1543 (2010).

▪ Patent

101 Bretschger O: US0137000 (2013).